Prompt Production of Hadronic Molecules and Rescattering of Final States in Heavy Hadron Decays

Dissertation
zur
Erlangung des Doktorgrades (Dr. rer. nat.)
der
Mathematisch-Naturwissenschaftlichen Fakultät
der
Rheinischen Friedrich-Wilhelms-Universität Bonn

von
Zhi Yang
aus
Sichuan, China

Bonn, 2016

Dieser Forschungsbericht wurde als Dissertation von der Mathematisch-Naturwissenschaftlichen Fakultät der Universität Bonn angenommen und ist auf dem Hochschulschriftenserver der ULB Bonn `http://hss.ulb.uni-bonn.de/diss_online` elektronisch publiziert.

1. Gutachter:	Prof. Dr. Ulf-G. Meißner
2. Gutachterin:	Prof. Dr. Feng-Kun Guo
Tag der Promotion:	7.7.2016
Erscheinungsjahr:	2016

Abstract

The B factories and high energy hadron colliders have accumulated unprecedented data samples in the past decade, and a dramatic progress has been made in hadron spectroscopy. The discovery of many new unexpected states in the open and hidden heavy flavor spectrum is extremely interesting as they can not be simply explained by the conventional quark model, and it triggers a campaign of revealing their internal structure.

It calls for more complex structures. Different explanations for the underlying structure have been proposed, for instance tetraquark, hybrid, hadro-quarkonium and hadronic molecule. The hadrons can form hadronic molecule, just like two nucleons form the deuteron. Especially for the exotic states very close to the threshold of two conventional hadrons, they are very likely to be S-wave loosely bound states. The $X(3872)$ is one promising candidate of a hadronic molecule.

To clarify the intriguing properties and finally decipher the internal nature, more accurate data and new processes involving the production and decays of the exotic states will be helpful. In this thesis, we investigated the mechanism for the inclusive prompt production of the exotic state under the molecular scenario. The mechanism is as follows: the constituent mesons would be produced by using the Monte Carlo event generator first, and the formation of the bound state occurs afterward through the final state interaction which can be described by the effective field theory. The well separated energy scales associated in the process make the mechanism valid. And a factorization formula can be obtained by using the Migdal-Watson theorem. We applied this mechanism to predict the production rate of the exotic charm-strange hadrons D_{sJ}, the $X(3872)$ and and its bottom analogs and spin partner at hadron colliders.

We also investigated the kinematical effect in the triangle diagram. The effect can play a important role in certain transitions, as it might cause an enhancement or a peak. We thus find the ideal energy range to search for the spin partner of the $X(3872)$ in electron–position collisions associated with one emitted photon. In addition, we studied the hindered $M1$ transition between two bottomia as the kinematical effect in the triangle diagram is expected to lead to partial widths much larger than the prediction of the quark model. Moreover, we studied the motion of the anomalous threshold singularity of the triangle diagram of process $\Lambda_b \to J/\psi\pi K$ in the complex energy plane. And we found that the intermediate states $\Lambda(1890)$, χ_{c1} and p can make the singularity appear at the $\chi_{c1}p$ threshold, where the narrow pentaquark-like structure $P_c(4450)$ observed by LHCb is located.

Contents

CHAPTER 1

Introduction

In particle physics, the standard model has enjoyed great successes in the last half century in exploring the fundamental particles and the interactions between them, although it falls short of incorporating the theory of gravitation. All the elementary particles including quarks, leptons, gauge bosons and the Higgs boson in the standard model have been observed, which gives credit to the model.

Among the fundamental particles, the quarks make up the most part of our observable matter. The strong interaction between the quarks and gluons can be described by Quantum Chromodynamics (QCD). In the high energy region, the quarks and gluons can freely move which is known as asymptotic freedom. In the low energy region, the interaction between the quarks and gluons becomes strong enough to bind the quarks to hadrons and the theory cannot be solved perturbatively any more.

A scheme to classify the hadrons is the quark model which was proposed by Zweig and Gell-Mann in 1964 before the birth of QCD [1, 2]. The model successfully classifies the large number of hadrons in terms of the small number of quarks. Mesons and baryons have baryon number 0 and 1, respectively. In the quark model, mesons are made of valence quark-antiquark pairs $q\bar{q}$ and baryons are made of three valence quarks qqq. In the most general case, they may also have any number of quark-antiquark pairs. The valence quarks give rise to the quantum numbers of the hadrons. In addition to flavour and spin degrees of freedom, the quarks also carry color which is the quantum number introduced to explain the existence of baryons with three identical quarks, for instance the Δ^{++} (uuu) and the Ω^{-} (sss). However, the hadrons are color-neutral and no colorful objects have been observed in experiments as asymptotic states. This leads to the conjecture of color confinement.

Nevertheless, the color-neutral hadrons can have much more complicated structures than the quark model allows. There may exist hadrons beyond the simple quark model. For example, the glueballs which only contain valence gluons, the hybrids which contain valence quarks and gluons as well, especially the exotic hadrons with multiquarks. At the beginning of this century, the famous $X(3872)$ was observed by the Belle Collaboration. Its properties are in conflict with quark model expectations for any normal $c\bar{c}$ charmonium, and thus the $X(3872)$ presents a prominent example of a hadron beyond the simple quark model. So far, the $X(3872)$ has received the most intensive attention. Its discovery opens a new era of revealing the intriguing hadron structure with multiquarks.

For the multiquark states with more than three quarks, i.e. tetraquarks or pentaquarks, they can be loosely bound states of two mesons or baryons which is the generalization of the classical light nuclei to systems of other hadrons, or compact multiquark states. As we know, in the quantum field theory all possible configurations can mix with each other in various ways as long as they have the same quantum numbers. Thus strictly speaking, the wave function of a hadron is actually a superposition of all possible configurations. Yet, if the hadron is very close the threshold of other two hadrons, one may construct an

effective field theory to describe it with hadronic degrees of freedom. In fact, many of the newly observed structures were suggested to be hadronic molecules, and may be described by such an approach.

In the open charm sector, the $D^*_{s0}(2317)$ was observed by Babar in $D_s\pi^0$ final state [3] and $D_{s1}(2460)$ was observed by CLEO in the $D^*_s\pi^0$ channel [4]. They can not fit in the simple quark model scheme and are possible candidates for DK and D^*K bound states, respectively. Their mass splitting is approximately equal to the mass splitting between pseudoscalar and vector charmed mesons, which is the consequence of heavy quark spin symmetry in the picture of hadronic molecule.

In the hidden charm and bottom sector, one also has the so-called XYZ state or quarkonium-like state, which can decay to final states containing a heavy quark Q and a heavy antiquark $\bar{Q}$, with Q the charm or bottom quark, but cannot be easily accommodated as a conventional quarkonium. Unlike the light quarks, charm and bottom quarks are so heavy that their pair production from the vacuum would be heavily suppressed. Therefore the heavy quarks in the final states are likely to exist as initial constituents. Some of them, if confirmed as real resonances rather than kinematical effects, are necessarily exotic hadrons, especially for the charged charmonium-like states $Z_c(3900)$, $Z_c(4020)$, $Z^+(4051)$, $Z^+(4430)$ and so on. They cannot be just charge-neutral $Q\bar{Q}$ configuration but contain at least four quarks. In the bottomium sector, we can expect the existence of similar exotic states. Actually, the charged bottomium-like states $Z_b(10610)$ and $Z_b(10650)$ were observed by Belle in the invariant mass spectra for the decays of $\Upsilon(5S)$ into $\Upsilon(1S, 2S, 3S)\pi\pi$, $h_b(1P, 2P)\pi\pi$ and $B^{(*)}\bar{B}^{(*)}\pi$ [5].

Let us take the $X(3872)$ as an example. The production of the $X(3872)$ can be achieved through the weak decay of b hadrons and the prompt production through QCD mechanisms. Since the $X(3872)$ is very close to the $D^0\bar{D}^{*0}$ threshold, it is quite reasonable that it is an S-wave bound state of $D\bar{D}^*$. After the discovery of the $X(3872)$, dozens of charmonium-like XYZ states have been observed, mainly through B hadron decays. Fig. 1.1, which is taken from Ref. [6], lists five groups of observed charmonlum-like states according to their production mechanisms. In addition to b hadron decays, the charmonium-like XYZ state can be produced through the initial state radiation technique (ISR) in the e^+e^- annihilation, the double charmonium production processes, the two photon fusion processes, and the the hadronic decays of the $Y(4260)$ as well. What is more interesting is that BESIII reported the $X(3872)$ events in the radiative decay of $Y(4260)$, $Y(4260) \to X(3872)\gamma$ [7], which may be regarded as a support of the dominantly molecular structure of the $X(3872)$ [8].

Our understanding of hadron spectroscopy can be largely improved by studies of the exotic states. Great progress has been made in the past decades, see Ref. [9, 10] and references therein. One of the most important aspects is the discrimination of a compact multiquark configuration and a loosely bound hadronic molecule. Different theoretical predictions based on different scenarios are necessary on the masses, decays and productions of the exotic states. Comparing these predictions with experiments, one can make progress towards understanding these new structures, and eventually getting hints of how confinement occurs.

Under the hadronic molecular configuration, we can use the observed candidates as inputs to predict their spin partners and charm or bottom analogs according to the heavy quark symmetry. At the leading order, the scattering of a Goldstone boson off a matter field is universally dominated by the Weinberg-Tomozawa term [11, 12], one can predict more bound states of a kaon and a heavy meson with $D^*_{s0}(2317)$. On the other hand, some of the leading order interaction between two heavy mesons are identical, there exist the spin partner of the $X(3872)$ and their bottom analogs [13]. The discovery of these spin partners and analogs can be not only important for the study of their properties, but also for identifying the the molecular configuration of the $X(3872)$.

The production mechanism for the prompt hadronic molecules by using Monte Carlo event generators was first proposed in Ref. [14]. In this thesis, we will use the event generators together with the effective field theory which is used for describing the final state interaction to establish the factorization formula

of the cross sections, and estimate the production rates of the bound states in the open and hidden heavy flavour sectors.

For the pentaquarks, a peak was reported by the LEPS experiment in the K^+n invariant mass distribution in the reaction $\gamma n \to K^+K^-n$ in 2003 [15] and this structure was declared as a pentaquark called Θ^+. However, it turned out to be caused by an artificial prescription for the calculation of unmeasured neutron momentum. And the peak disappeared in later experiments with high statistics by CLAS [16] and J-PARC [17]. Thus this claimed observation of the pentaquark is spurious. In 2015, two charmonium-pentaquark-like states were observed in the $J/\psi p$ channel in the $\Lambda_b^0 \to J/\psi K^- p$ decays [18]. One is called $P_c(4380)$, and the other one is $P_c(4450)$.

However, the rescattering effect of the final state could cause an enhancement in the invariant mass distribution. The near-threshold structure was discovered in the invariant mass spectrum of $p\bar{p}$ by BESII [19] and BESIII [20] in the J/ψ and ψ' radiative decays to $\gamma p\bar{p}$, and in the decays $B \to xp\bar{p}$ with x being π^+, K^+, K^0 and K^{*+} by Belle [21, 22]. A number of theoretical proposal were $p\bar{p}$ bound state or baryonium [23] and glueball state [24, 25]. In addition to the speculation of genuine state, the near-threshold enhancement can be reproduced by simply the final state interaction between the outgoing proton and antiproton [26–30]. For the $P_c(4450)$, it is located exactly at the $\chi_{c1}p$ threshold and could be caused by a kinematical singularity in the rescattering process. In this thesis, we will also study the kinematical effect of the scattering of $\chi_{c1}p \to J/\psi p$ which can cause a peak located at the same position as the $P_c(4450)$.

This thesis is organised as follows:

- In Chapter 2, we will first give an short introduction to hadron physics. Then we will also briefly introduce the effective field theories, such as chiral perturbation theory, heavy quark effective theory, heavy hadron chiral perturbation theory and nonrelativistic field theory, which we are going to use in later chapters. And we will discuss the dynamical generation of hadronic molecules.

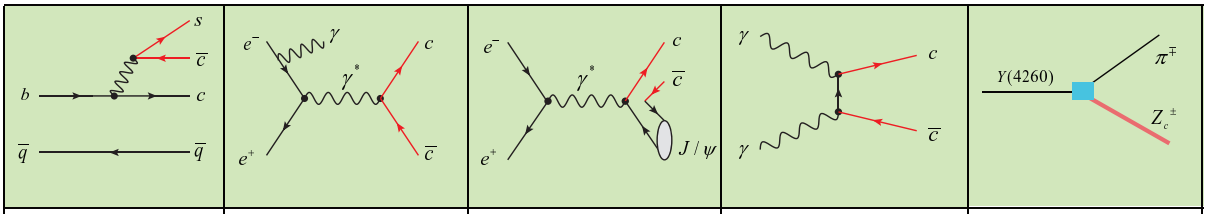

$X(3872)$	$Y(4260)$	$X(3940)$	$X(3915)$	$Z_c(3900)$
$Y(3940)$	$Y(4008)$	$X(4160)$	$X(4350)$	$Z_c(4025)$
$Z^+(4430)$	$Y(4360)$		$Z(3930)$	$Z_c(4020)$
$Z^+(4051)$	$Y(4630)$			$Z_c(3885)$
$Z^+(4248)$	$Y(4660)$			
$Y(4140)$				
$Y(4274)$				
$Z_c^+(4200)$				
$Z^+(4240)$				
$X(3823)$				

Figure 1.1: The five production mechanisms and the charmion-like states observed. This picture is taken from Ref. [6]. The first, second, third, and fourth columns are the mechanisms via B hadron decays, initial state radiation technique (ISR) in the e^+e^- annihilation, the double charmonium production processes, and two photon fusion processes, respectively. And the last one shows the hadronic decays of the $Y(4260)$.

- In Chapter 3, we will investigate the charm-strange hadronic molecules and their prompt production at the hadron colliders by using event generators and unitarized heavy hadron chiral perturbative theory.
- In Chapter 4, we will investigate the general factorization formula for the inclusive production of the hadronic molecules and calculate the cross sections for the production of the $X(3872)$ and its spin partner and bottom analogs.
- In Chapter 5, we will study the production of the spin partner of the $X(3872)$ at electron-positron collider through the charmonium decays. We will show the ideal energy region to produce this state.
- In Chapter 6, we will study the hindered $M1$ transition between two bottomia with coupled channel effects. The partial widths of these transitions could be much larger than the predictions from quark model.
- In Chapter 7, we will investigate the kinematical effect in the narrow $P_c(4450)$ structure. From the motion of the anomalous threshold singularity, we can find the triangle diagram that would contribute to the peak located at the same position as the $P_c(4450)$.

CHAPTER 2

Hadron structure and theories

In the realm of hadron physics, the fundamental field theory, i.e. the quantum chromodynamics (QCD) for describing the strong interactions, encounters extreme difficulties because at long distances QCD exhibits color confinement and is nonperturbative. Then alternative approaches have to be used instead, for example lattice QCD and effective field theories.

This chapter is organized as follows. In Section 2.1, we will first give a brief review on hadron structure. In Section 2.2, we will also show some relevant effective field theories which we will use in the latter chapters. At last in Section 2.3, we will discuss the dynamical generation of hadronic molecules.

2.1 Hadron structure

The strongly interacting particles in the Standard Model are the colored quarks and gluons. In nature, the quarks and gluons are bound to color-neutral hadrons as the strength of their color interactions increases as the involved energy scale decreases.

2.1.1 Conventional hadrons

In the conventional quark model, a meson is composed of a pair of quark and antiquark and a baryon is composed of three quarks. Additionally, they may also have any number of quark-antiquark pairs in the most general case. We show an illustration for the conventional hadrons in Fig. 2.1. The valence quarks give rise to the quantum numbers of hadrons. These quantum numbers are labels classifying the hadrons. We can use the set coming from the Poincaré symmetry—J^{PC}, where J, P and C stand for the total angular momentum, P-symmetry, and C-symmetry, respectively. For a pair of quark and anti-quark, $P = (-1)^{L+1}$ and $C = (-1)^{L+S}$ (only for mesons with vanishing additive quantum numbers such as electric charge and strangeness), where L and S are the orbital and spin angular momentum, respectively. The quark model allows the meson $q\bar{q}$ to have the quantum numbers

$$0^{++},\ 0^{-+},\ 1^{--},\ 1^{+-},\ 1^{++},\ 2^{--},\ 2^{-+},\ 2^{++},\cdots \tag{2.1}$$

while

$$0^{--},\ \text{even}^{-+},\ \text{odd}^{-+} \tag{2.2}$$

are called exotic quantum numbers which can not be formed by a pair of q and $\bar{q}$.

In contrast, the qqq baryon in the quark model can exhaust all the quantum number

$$\frac{1}{2}^{\pm}, \frac{3}{2}^{\pm}, \frac{5}{2}^{\pm}, \cdots. \tag{2.3}$$

In the quark model with assumed and QCD-motivated quark-quark interaction, the mass spectrum of the hadrons can be obtained by solving the Schrödinger equation. The Schrödinger equation is nonrelativistic, and the relativistic corrections are necessary in more general cases, for instance the heavy-light mesons. For the relativistic corrections, we refer to the literatures by Basdevant and Boukraa [31], Godfrey and Isgur [32] and the Bonn Group for mesons [33, 34] and baryons [35]. The Godfrey-Isgur (GI) relativized potential quark model was very successful in the description of the spectrum and static properties of the mesons and baryons. Here we give a brief introduction to the GI model for mesons based on Ref. [32]. In the GI model, the rest-frame Schrödinger-type equation is written as

$$\mathcal{H}\,|\psi\rangle = E\,|\psi\rangle \tag{2.4}$$

where the Hamiltonian $\mathcal{H} = H_0 + V$ describes the interaction between the quark and antiquark, and the relativistic kinetic term

$$H_0 = \sqrt{\mathbf{p}^2 + m_1^2} + \sqrt{\mathbf{p}^2 + m_2^2} \tag{2.5}$$

with $m_{1,2}$ the constituent quark masses and $V = V(\mathbf{p}, \mathbf{r})$ is the effective momentum-dependent potential of the $q\bar{q}$ system with $\mathbf{p} = \mathbf{p}_1 = \mathbf{p}_2$ the center-of-mass momentum and $\mathbf{r}$ is the usual spatial coordinate in the nonrelativistic limit. The above subscripts 1 and 2 denote the quark and antiquark, respectively.

As for the effective potential, it can be obtained from the on-shell $q\bar{q}$ scattering amplitudes in the center-of-mass frame. The two key ingredients are the short-distance one-gluon-exchange interaction and the long-distance linear confining interaction. The latter one was at first employed by the Cornell group and later confirmed by the lattice QCD simulations. More details of the relativistic GI model can be found in the appendices of Ref. [32].

The relativistic effects are taken into account in the GI model for all mesons in a unified and physically motivated way. However, the nonrelativistic approximation can well describe the heavy-quark systems. In the nonrelativistic limit, Eq. (2.4) turns out to be the familiar Schrödinger equation with

$$H_0 \to \sum_{i=1}^{2}\left(m_i + \frac{\mathbf{p}^2}{2m_i}\right) \tag{2.6}$$

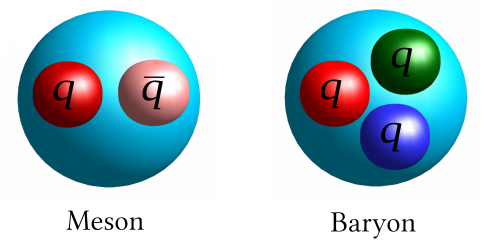

Figure 2.1: An illustration of the normal hadrons in the quark model.

$n\,^{2s+1}l_J$ J^{PC}	$c\bar{c}$	$c\bar{s}$; $\bar{c}s$
$1\,^1S_0$ 0^{-+}	$\eta_c(1S)$	$D_s^{\pm}$
$1\,^3S_1$ 1^{--}	$J/\psi(1S)$	$D_s^{*\pm}$
$1\,^1P_1$ 1^{+-}	$h_c(1P)$	$D_{s1}(2536)^{\pm}$
$1\,^3P_0$ 0^{++}	$\chi_{c0}(1P)$	
$1\,^3P_1$ 1^{++}	$\chi_{c1}(1P)$	
$1\,^3P_2$ 2^{++}	$\chi_{c2}(1P)$	$D_{s2}^{*}(2573)^{\pm}$
$1\,^3D_1$ 1^{--}	$\psi(3770)$	$D_{s1}^{*}(2700)^{\pm}$
$2\,^1S_0$ 0^{-+}	$\eta_c(2S)$	
$2\,^3S_1$ 1^{--}	$\psi(2S)$	
$2\,^1P_1$ 1^{+-}		
$2\,^3P_{0,1,2}$ $0^{++}, 1^{++}, 2^{++}$	$\chi_{c2}(2P)$	

Table 2.1: $q\bar{q}$ quark model assignments for the observed charmonia and charm-strange mesons with established J^{PC}.

and

$$V_{ij}(\mathbf{p},\mathbf{r}) \to H_{ij}^{\text{conf}} + H_{ij}^{\text{hyp}} + H_{ij}^{\text{SO}}\,. \tag{2.7}$$

The first term H_{ij}^{conf} includes the spin-independent linear confinement and Coulomb-type interaction, the second term H_{ij}^{hyp} is the color-hyperfine interaction and third term H^{SO} is the spin-orbit interaction including the color-magnetic term and the Thomas-precession term. More details about the explicit expressions can be found in Ref. [32].

In Tab. 2.1, we show the observed charmonia and charm-strange mesons with established J^{PC} in quark model. Together with the experimental results, the spectra of charm-strange mesons and charmonia predicted in the GI model will be shown in Chapter 3 and Chapter 4, respectively.

2.1.2 Exotic hadrons

In addition to the naive quark model, QCD allows much richer hadron spectrum. Actually, Gell-Mann and Zweig proposed not only the existence of meson and baryon but also the possible existence of the multiquark states [2, 36]. To be a multiquark state, it can be the loosely bound state of two or more hadrons or the compact tetraquark, pentaquark etc. On the other hand, the gluons interact among themselves because they carry color charges. Therefore two or more gluons may form the color-singlet glueball. And one or more gluons may bind with a pair of quark and antiquark to form a hybrid meson. The multiquark state or glueball or hybrid can carry all the exotic quantum numbers mentioned in Eq. 2.2. We show an illustration for these different types of exotic hadrons in Fig. 2.2.

2.2 Effective field theory

The fundamental field theory is one of the ultimate aims in particle physics, while the effective field theory (EFT) has become a practical tool which can avoid unnecessarily complicated calculations in the fundamental theory or provide insights even without knowing details of the fundamental theory. The very

basic ingredients of an EFT is scale separation, which allows for a power counting and thus a systematic expansion, and symmetry constraints. An EFT can be constructed at low energy as a Taylor expansion of the Lagrangian of an fundamental theory in powers of the external momentum of the light fields divided by the scale of heavy physics p/Λ, the value of Λ depends on the theory under investigation. This is an approximation, and the truncation of the series depends on the accuracy we desire. In addition, the larger the separation between the energy scale of interest and the energy scale of the fundamental dynamics is, the more accurate the EFT can be. To simplify the calculation, an EFT uses suitable degrees of freedom in the low energy region and the degrees of freedom at higher energy scale are integrated out.

A well-known example of an EFT is the Fermi theory of beta decay for weak interactions. If we are concerned with the interaction between hadrons, we also need the EFT of theory for the strong interaction.

In the standard model, quantum chromodynamics (QCD) is the theory describing the strong interactions between quarks and gluons. The dynamics of the quarks and gluons are controlled by the gauge invariant QCD Lagrangian

$$\mathcal{L}_{\mathrm{QCD}} = \bar{\psi}_i \left(i \not{D} - m_i \right) \psi_i - \frac{1}{4} G^a_{\mu\nu} G^{\mu\nu}_a, \tag{2.8}$$

where ψ_i is the quark field labelled by i, $D_\mu = \partial_\mu + igA^a_\mu \lambda_a/2$ is the covariant derivative, with A^a_μ the gluon fields and $G^a_{\mu\nu} = \partial_\mu A^a_\nu - \partial_\nu A^a_\mu + g f^{abc} A^b_\mu A^c_\nu$ is the gauge invariant gluon field strength tensor, where the f^{abc} are the structure constants of SU(3). The constants m and g are the quark mass and coupling constant of the theory, respectively. It is well-known that QCD presents two peculiar properties due to the

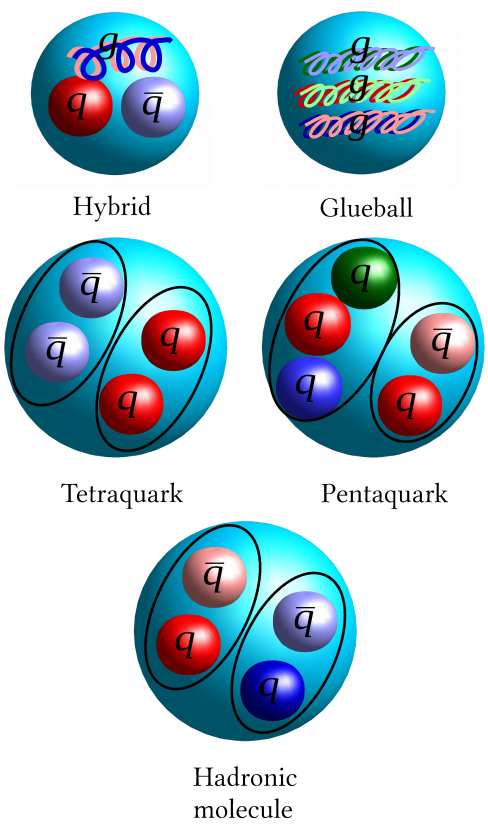

Figure 2.2: An illustration of the exotic hadrons beyond the simpler states in the quark model.

coupling constant behave differently in the high energy and low energy regions related to the QCD scale, $\Lambda_{QCD} \sim 220$ MeV. In the high energy region much larger than Λ_{QCD}, the coupling constant becomes very weak which makes the quarks and gluons move almost freely. This phenomenon is known as asymptotic freedom and the physics can be dealt with in perturbation theory. However, in the low energy region smaller than Λ_{QCD}, the constant becomes so strong that the quarks and gluon are bound into hadrons, which is known as confinement. The perturbative theory is no longer valid.

The EFTs can be constructed according to the fact that

$$m_u, m_d, m_s \ll \Lambda_{QCD} \ll m_c, m_b. \tag{2.9}$$

The top quark is even much heavier than Λ_{QCD}, while it decays too quickly to form any bound state and therefore not suitable to be included in the EFT at low energy region. From the above equation, we know that $m_{u,d,s}/\Lambda_{QCD} \ll 1$ and get the Chiral Perturbation Theory (ChPT) for light sector, while $\Lambda_{QCD}/m_{c,b} \ll 1$ and get the Heavy Quark Effective Theory (HQEFT) for heavy sector. Since the mass of strange quark is not very small compared to Λ_{QCD}, the high order contributions would be more important when expanding the quantities of interest in m_s.

2.2.1 Chiral perturbation theory for light pseudoscalar meson

Chiral perturbation theory (ChPT) is the EFT of the QCD in the low energy region. It describes the interactions among the light pseudoscalar mesons in the manner of a low momentum expansion in momenta and meson masses. It is based on the spontaneous breaking of the approximate chiral symmetry of QCD and Weinberg's theorem [37]. The next-to-leading order (NLO) was constructed by Gasser and Leutwyler in the 1980s [38, 39]. Here we will give a brief introduction following the discussion in Ref. [40–42].

Let us first consider the part with only three light quarks in the QCD Lagrangian in Eq. (2.8)

$$\mathcal{L}_{light} = \bar{q}\left(i\not{D} - m_q\right)q, \tag{2.10}$$

where $q = (u, d, s)$ are the light quark fields. With the right- and left-handed projectors $P_{R/L} = (1 \pm \gamma_5)/2$, we have the right- and left-handed fields $q_R = P_R q, q_L = P_L q$ and the relation

$$\bar{q}\gamma^\mu q = \bar{q}_R\gamma^\mu q_R + \bar{q}_L\gamma^\mu q_L, \quad \bar{q}m_q q = \bar{q}_R m_q q_L + \bar{q}_L m_q q_R. \tag{2.11}$$

With this, we can write the Lagrangian as

$$\mathcal{L}_{light} = \bar{q}_R i\not{D} q_R + \bar{q}_L i\not{D} q_L - \bar{q}_R \mathcal{M} q_L - \bar{q}_L \mathcal{M} q_R, \tag{2.12}$$

where $\mathcal{M}$ is the light quark mass matrix, $\mathcal{M} = \mathrm{diag}(m_u, m_d, m_s)$. If we ignore the quark mass term above, the right- and left-handed fields decouple and the Lagrangian is symmetric under the chiral transformation $SU(3)_L \times SU(3)_R$

$$q_R \to q'_R R q_R, \quad q_L \to q'_L = L q_L \tag{2.13}$$

wiht $R \in SU(3)_R$ and $L \in SU(3)_L$. The quark mass term in the Lagrangian leads to an explicit symmetry breaking. On the other hand, due to the nonvanishing scalar singlet quark condensate the chiral symmetry $SU(3)_L \times SU(3)_R$ is spontaneously broken to its diagonal subgroup $SU(3)_V$. As a result, the massless Goldstone bosons appear as new degrees of freedom. The eight Goldstone bosons are the light pseudoscalars (π, K and η).

The eight Goldstone bosons can be parametrized in a unitary 3×3 matrix and it transforms under $SU(3)_L \times SU(3)_R$ as

$$U \to U' = RUL^\dagger. \tag{2.14}$$

A popular choice for U is

$$U = \exp\left(\frac{i\phi_a\lambda_a}{F_0}\right), \tag{2.15}$$

where F_0 is constant here, and it is referred to as the pion-decay constant in the chiral limit. Its value can be obtained from the weak decay of the pion $\pi^+ \to \mu^+\nu_\mu$, and λ_a are the Gell-Mann matrices. We can use a matrix ϕ to parametrize the physical octet Goldstone bosons in terms of the Cartesian components ϕ_a, it reads

$$\phi = \sum_{a=1}^{8} \phi_a\lambda_a \equiv \sqrt{2}\begin{pmatrix} \frac{1}{\sqrt{2}}\pi^0 + \frac{1}{\sqrt{6}}\eta & \pi^+ & K^+ \\ \pi^- & -\frac{1}{\sqrt{2}}\pi^0 + \frac{1}{\sqrt{6}}\eta & K^0 \\ K^- & \bar{K}^0 & -\frac{2}{\sqrt{6}}\eta \end{pmatrix}. \tag{2.16}$$

Then we are ready to construct to effective Lagrangian order by order in the momentum expansion with the use of U. According to the counting scheme of chiral perturbation theory, the elements count as

$$U = O(q^0), \quad \partial_\mu U = O(q). \tag{2.17}$$

We know that the momentum is due to the derivative of the field. Only even numbers of derivatives are possible as required by the Lorentz invariance. Thus the the Lagrangian is expanded as $p^0/\Lambda_\chi^0 + p^2\Lambda_\chi^2 + p^4/\Lambda_\chi^4 + \ldots$ with $\Lambda_\chi = 4\pi F_0 = O(1\,\text{GeV})$ the chiral symmetry breaking scale, that is

$$\mathcal{L}_{eff} = \mathcal{L}^{(0)} + \mathcal{L}^{(2)} + \mathcal{L}^{(4)} + \ldots. \tag{2.18}$$

The first term $\mathcal{L}^{(0)}$ is proportional to $\text{Tr}[UU^\dagger] = 3$. We should omit it because it is irrelevant for the dynamics of the Goldstone bosons. Then the leading order effective Lagrangian reads

$$\mathcal{L}^{(2)} = \frac{F_0^2}{4}\text{Tr}[\partial_\mu U(\partial^\mu U)^\dagger]. \tag{2.19}$$

Due to the finite quark masses, we need to incorporate the explicit chiral symmetry breaking by adding the quark mass term in the effective Lagrangian. If we use the trick to assume that the mass matrix of the light quarks transform as

$$\mathcal{M} \to \mathcal{M}' = R\mathcal{M}L^\dagger. \tag{2.20}$$

Then one can construct the terms which is invariant under Eqs. (2.14) and (2.20). At lowest order in $\mathcal{M}$, we have

$$\mathcal{L}_{\chi SB} = \frac{F_0^2 B_0}{2}\text{Tr}[\mathcal{M}U^\dagger + U\mathcal{M}^\dagger], \tag{2.21}$$

where B_0 is related to the scalar singlet quark condensate. Expanding the Lagrangian, one gets

$$\begin{aligned}\mathcal{L}_{\chi SB} &= -\frac{B_0}{2}\mathrm{Tr}[\phi^2\mathcal{M}] + \text{higher orders of } \phi \\ &= -\frac{B_0}{2}\Big(2(m_u+m_d)\pi^+\pi^- + 2(m_u+m_s)K^+K^- + 2(m_d+m_s)K^0\bar{K}^0 + (m_u+m_d)\pi^0\pi^0 \\ &\quad + \frac{2}{\sqrt{3}}(m_u-m_d)\pi^0\eta + \frac{m_u+m_d+4m_s}{3}\eta^2\Big). \end{aligned} \tag{2.22}$$

Then we can obtain the masses of the Goldstone bosons in terms of the quark masses

$$\begin{aligned} M_\pi^2 &= B_0(m_u+m_d), \\ M_{K^0}^2 &= B_0(m_d+m_s), \\ M_{K^\pm}^2 &= B_0(m_u+m_s). \end{aligned} \tag{2.23}$$

The matrix for $\pi^0-\eta$ mixing is

$$M_{\pi^0\eta} = \begin{pmatrix} B_0(m_u+m_d) & B_0\frac{m_u-m_d}{\sqrt{3}} \\ B_0\frac{m_u-m_d}{\sqrt{3}} & B_0\frac{m_u+m_d+4m_s}{3} \end{pmatrix}, \tag{2.24}$$

where the off-diagonal terms describing the $\pi^0-\eta$ mixing at LO vanishes in the isospin-symmetric limit $m_u = m_d$. In order to get the masses of π^0 and η, one needs diagonalize the above matrix.

On the other hand, from Eq. (2.24) we know that the quark mass is counted as $O(p^2)$, and so is chiral symmetry breaking Lagrangian $\mathcal{L}_{\chi SB}$. In total, the effective Lagrangian at the lowest order $O(p^2)$ reads

$$\mathcal{L}_{eff} = \frac{F_0^2}{4}\mathrm{Tr}[\partial_\mu U(\partial^\mu U)^\dagger] + \frac{F_0^2 B_0}{2}\mathrm{Tr}[\mathcal{M}U^\dagger + U\mathcal{M}^\dagger]. \tag{2.25}$$

2.2.2 Chiral perturbation theory for heavy-light meson

As we already know, ChPT is constructed to describe the interaction involving light pseudoscalar mesons. When the heavy mesons are also involved, in other words if we want to describe the low-energy interaction between heavy mesons with the light pseudoscalar mesons, we need combine the heavy quark symmetry together with the chiral $SU(3)_L \times SU(3)_R$ symmetry [43, 44]. The heavy meson chiral perturbation theory (HMChPT) focuses on such a purpose.

2.2.2.1 Heavy quark effective theory

Let us first give a brief introduction to the heavy quark effective theory (HQET). For more details, we refer to the review in Ref. [45] and the textbook by Manohar and Wise [46].

In the light quark limit $m_{u,d,s} \to 0$, the dynamics of the QCD respects the chiral symmetry. On the other side, it exhibits the heavy quark flavor and spin symmetry in the heavy quark limit $m_{c,b} \to \infty$. The top quark is not included as it decay too fast to form any bound state. The relevant part in the QCD Lagrangian for the heavy quark reads

$$\mathcal{L}_Q = \bar{Q}\,(i\not{D} - m_Q)\,Q, \tag{2.26}$$

where Q is the field for the heavy quarks c and b.

Due to the fact that the heavy quark in a heavy-light hadron moves almost with the same speed as the hadron and is almost on shell, we can decompose its the momentum as

$$p_Q^\mu = m_Q v^\mu + k^\mu, \tag{2.27}$$

where v is the four-velocity of the heavy hadron normalized to $v^2 = 1$ and k is the so-called residual momentum. In a heavy hadron the light degree of freedom can have momenta k^μ of the order $O(\Lambda_{QCD})$, that is to say $k^\mu \ll m_Q$. The propagator of the heavy quark in QCD reads

$$\frac{i}{\not{p}_Q - m_Q} = i\frac{1+\not{v}}{2v\cdot k} + O\left(\frac{k}{m_Q}\right). \tag{2.28}$$

We can use the projection operators $P_\pm = (1 \pm \not{v})/2$ to project out the large- and small-component fields, h_v and H_v. By defining $h_v(x) = e^{im_Q v\cdot x} P_+ Q(x)$ and $H_v(x) = e^{im_Q v\cdot x} P_- Q(x)$, we can decompose the heavy quark field as

$$Q(x) = e^{-im_Q v\cdot x}[h_v(x) + H_v(x)]. \tag{2.29}$$

In the rest frame $v^\mu = (1,0,0,0)$, h_v and H_v correspond to the annihilation of a heavy quark and creation of a heavy antiquark, respectively. Then the heavy quark part of QCD Lagrangian in terms of the new fields reads

$$\mathcal{L}_Q = \bar{h}_v iv\cdot D\, h_v - \bar{H}_v(iv\cdot D + 2m_Q)H_v + \bar{h}_v i\not{D}_\perp H_v + \bar{H}_v i\not{D}_\perp h_v, \tag{2.30}$$

where $D_\perp^\mu = D^\mu - v^\mu v\cdot D$ is orthogonal to the heavy quark velocity. Using the equation of motion, we have $H_v = i\not{D}_\perp h_v/(2m_Q + iv\cdot D)$. The Lagrangian can be written as

$$\begin{aligned}\mathcal{L}_Q &= \bar{h}_v iv\cdot D\, h_v + \frac{1}{2m_Q}\sum_{n=0}^{\infty}\bar{h}_v i\not{D}_\perp\left(-\frac{iv\cdot D}{2m_Q}\right)^n i\not{D}_\perp h_v \\ &= \bar{h}_v iv\cdot D\, h_v + \frac{1}{2m_Q}\bar{h}_v(iD_\perp)^2 h_v + \frac{g_s}{4m_Q}\bar{h}_v\sigma_{\mu\nu}G^{\mu\nu}h_v + O\left(\frac{1}{m_Q^2}\right).\end{aligned} \tag{2.31}$$

In the heavy quark limit $m_Q \to \infty$, only the first term survives and we get the HQET Lagrangian

$$\mathcal{L}_{HQET} = \bar{h}_v iv\cdot D\, h_v, \tag{2.32}$$

which is spin and flavor independent. Thus we have heavy quark spin and flavor symmetry. From the above Lagrangian we can get the Feynman rule for the heavy quark propagator which is consistent with Eq. (2.28) if one notices that h_v contains the projector P_+.

One important consequence of the heavy quark symmetry is that the pseudoscalar D (B) mesons and the vector D^* (B^*) mesons form a $SU(2)_S$ spin multiplet, the symmetry breaking effect is at the order of Λ_{QCD}/m_Q. And the interaction involving the charmed and bottom meson are the same, thus we also have the $SU(2)_F$ flavor symmetry with the symmetry breaking effect at the order of $1/m_c - 1/m_b$.

On the other hand, as Eq. (2.31) shows, the third term which corresponds to the chromomagnetic coupling of the heavy quark spin to the gluon vanishes in the heavy quark limit. That means the spin of the heavy quark s_Q and the total angular momentum of light degrees of freedom s_ℓ are decoupled. We know that their sum $\vec{J} = \vec{s}_Q + \vec{s}_\ell$ is conserved, and in the heavy quark limit they are also conserved separately.

As a result of the heavy quark symmetry, the wave function of a heavy-light meson $Q\bar{q}$ must be independent of the flavor and spin of its heavy quark Q. Therefore the wave function can be characterized by the total angular momentum of the light degrees of freedom s_l. And we can use the value of s_l to classify the heavy-light meson and collect them in doublets with total spin $J = s_\ell \pm \frac{1}{2}$. For example, when the orbital angular momentum of the light degrees of freedom $l = 0$, the state $s_\ell^P = \frac{1}{2}^-$ with parity $P = (-1)^{l+1}$ corresponds to the spin symmetry doublet of pseudoscalar meson P and the vector meson P^*. The spin doublet (P, P^*) with negative parity can be represented by a 4×4 matrix H, which denotes the effective field for heavy-light mesons

$$H = \frac{1+\not{v}}{2}[P^*_\mu \gamma^\mu - \gamma_5 P], \tag{2.33}$$

and its hermitian conjugate multiplet is

$$\begin{aligned} \bar{H} &= \gamma_0 H^\dagger \gamma_0 \\ &= [P^{*\dagger}_\mu \gamma^\mu + \gamma_5 P^\dagger] \frac{1+\not{v}}{2}, \end{aligned} \tag{2.34}$$

where the factors $\sqrt{M_P}$ and $\sqrt{M_{P^*}}$ have been absorbed into the definition of the heavy fields $P(v)$ and $P^*(v, \epsilon)$ as will be shown later. The field H satisfy the constraints $\not{v}H = -H\not{v} = H$.

2.2.2.2 Heavy meson chiral perturbation theory

Here we follow the discussions in Refs. [47, 48] to introduce the effective Lagrangian describing the interaction between heavy mesons and light pseudoscalar mesons which we will use later. As a heavy-light meson contains a heavy quark Q and a light antiquark $\bar{q}$, we can construct the fields for the mesons according to their quantum numbers

$$P(v) = \bar{q}\gamma_5 h_v \sqrt{M_p}, \tag{2.35}$$

$$P^*(v, \epsilon) = \bar{q}\not{\epsilon} h_v \sqrt{M^*_p}, \tag{2.36}$$

where M_p and M^*_p are the masses of the pseudoscalar 0^- and vector 1^-, meson, respectively. ϵ is the polarization of the vector meson and v is the four-velocity. Here the small-component fields H_v in Eq. (2.29) is ignored.

In order to describe the coupling of Goldstone bosons to the heavy hadrons, it is convenient to introduce a new matrix, the coset field ξ. It is the key ingredient in the theory of non-linear realization of chiral symmetry [49, 50]. In this theory, the field ξ is simply related to the Goldstone bosons as

$$\xi = U^{1/2}, \tag{2.37}$$

where U is the exponential represented unitary matrix in terms of the physical octet Goldstone bosons defined in Eq. (2.29). ξ transforms under chiral $SU(3)_L \times SU(3)_R$ transformations as

$$\xi \to L\xi h^\dagger = h\xi R^\dagger, \tag{2.38}$$

where h is the unitary matrix belongs to the $SU(3)_V$ unbroken subgroup, and depends on L and R. With

ξ, one can construct a vector field V_μ and an axial vector field A_μ

$$V_\mu = \frac{1}{2}(\xi^\dagger\partial_\mu\xi + \xi\partial_\mu\xi^\dagger), \tag{2.39}$$
$$A_\mu = \frac{i}{2}(\xi^\dagger\partial_\mu\xi - \xi\partial_\mu\xi^\dagger).$$

In the chiral transformation, the vector field acts like a gauge field, while the axial vector field is just an $SU(3)$ octet. They transform as

$$V_\mu \to hV_\mu h^\dagger + h\partial_\mu h^\dagger, \quad A_\mu \to hA_\mu h^\dagger. \tag{2.40}$$

For the heavy-light mesons, they have the transformation rule

$$P \to Ph^\dagger, \quad P^* \to P^* h^\dagger. \tag{2.41}$$

Then the guage-covariant derivative can be constructed in terms of the vector field V_μ as

$$\begin{aligned} D_\mu P^\dagger &= (\partial_\mu + V_\mu)\, P^\dagger, \\ D_\mu P &= \partial_\mu\, P + P\, V^*_\mu. \end{aligned} \tag{2.42}$$

The Lagrangian for the strong interaction between the heavy mesons with the Goldstone bosons has to satisfy Lorentz invariance as well as the C, P, T invariance. Furthermore, we require the chiral invariance. The leading order Lagrangian with only one single derivative can be constructed as

$$\begin{aligned} \mathcal{L} &= \mathcal{D}_\mu P \mathcal{D}^\mu P^\dagger - M_P^2 P P^\dagger + f_Q(P A^\mu P^{*\dagger}_\mu + P^*_\mu A^\mu P^\dagger) - \frac{1}{2}P^{*\mu\nu}P^{*\dagger}_{\mu\nu} + M^2_{P^*}P^{*\mu}P^{*\dagger}_\mu \\ &\quad + \frac{1}{2}g_Q\epsilon_{\mu\nu\lambda\kappa}(P^{*\mu\nu}A^\lambda P^{*\kappa\dagger} + P^{*\kappa}A^\lambda P^{*\mu\nu\dagger}), \end{aligned} \tag{2.43}$$

where

$$\begin{aligned} P^{*\dagger}_{\mu\nu} &= D_\mu P^{*\dagger}_\nu - D_\nu P^{*\dagger}_\mu, \\ P^*_{\mu\nu} &= P^{*\dagger}_\nu(\overleftarrow{\partial}_\mu + V^*_\mu) - P^{*\dagger}_\mu(\overleftarrow{\partial}_\nu + V^*_\nu). \end{aligned} \tag{2.44}$$

There are two coupling constants f_Q and g_Q in the Lagrangian. In addition to the chiral invariance, we also require the heavy quark symmetry at the leading order in the $1/M_{P,P^*}$ expansion. Once we apply the heavy quark spin symmetry, the two constants are related as

$$g_Q = \frac{f_Q}{2\sqrt{M_P M_{P^*}}}. \tag{2.45}$$

And the heavy quark flavor symmetry will relate them to the masses of heavy mesons.

2.2.3 Nonrelativistic effective field theory

For the purpose of studying the charmed meson loops in the decays $\psi' \to J/\psi\pi^0(\eta)$, a nonrelativistic effective field theory (NREFT) is constructed in Ref. [51]. The interaction between quarkonia with heavy-light mesons can be treated nonrelativistically due to the fact that the quarkonia are close to the thresholds of corresponding mesons.

2.2.3.1 Framework

In the nonrelativistic limit, it is convenient use the effective fields to study the phenomenology of the heavy mesons and quarkonia belonging to doublets or multiplets, and the effective fields will be shown below. For heavy mesons as well as quarkonia, we choose to use the two-component notation introduced in Ref. [52]. The notation employs 2×2 matrix fields, and can be simplified by using the nonrelativistic approximation. Here we will give a brief discussion on the effective fields for the heavy-light meson and quarkonium separately.

Heavy-light meson

As discussed in Section 2.2.2, the heavy-light $Q\bar{q}$ mesons can be classified according to the total angular momentum of the light degree of freedom s_ℓ which is half-integral and collected in doublets with total spin $J = s_\ell \pm \frac{1}{2}$ and parity $P = (-1)^{l+1}$, where again l is the orbital angular momentum of the light degree of freedom . The total angular momentum of the light degrees of freedom satisfies $\vec{s}_\ell = \vec{l} + \vec{s}_q$, where s_q is the light antiquark spin.

For $l = 0$, we have only $s_\ell^P = \frac{1}{2}^-$, which corresponds to the doublet containing the lowest lying heavy mesons (P, P^*) with quantum number $(0^-, 1^-)$, and denote it as H. For $l = 1$, we have either $s_\ell^P = \frac{1}{2}^+$ or $s_\ell^P = \frac{3}{2}^+$, corresponding to two doublet containing the heavy mesons (P_0^*, P_1') with quantum number $(0^+, 1^+)$ and (P_1, P_2) with quantum number $(1^+, 2^+)$,respectively, and denote them as S and T, respectively. For $l = 2$, we have either $s_\ell^P = \frac{3}{2}^-$ or $s_\ell^P = \frac{5}{2}^-$, corresponding to two doublet containing the heavy mesons (P_1^*, P_2^*) with quantum number $(1^-, 2^-)$ and $(P_2^{*\prime}, P_3)$ with quantum number $(2^-, 3^-)$, respectively, and denote them as X and X', respectively.

Here we will give the explicit expressions for the effective fields H, S, T and X. The general form for the effective fields has been derived in Refs. [53, 54], it is a traceless and symmetric Lorentz tensor

$$H_a^{\mu_1 \cdots \mu_k}, \quad k = s_\ell - \frac{1}{2}. \tag{2.46}$$

The tensor satisfies $v_{\mu_1} H_a^{\mu_1 \cdots \mu_k} = \gamma_{\mu_1} H_a^{\mu_1 \cdots \mu_k} = 0$ and $a = u, d, s$ is the flavor label for the light quarks. It transforms under the Lorentz transformations as

$$H_a^{\mu_1 \cdots \mu_k} \to D(\Lambda) \Lambda_{\nu_1}^{\mu_1} \cdots \Lambda_{\nu_k}^{\mu_k} H_a^{\mu_1 \cdots \mu_k} D^\dagger(\Lambda), \tag{2.47}$$

where $D(\Lambda)$ is an element of the 4×4 matrix representation of the Lorentz group. For light degrees of freedom with parity $(-1)^{s_\ell - 1/2}$, we have the doublet of states $P^*_{s_\ell + 1/2}$ and $P_{s_\ell - 1/2}$,

$$\begin{aligned} H_a^{\mu_1 \cdots \mu_k} &= \frac{1 + \not{v}}{2} \Bigg\{ (P^*_{s_l + 1/2})_a^{\mu_1 \ldots \mu_{k+1}} \gamma_{\mu_{k+1}} - \sqrt{\frac{2k+1}{k+1}} \gamma_5 (P_{s_l - 1/2})_a^{\nu_1 \ldots \nu_k} \\ &\quad \Big[g_{\nu_1}^{\mu_1} \ldots g_{\nu_k}^{\mu_k} - \frac{1}{2k+1} \gamma_{\nu_1} (\gamma^{\mu_1} - v^{\mu_1}) g_{\nu_2}^{\mu_2} \ldots g_{\nu_k}^{\mu_k} - \cdots \\ &\quad - \frac{1}{2k+1} g_{\nu_1}^{\mu_1} \ldots g_{\nu_{k-1}}^{\mu_{k-1}} \gamma_{\nu_k} (\gamma^{\mu_k} - v^{\mu_k}) \Big] \Bigg\}, \end{aligned} \tag{2.48}$$

while for parity $(-1)^{s_\ell+1/2}$, we have $P_{s_\ell+1/2}$ and $P^*_{s_\ell-1/2}$,

$$\begin{aligned} H_a^{\mu_1\cdots\mu_k} &= \frac{1+\not{v}}{2}\Big\{(P_{s_l+1/2})_a^{\mu_1\ldots\mu_{k+1}}\gamma_5\gamma_{\mu_{k+1}} - \sqrt{\frac{2k+1}{k+1}}(P^*_{s_l-1/2})_a^{\nu_1\ldots\nu_k} \\ &\quad \Big[g^{\mu_1}_{\nu_1}\ldots g^{\mu_k}_{\nu_k} - \frac{1}{2k+1}\gamma_{\nu_1}(\gamma^{\mu_1}+v^{\mu_1})g^{\mu_2}_{\nu_2}\ldots g^{\mu_k}_{\nu_k} - \cdots \\ &\quad -\frac{1}{2k+1}g^{\mu_1}_{\nu_1}\ldots g^{\mu_{k-1}}_{\nu_{k-1}}\gamma_{\nu_k}(\gamma^{\mu_k}+v^{\mu_k})\Big]\Big\}, \end{aligned} \tag{2.49}$$

where the phase difference between the P and P^* terms is arbitrary.

The quark and antiquark have opposite parity, so do the light degree of freedom and meson. Therefore $s_\ell^P = \frac{1}{2}^-$ and $s_\ell^P = \frac{3}{2}^+$ doublets correspond to the case in Eq. (2.48), while $s_\ell^P = \frac{1}{2}^+$ and $s_\ell^P = \frac{3}{2}^-$ doublets correspond to the case in Eq. (2.49). Then

$$\begin{aligned} H_a &= \frac{1+\not{v}}{2}[P^*_{a\mu}\gamma^\mu - P_a\gamma_5] \\ S_a &= \frac{1+\not{v}}{2}[P'^\mu_{1a}\gamma^\mu\gamma_5 - P^*_{0a}], \\ T_a^\mu &= \frac{1+\not{v}}{2}\left[P^{\mu\nu}_{2a}\gamma_\nu - \sqrt{\frac{3}{2}}P^\nu_{1a}\gamma_5\Big(g^\mu_\nu - \frac{1}{3}\gamma_\nu(\gamma^\mu - v^\mu)\Big)\right], \\ X_a^\mu &= \frac{1+\not{v}}{2}\left[P^{*\mu\nu}_{2a}\gamma_5\gamma_\nu - \sqrt{\frac{3}{2}}P'^{*\nu}_{1a}\Big(g^\mu_\nu - \frac{1}{3}\gamma_\nu(\gamma^\mu + v^\mu)\Big)\right]. \end{aligned} \tag{2.50}$$

With the Dirac representation of the gamma matrices

$$\gamma^0 = \begin{pmatrix} \mathbb{1} & 0 \\ 0 & -\mathbb{1} \end{pmatrix},\ \gamma^i = \begin{pmatrix} 0 & \sigma^i \\ -\sigma^i & 0 \end{pmatrix},\ \gamma^5 = \begin{pmatrix} 0 & \mathbb{1} \\ \mathbb{1} & 0 \end{pmatrix}, \tag{2.51}$$

where the σ_i are the Pauli matrices. In the rest-frame of the heavy-light meson, the velocity is given by $v = (1,0,0,0)$, and then the effective fields can be simplified. Let us take H_a and T_a^μ as examples. For the $s_\ell^P = \frac{1}{2}^-$ doublet, one easily get

$$H_a = \begin{pmatrix} P_a^{*0} & -\vec{\sigma}\cdot\vec{P}^*_a - P_a \\ 0 & 0 \end{pmatrix} \approx \begin{pmatrix} 0 & -\vec{\sigma}\cdot\vec{P}^*_a - P_a \\ 0 & 0 \end{pmatrix}, \tag{2.52}$$

where the time-like component of the heavy meson field can be neglected because it is suppressed by a factor of $\vec{p}/m$ which tends to zero in the nonrelativistic limit. $\vec{p}$ and m are the momentum and mass of the heavy meson, respectively. For $s_\ell^P = \frac{3}{2}^+$ doublet, we have

$$\begin{aligned} T_a^\mu &\approx \begin{pmatrix} 0 & -P^{\mu j}_{2a}\sigma^j - \sqrt{\frac{3}{2}}\,P^\mu_{1a} + \sqrt{\frac{1}{6}}\,\vec{P}_{1a}\cdot\vec{\sigma}\sigma^j\delta^{\mu j} \\ 0 & 0 \end{pmatrix} \\ &\approx \begin{pmatrix} 0 & -P^{ij}_{2a}\sigma^j - \sqrt{\frac{2}{3}}\,P^i_{1a} - i\sqrt{\frac{1}{6}}\,\epsilon_{ijk}P^j_{1a}\sigma^k \\ 0 & 0 \end{pmatrix}. \end{aligned} \tag{2.53}$$

Parity	Charge conjugation
$H_a \to -H_a$	$H_a \to \sigma_2 \bar{H}_a^T \sigma_2$
$\bar{H}_a \to -\bar{H}_a$	$\bar{H}_a \to \sigma_2 H_a^T \sigma_2$
$T_a^i \to T_a^i$	$T_a^i \to \sigma_2 \bar{T}_a^{iT} \sigma_2$
$\bar{T}_a^i \to \bar{T}_a^i$	$\bar{T}_a^i \to \sigma_2 T_a^{iT} \sigma_2$

Table 2.2: Properties of the superfields under parity and charge conjugation transformations.

Therefore, we can define the fields for the heavy meson states in two component representation. They are

$$H_a = \vec{P}_a^* \cdot \vec{\sigma} + P_a \tag{2.54}$$

$$T_a^i = P_{2a}^{ij} \sigma^j + \sqrt{\frac{2}{3}} P_{1a}^i + i \sqrt{\frac{1}{6}} \epsilon_{ijk} P_{1a}^j \sigma^k, \tag{2.55}$$

for $s_\ell^P = \frac{1}{2}^-$ (S-wave) where $s_\ell^P = \frac{3}{2}^+$ (P-wave) heavy-light mesons, respectively. In the above equations, P_a and P_a^* annihilate the pseudoscalar and vector heavy mesons, respectively, and P_{1a} and P_{2a} annihilate the excited axial-vector and tensor heavy mesons, respectively.

As we know only the flavor neutral mesons are eigenstates of the charge parity, and the heavy-light mesons do not have definite charge parity. Therefore we have to clarify the phase convention of such mesons under charge conjugation. Here we use the same phase convention for charge conjugation specified in Ref. [8], they are

$$CPC^{-1} = \bar{P}, \;\; CP^*C^{-1} = \bar{P}^*, \;\; CP_1C^{-1} = \bar{P}_1, \;\; CP_2C^{-1} = \bar{P}_2. \tag{2.56}$$

Under these conventions, the fields for annihilating the $s_l^P = \frac{1}{2}^+$ heavy mesons containing a heavy antiquark is [55]

$$\bar{H}_a = \sigma_2 \left(\vec{P}_a^* \cdot \vec{\sigma}^T + \bar{P}_a \right) \sigma_2 = -\vec{P}_a^* \cdot \vec{\sigma} + \bar{P}_a. \tag{2.57}$$

For the $s_l^P = \frac{3}{2}^+$ heavy mesons, the corresponding field has the form

$$\bar{T}_a^i = -\bar{P}_{2a}^{ij} \sigma^j + \sqrt{\frac{2}{3}} \bar{P}_{1a}^i - i \sqrt{\frac{1}{6}} \epsilon_{ijk} \bar{P}_{1a}^j \sigma^k. \tag{2.58}$$

The transformation properties of the relevant doublets are shown in Tab. 2.2.

Heavy quarkonium

In the case of a heavy quarkonium, the flavour symmetry can not be applied so that the each multiplet describes states with a defined heavy flavour [56]. For a quarkonium ($Q\bar{Q}$ pair) with relative orbital angular momentum $L = 0$, the multiplet reads [48]

$$J = \frac{1 + \not{v}}{2} \left[H_1^\mu \gamma_\mu - H_0 \gamma_5 \right] \frac{1 - \not{v}}{2} \, . \tag{2.59}$$

Here, H denotes the quarkonium field. For $L \neq 0$, the multiplet has the generic expression

$$\begin{aligned} J^{\mu_1\ldots\mu_L} &= \frac{1+\not{v}}{2}\Bigg(H_{L+1}^{\mu_1\ldots\mu_L\alpha}\gamma_\alpha + \frac{1}{\sqrt{L(L+1)}}\sum_{i=1}^{L}\epsilon^{\mu_i\alpha\beta\gamma}v_\alpha\gamma_\beta H_{L\gamma}^{\mu_1\ldots\mu_{i-1}\mu_{i+1}\ldots\mu_L} \\ &+\frac{1}{L}\sqrt{\frac{2L-1}{2L+1}}\sum_{i=1}^{L}(\gamma^{\mu_i}-v^{\mu_i})H_{L-1}^{\mu_1\ldots\mu_{i-1}\mu_{i+1}\ldots\mu_L} \\ &-\frac{2}{L\sqrt{(2L-1)(2L+1)}}\sum_{i<j}(g^{\mu_i\mu_j}-v^{\mu_i}v^{\mu_j})\gamma_\alpha H_{L-1}^{\alpha\mu_1\ldots\mu_{i-1}\mu_{i+1}\ldots\mu_{j-1}\mu_{j+1}\ldots\mu_L} + K_L^{\mu_1\ldots\mu_L}\gamma_5\Bigg)\frac{1-\not{v}}{2}, \end{aligned} \tag{2.60}$$

where H_A, K_A are the effective fields of the multiplets with total spin $J = A$, and K_A is the spin singlet, H_A represent the spin triplet. From above formula, we can obtain

- $L = 1$ multiplet:

$$J^\mu = \frac{1+\not{v}}{2}\left\{H_2^{\mu\alpha}\gamma_\alpha + \frac{1}{\sqrt{2}}\epsilon^{\mu\alpha\beta\gamma}v_\alpha\gamma_\beta H_{1\gamma} + \frac{1}{\sqrt{3}}(\gamma^\mu - v^\mu)H_0 + K_1^\mu\gamma_5\right\}\frac{1-\not{v}}{2}\ ; \tag{2.61}$$

- $L = 2$ multiplet:

$$\begin{aligned} J^{\mu\nu} &= \frac{1+\not{v}}{2}\Bigg\{H_3^{\mu\nu\alpha}\gamma_\alpha + \frac{1}{\sqrt{6}}\left(\epsilon^{\mu\alpha\beta\gamma}v_\alpha\gamma_\beta H_{2\gamma}^\nu + \epsilon^{\nu\alpha\beta\gamma}v_\alpha\gamma_\beta H_{2\gamma}^\mu\right) + \frac{1}{2}\sqrt{\frac{3}{5}}\Big[(\gamma^\mu - v^\mu)H_1^\nu \\ &+(\gamma^\nu - v^\nu)H_1^\mu\Big] - \frac{1}{\sqrt{15}}(g^{\mu\nu}-v^\mu v^\nu)\gamma_\alpha H_1^\alpha + K_2^{\mu\nu}\gamma_5\Bigg\}\frac{1-\not{v}}{2}\ . \end{aligned} \tag{2.62}$$

It is convenient to write the corresponding multiplets through the above formulae in the nonrelativistic limit in the two-component notation. The S, P and D wave states are

$$J = \vec{H}_1\cdot\vec{\sigma} - H_0\ , \tag{2.63}$$

$$J^i = H_2^{ij}\sigma_j - \frac{1}{\sqrt{2}}\epsilon^{ijk}\sigma_j H_{1k} + \frac{1}{\sqrt{3}}H_0\sigma^i + K_1^i\ , \tag{2.64}$$

and

$$\begin{aligned} J^{ij} &= H_3^{ijk}\sigma_k - \frac{1}{\sqrt{6}}\left(\epsilon^{ilm}\sigma_l H_{2m}^j + \epsilon^{jlm}\sigma_l H_{2m}^i\right) + \frac{1}{2}\sqrt{\frac{3}{5}}\Big[H_1^j\sigma^i + H_1^i\sigma^j\Big] \\ &-\frac{1}{\sqrt{15}}\delta^{ij}\vec{H}_1\cdot\vec{\sigma} + K_2^{ij}\ , \end{aligned} \tag{2.65}$$

respectively.

The interaction of heavy mesons and quarkonia with other fields can be described by an effective Lagrangian in terms of above doublets and multiplets.

2.2.3.2 Power counting

In effective theories, an infinite number of terms in the Lagrangian and diagrams arise. The purpose of the power counting is to classify the importance of each one. In the NREFT, the intermediate heavy

mesons are nonrelativistic with velocity $v \ll 1$. The power counting scheme of NREFT is performed in terms of the velocity. The velocity is estimated as

$$\sqrt{\frac{|m_a + m_b - M|}{\bar{m}_{ab}}} \tag{2.66}$$

where m_a and m_b are the masses of heavy mesons, with $\bar{m}_{ab} = (m_a + m_b)/2$, and M is the mass of quarkonium. We have the following scaling rules:

- The three-momentum scales as v,
- The kinetic energy scales as v^2,
- The Feynman propagator, as in the nonrelativistic expansion, has the form

$$\frac{1}{l^2 - m + i\epsilon} \approx \frac{1}{2m(l^0 - \frac{\vec{l}^2}{2m} + i\epsilon)}, \tag{2.67}$$

  and thus it scales as v^{-2},
- The S-wave momentum independent coupling scales as v^0,
- The P-wave coupling scales as v.

If all the three vertices are S-wave, the amplitude scales as

$$\frac{v^5}{(v^2)^3} = \frac{1}{v}, \tag{2.68}$$

which is greatly enhanced if the velocity is small.

2.3 Dynamical generation of hadronic molecules

For a effective field theory containing the constituents of hadronic molecules as the degrees of freedom, the hadronic molecules appear as poles of the scattering amplitudes, which are so-called dynamically generated. The dynamical generation of a hadronic molecule from the effective field theory is a non-perturbative phenomenon. The hadronic molecule does not appear phenomenologically in the Lagrangian as a degree of freedom, but it can be obtained by using the interaction of the constituent particles.

The Lippmann-Schwinger equation reads

$$T = \frac{V}{1 - G \cdot V}, \tag{2.69}$$

where V is the tree-level interaction of the consistent particles and G is the two-point loop integral. It is the infinite sum of the scattering amplitude and allows the dynamical generation of poles, namely

$$1 - G \cdot V = 0. \tag{2.70}$$

There are three kinds of poles on the complex energy plane of scattering amplitude. They are bound state, virtual state and resonance. All the three poles are called hadronic molecule. Let us take a simple case as example, in which only one channel is considered:

- A bound states is associated with a pole below the threshold of two hadrons in the real axis on the first Riemann sheet of the complex energy plane. The three-momentum of the scattered hadron in the center of mass frame of the two hadrons satisfies

$$\mathrm{Im}\, p_{cm} > 0, \;\; \mathrm{Re}\, p_{cm} = 0. \tag{2.71}$$

- A virtual state is to be identified with a pole below the threshold of two hadrons in the real axis on the second Riemann sheet. The three-momentum satisfies

$$\mathrm{Im}\, p_{cm} < 0, \;\; \mathrm{Re}\, p_{cm} = 0. \tag{2.72}$$

- A resonance happens at a pole above the threshold of two hadrons below the real axis on the second Riemann sheet, namely

$$\mathrm{Im}\, p_{cm} < 0. \tag{2.73}$$

In the case of coupled channel, the situation is somewhat more complicated. For more detailed relations, we refer to Ref. [57].

Part I

Inclusive prompt production of S-wave loosely bound states

CHAPTER 3

Production of charm-strange hadronic molecules at the LHC

In this chapter, we will provide a theoretical exploration on the hadroproduction of the $D_{s0}^*(2317)$, $D_{s1}(2460)$ and $D_{sJ}(2860)$ at the large hadron collider (LHC). Besides, the predicted spin partner of the $D_{sJ}(2860)$, called $D_{s2}(2910)$ hereafter, is also investigated. Most of the calculations and discussions presented here are taken from our published paper in Ref. [58]. For the production of the exotic states, there have been some literatures devoted to such investigation at the hadron colliders, especailly under the hadronic molecule picture [14, 59–62].

The assumption used in our calculation is that the four charm-strange states are all S-wave hadron molecules which are the composite particles of a kaon and a nonstrange charmed meson. Based on this assumption, the charmed meson–kaon pairs will be produced first. And for the production of the pairs, we will make use of two Monte Carlo (MC) event generators, Herwig and Pythia, to do the simulation. After the production of the constituents, these D_{sJ} states will be formed through the final state interactions between them. The approach we used is similar to that used in Ref. [59, 60] for the study of the production of the $X(3872)$ and Ref [62] for other heavy quarkonium-like states. The difference is that the universal elastic scattering amplitude is used there to cope with the final state interaction, while we use the effective field theory (EFT) to get the scattering amplitude for the kaon and charmed meson. One may note that the effect of the rescattering of constituents is ignored in Ref. [14], and we will discuss this in more detail in Chapter 4. Finally, we are able to derive an estimate of the production rates for these particles at an order-of-magnitude accuracy. It presents a promising prospect to observe these states at the LHC based on the accumulated data according to the results we will show in the following. This calls for an experimental analysis.

This chapter is organised as follows. In Section 3.1, we first give an introduction about the four charm-strange states. Then an overview of the effective field theory description of the kaonic bound states will be presented in Section 3.2. Based on the MC event generators, we will derive the production rates of the molecular states in Section 3.3, while the numerical results are presented subsequently in Section 3.4. At last, we will summarize this chapter in Section 3.5.

3.1 Introduction

In the past years, many of the charm-strange mesons have been observed at varieties of experimental facilities. This kind of heavy-light mesons is particular and can provide a unique platform to study the heavy quark dynamics and non-perturbative QCD in the presence of a heavy quark. The discoveries

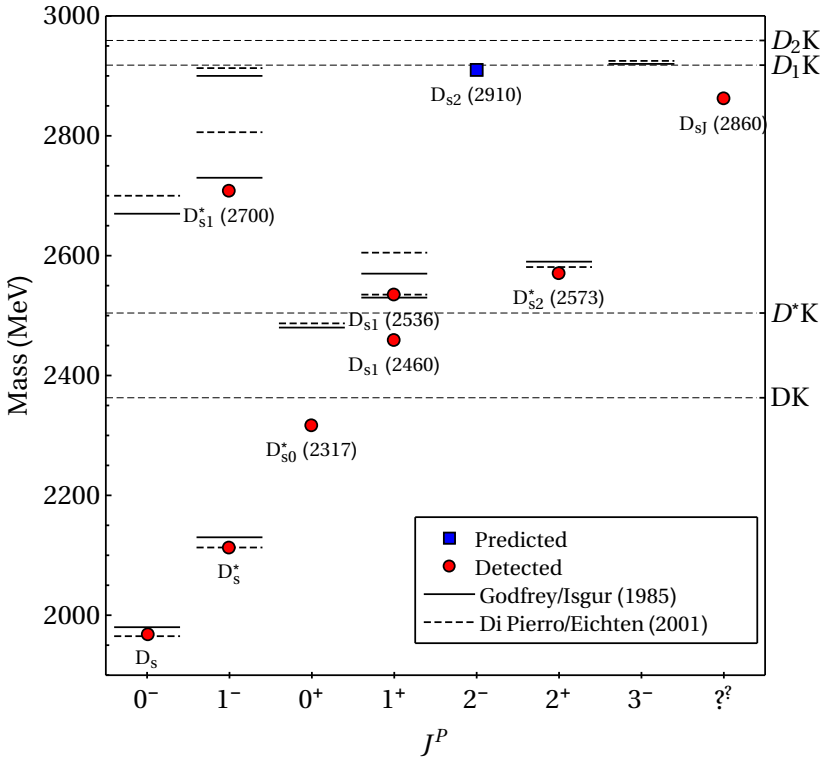

Figure 3.1: Spectroscopy of the charm-strange mesons, where the solid and dashed lines are for the values from the relativized Godfrey-Isgur (GI) model [32] and the Ref. [64], respectively. The circles are the observed particles and the squre is the $D_{s2}(2910)$ predicted in Ref. [65].

have not only enriched the particle zoo of the conventional $c\bar{s}$ family, but also have found unexpected candidates for exotic states beyond the conventional quark model for mesons. Among them, the $D^*_{s0}(2317)$ is the first one discovered by the Babar Collaboration in the inclusive $D_s\pi^0$ mass distribution in 2003 from e^+e^- annihilation data at energies near 10.6 GeV [3]. At the same year, the $D_{s1}(2460)$ was observed by the CLEO Collaboration in the $D^*_s\pi^0$ final state [4], followed by the discovery of the $D^*_{sJ}(2860)$ by the BABAR Collaboration in the DK channel [63].

We plot the spectrum of the charm-strange mesons in Fig. 3.1, where the lines are the results by the QCD motivated quark model: the solid and dashed ones are for the values from the relativized Godfrey-Isgur (GI) model [32] and the model uses the relativistic Dirac Hamiltonian and includes the $1/m_c$ order corrections [64], respectively. The circles are the observed particles and the square is the speculated $D_{s2}(2910)$. It is likely that the $D^*_{s0}(2317)$ and $D_{s1}(2460)$ are spin partners, because the mass difference between them is not large. A more important feature of the above mentioned two charm-strange mesons is that their masses are quite far below the potential model predictions for the lowest states with the same quantum numbers as we can see from the data. As the GI model is a typical quenched quark model, Ref.[66] takes the screening effect into account to modify it. However the masses of $D_{s1}(2460)$ and $D^*_{s0}(2317)$ are still far below the modified model. There exists various explanations for their nature. For instance, $D^*_{sJ}(2860)$ is regarded as the conventional $1^3D_3(c\bar{s})$ in Ref. [67], where the authors propose that the measurement of its spin can be used to verify the explanation. We refer to the reviews in Ref. [9,

	$D^*_{s0}(2317)$	$D_{s1}(2460)$	$D^*_{sJ}(2860)$
constituents	DK	D^*K	D_1K
mass	2317.8 ± 0.6	2459.6 ± 0.6	$2863.2^{+4.0}_{-2.6}$
relative energy (E_0)	-45.1 ± 0.4	-44.7 ± 0.4	$-54.8^{+2.5}_{-1.1}$

Table 3.1: Masses of the $D^*_{s0}(2317)$, $D_{s1}(2460)$ and $D_{sJ}(2860)$ taken from the Particle Data Group [77], and the relative energy E_0 of the exotic states to the corresponding meson-meson thresholds (in units of MeV).

10] for more details.

One particular interesting assumption for the underlying structure is that the $D^*_{s0}(2317)$ and $D_{s1}(2460)$ are hadronic molecules, i.e. the DK and D^*K bound states, respectively [68–72]. As the Tab. 3.1 shows, the mass splittings $M_{D_{s1}(2460)} - M_{D^*_{s0}(2317)} \simeq 142$ MeV and $M_{D^*} - M_D \simeq 143$ MeV are approximately equal. It is a natural consequence of heavy quark spin symmetry in the picture of hadronic molecules [73]. We can also resort to the parity doublet assumption [74–76] to explain the equality. The $D^*_{s0}(2317)$ and $D_{s1}(2460)$ are below the DK and D^*K thresholds, respectively. Moreover both have narrow widths, less than 3.8 MeV and 3.5 MeV, respectively [77]. The small widths of the two arise from the radiative decays and isospin-violating hadronic decay modes. Under different interpretations of the internal structure, these decay modes have been intensively explored. The isospin-violating decay can occur through the $\eta - \pi^0$ mixing [78]. While in the hadronic molecule picture, an additional mechanism for the decay exists due to D^*K meson loops and the direct coupling of the $D^{(*)}$ and $K^{(*)}$ mesons to π^0. The mass differences between the neutral and charged charmed meson and kaons would give rise to isospin-violating decay even dominate over the contribution from the $\eta - \pi^0$ mixing [79–82]. Therefore the isospin breaking decays can be used to distinguish the hadronic molecule picture from the others. It is necessary to measure the width of the order of 100 keV predicted in the hadronic molecule picture. At present, the experimental resolution is not high enough. Only the planned $\overline{\mathrm{P}}$ANDA experiment is expected to have the ability to perform such a measurement [83]. Nevertheless, the hadronic molecule picture is supported by some lattice QCD calculations of the charmed meson–light meson scattering lengths [84, 85].

The kaons can be regarded as pseudo-Goldstone bosons of the spontaneous breaking of chiral symmetry $SU(3)_L \times SU(3)_R \to SU(3)_V$. As a consequence of chiral symmetry, the leading order interaction between an narrow excited heavy meson and the kaon should be the same as that for the ground state charmed mesons when Born terms are neglected, which is a very good approximation for S-wave scattering [86]. The excited state must be narrow enough so that its width is small compared to the inverse of the range of forces between the heavy meson and the kaon. If not, a new large energy scale would be introduced, and we can not make the analogy to the ground state mesons any more. We can expect more kaonic bound states analogous to the $D^*_{s0}(2317)$ and $D_{s1}(2460)$ as the DK and D^*K bound states. Especially, the ratio of branching fractions $\mathcal{B}(D^*_{sJ}(2860) \to DK)/\mathcal{B}(D^*_{sJ}(2860) \to D^*K)$ is difficult to be accounted for in other models. But the interpretation as $D_1(2420)K$ bound state can explain the experimental data for the $D^*_{sJ}(2860)$ very well. Besides, a spin partner of the $D^*_{sJ}(2860)$, the $D_{s2}(2910)$ as a $D_2(2460)K$ bound state, was predicted to have a mass and a width around 2910 MeV and 10 MeV, respectively. This state is expected to have quantum numbers $J^P = 2^-$ and decays into the D^*K and $D^*_s\eta$.

Until now, most of the available studies of the exotic candidates from both experimental and theoretical sides in the charm-strange sector have been mainly focused on the spectrum and decays or the production through B meson decays in the e^+e^- collisions. The underlying structure of the D_{sJ} states is a longstanding problem that needs to be solved. For the purpose of revealing their nature, more data and processes involving these states would be equally important and urgent. For example, the processes include

heavy-ion collisions [87, 88] and the hadroproduction due to the large number of charm quarks that could be produced. At low energy regions, the forthcoming $\overline{\text{P}}$ANDA experiment is a promising facility to reach such a purpose. First it has a particular focus on the hadroproduction of $D^*_{s0}(2317)$ state [89], and secondly it is supposed to have the ability to measure the decay width of the $D^*_{s0}(2317)$ at the 100 keV level which is important as we discussed above. We note that in high collision energy regions at hadron colliders like the LHC, the charm quark will be abundantly produced via the QCD processes, which makes it an ideal platform for the study of these new exotic hadrons and in particular for searching for the predicted $D_{s2}(2910)$. Moreover, the LHCb Collaboration has already reported some measurements about the states in charm-strange sector, such as the decays of the $D^*_{s1}(2710)$, which is the first radially excited state of the D^*_s with $J^P = 1^-$, and the decay of $D_{sJ}(2860)$ into the $D^+K^0_S$ and D^0K^+ final states with small statistical uncertainties [90].

3.2 Dynamical generation of the kaonic bound states

For D_{sJ} states which can be dynamically generated from the interaction between charmed mesons and kaons in the isoscalar channel, the assumed molecular structures can be explicitly decomposed as

$$|D_{sJ}\rangle = -\frac{1}{\sqrt{2}}\left(\left|C^+K^0\right\rangle + \left|C^0K^+\right\rangle\right),$$

where C denotes the D, D^*, D_1 and D_2 charmed mesons. We use the isospin phase conventions

$$\begin{aligned}\left|C^+\right\rangle &= -\left|1/2, 1/2\right\rangle, \left|C^0\right\rangle = \left|1/2, -1/2\right\rangle,\\ \left|K^+\right\rangle &= \left|1/2, 1/2\right\rangle, \left|K^0\right\rangle = \left|1/2, -1/2\right\rangle,\end{aligned}$$

which corresponds to the convention for the d quark $\left|\bar{d}\right\rangle = -\left|1/2, 1/2\right\rangle$. The two numbers in $|\cdots, \cdots\rangle$ are the isospin I and its third component I_3. The scattering amplitude may differ in sign under different phase conventions, however, the final physical observables remain the same.

3.2.1 Scattering of the Goldstone bosons off the charmed mesons

As we can see that all the considered bound states contain the light pseudoscalar kaon, and it can be considered as a Goldstone boson of the spontaneous chiral symmetry breaking from $\text{SU}(3)_L\times\text{SU}(3)_R$ to $\text{SU}(3)_V$. As shown in Section 2.2.2, the interaction between the Goldstone bosons and the heavy mesons can be described by the heavy meson chiral perturbation theory (HMChPT) [43, 44, 47], which combines the chiral and heavy quark symmetries in the light and heavy quark sectors, respectively. More details about the HMChPT can be found there. It is shown that the contribution from exchanging heavy mesons is negligible [86], therefore we can only consider the leading order contact terms interaction between the Goldstone boson and heavy meson, which comes from the kinetic term of the Lagrangian in Eq. (2.43)

$$\mathcal{L}_{\text{kin}} = \mathcal{D}_\mu H \mathcal{D}^\mu H^\dagger, \tag{3.1}$$

where H denotes the heavy charmed meson field with the composition $(c\bar{u}, c\bar{d}, c\bar{s})$, i.e. (D^0, D^+, D_s) and the chiral gauge derivative is given by

$$\mathcal{D}_\mu = \partial_\mu + \frac{1}{2}\left(u^\dagger\partial_\mu u + u\,\partial_\mu u^\dagger\right), \tag{3.2}$$

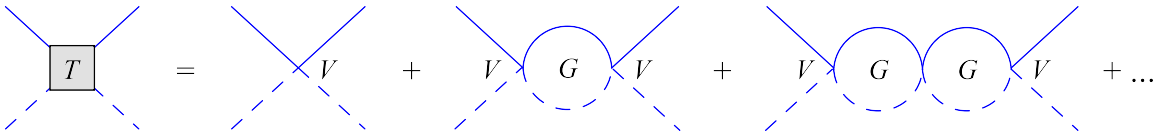

Figure 3.2: Sketch of the resummation of the amplitudes. Here, T denotes the total scattering amplitude, V is the leading order amplitude and G is the loop integral. The heavy meson H and kaon are represented by solid and dashed lines, respectively.

with $U = \exp\left(i\sqrt{2}\Phi/F\right)$ and $u = \sqrt{U}$. Here, Φ is the 3×3 matrix parametrizing the octet Goldstone bosons shown in Eq. (2.16), and F is the pion decay constant in the chiral limit. Since we will only consider the leading order interaction, $F = 92.2$ MeV will be used. The kinetic term in Eq. (2.43) can be written more explicitly as

$$\mathcal{L}_{\text{kin}} = \frac{1}{4F^2}((\partial^\mu H[\Phi, \partial_\mu\Phi]H^\dagger - H[\Phi, \partial_\mu\Phi]\partial^\mu H^\dagger). \tag{3.3}$$

It is shown in Ref. [71] that the kaon–charmed meson scattering with the isospin $I = 0$ is the most attractive one among all the channels for the light meson–heavy meson S-wave scattering. Hence we only consider the $I = 0$ case here. We can express the $\left|D^0K^+\right\rangle$ in terms of the isospin eigenstate as

$$\left|D^0K^+\right\rangle = \frac{1}{\sqrt{2}}\left|DK\right\rangle^{I=1} - \frac{1}{\sqrt{2}}\left|DK\right\rangle^{I=0}, \tag{3.4}$$

Thus the leading order scattering amplitude has the relation

$$\left\langle D^0K^+\right|\hat{V}\left|D^0K^+\right\rangle = \frac{1}{2}{}^{I=1}\left\langle DK\right|\hat{V}\left|DK\right\rangle^{I=1} + \frac{1}{2}{}^{I=0}\left\langle DK\right|\hat{V}\left|DK\right\rangle^{I=0}, \tag{3.5}$$

that is

$$V_{D^0K^+\to D^0K^+} = \frac{1}{2}V^{I=1}(s,t,u) + \frac{1}{2}V^{I=0}(s,t,u), \tag{3.6}$$

where s, t and u are the Mandelstam variables with the constraint $s + t + u = 2(m_H^2 + m_K^2)$ for the particles when they are on-shell, with m_H and m_K the mass of the charmed meson and kaon, respectively. One finds that $D^+K^+ \to D^+K^+$ is a purely $I = 1$ one,

$$V^{I=1}(s,t,u) = V_{D^+K^+\to D^+K^+}(s,t,u). \tag{3.7}$$

Eventually we have the relation from Eq. (3.6) and Eq. (3.7)

$$V^{I=0}(s,t,u) = 2V_{D^0K^+\to D^0K^+}(s,t,u) - V_{D^+K^+\to D^+K^+}(s,t,u). \tag{3.8}$$

From the Lagrangian, one can derive the leading order scattering amplitude. The tree level scattering amplitude of the process $HK \to HK$ in $I = 0$ reads

$$V(s,t,u) = -\frac{s-u}{2F^2}, \tag{3.9}$$

The Mandelstam variable u can be expressed in terms of the scattering angle θ between the incoming and

outgoing particles in the center-of-mass frame

$$-u(s,\cos\theta) = s - 2m_K^2 - \frac{1}{2s}(s+m_H^2-m_K^2)^2 + \frac{1}{2s}\lambda(s,m_H^2,m_K^2)\cos\theta. \tag{3.10}$$

where $\lambda(x,y,z) = x^2+y^2+z^2-2xy-2yz-2xz$ is the Källén function. More details about the kinematics of the two-body scattering are shown in the Appendix A. The scattering amplitude $V(s,t,u)$ can be decomposed by using the Legendre polynomials $P_L(\cos\theta)$ in terms of partical waves

$$V(s,t,u) = \sum_{L=0}^{\infty}(2L+1)P_L(\cos\theta)V_L(s) \tag{3.11}$$

where $V_L(s)$ are the partial wave amplitudes, and they can be projected out by using the orthogonality relation of the Legendre polynomials

$$V_L(s) = \frac{1}{2(\sqrt{2})^N}\int_{-1}^{1} P_L(\cos\theta)V(s,t(s,\cos\theta),u(s,\cos\theta))d\cos\theta$$

where $(\sqrt{2})^N$ is a factor due to the Bose symmetry. The parameter N depends on the number of times that identical particles appear in the partial wave amplitude. For instance, we have $N=2$ if both the initial and final states are identical, like $\pi\pi\to\pi\pi$; $N=1$ if the initial or final states are identical, like $\eta\eta\to K\bar{K}$; $N=0$ if both the initial and final states are not identical, like our case $DK\to DK$. The S-wave amplitude, i.e. $L=0$, can be projected out for on-shell particles

$$\begin{aligned} V_0(s) &= \frac{1}{2}\int_{-1}^{1} V(s,t(s,\cos\theta),u(s,\cos\theta))d\cos\theta \\ &= -\frac{2}{F^2}m_H E_K\left[1+O\left(\frac{k^2}{m_H^2}\right)\right], \end{aligned} \tag{3.12}$$

where $E_K = (s-m_H^2+m_K^2)/(2\sqrt{s})$ is the energy of the kaon, while k is the momentum in the center-of-mass frame. In the above equation, we have used the fact that the heavy meson is highly nonrelativistic in the energy region of interest.

We need to sum the scattering amplitudes up to infinite orders due to the strong interaction, and most importantly a perturbative expansion up to any finite order cannot account for the subthreshold states which appears as poles of the amplitude, for instance the $D_{s0}^*(2317)$. The summation shown in the Fig. 3.2 can be done by using the Bethe-Salpeter equation (BSE)

$$T(\boldsymbol{k}',\boldsymbol{k};s) = V(\boldsymbol{k}',\boldsymbol{k};s) + i\int\frac{d^4q}{(2\pi)^4}\frac{V(\boldsymbol{k}',\boldsymbol{q};s)\,T(\boldsymbol{q},\boldsymbol{k};s)}{(q^2-m_K^2+i\epsilon)[(p-q)^2-m_H^2+i\epsilon]}, \tag{3.13}$$

where $p^2=s$. Here the dependence of the amplitudes on the center-of-mass momenta both in the initial and final states are explicitly kept in the expression. The equation is an integral one and can be solved numerically. Here instead of solving the equation numerically, we will follow the approach developed by Ref. [91] and take the on-shell approximation, i.e. using the S-wave amplitude $V_0(s)$ as the kernel. The justification of this approximation can be found in Refs. [92, 93] by using dispersion relations or in Ref. [94] by taking the off-shell contribution into account. A critical discussion on the use of the on-shell approximation is given in Ref. [95]. Eventually, the integral equation can be simplified to an algebric

equation. The resummed S-wave scattering amplitude reads

$$T_0(s) = V_0(s)\,[1 - G(s)V_0(s)]^{-1}\,. \tag{3.14}$$

Notice that both here and in Eq. (3.9) we have neglected the polarizations of the charmed mesons with spin 1 or 2, which can be factorized out to be a overall factor of the resummed scattering amplitude. The justification is due to the fact that these charmed mesons are highly nonrelativistic in the energy region of interest. For more details we refer to Appendix B.

3.2.2 Loop function

In Eq. (3.14), $G(s)$ is the two-meson scalar loop function

$$G(s) \;=\; i\int \frac{d^4q}{(2\pi)^4}\frac{1}{q^2 - m_K^2 + i\epsilon}\frac{1}{(p-q)^2 - m_H^2 + i\epsilon}. \tag{3.15}$$

This integral is obviously divergent.

3.2.2.1 Relativistic formulation

The divergent integral can be regularized by adopting a three-momentum cutoff parameter [91]. Unfortunately, it give rise to an artificial singularity of the loop function which would have an impact when the momentum in the center-of-mass frame approaches the cutoff [96]. A feasible way is to use the once subtracted dispersion relation [92]

$$\begin{aligned} G(s) &= G(s_0) + \frac{s-s_0}{\pi}\int_{s_{th}}^{\infty} ds' \frac{\mathrm{Im}\,G(s')}{(s'-s)(s'-s_0)} \\ &= \frac{1}{16\pi^2}\Big\{a(\mu) + \log\frac{m_1^2}{\mu^2} + \frac{\Delta - s}{2s}\log\frac{m_1^2}{m_2^2} + \frac{\sigma}{2s}\big[\log(s-\Delta+\sigma) \\ &\quad + \log(s+\Delta+\sigma) - \log(-s+\Delta+\sigma) - \log(-s-\Delta+\sigma)\big]\Big\}, \end{aligned} \tag{3.16}$$

where $\mathrm{Im}\,G(s) = -\rho(s)\theta(s - s_{th})$ is the imaginary part of the loop function, with $\rho(s)$ the phase space factor, $a(\mu)$ is the subtraction constant related to $G(s_0)$, with μ the regularization scale which is related to subtraction point s_0 and $s_{th} = (m_1 + m_2)^2$ is the threshold square, and

$$\sigma = [-(s-(m_1+m_2)^2)(s-(m_1-m_2)^2)]^{1/2}, \quad \Delta = m_1^2 - m_2^2.$$

In Eq. (3.16), the regularization scale μ can have any arbitrary value since its change can always be absorbed into $a(\mu)$. The function $G(s)$ is symmetric under the exchange of the internal lines, i.e. $m_1 \leftrightarrow m_2$. Moreover the regularized loop function is only valid above the threshold, however, the value beyond the region can be obtained through analytical continuation.

J^P	State	Constituents	Thresholds	Predicted masses	Experimental data
0^+	$D^*_{s0}(2317)$	DK	2362.8	2317.8 (input)	2317.8 ± 0.6
1^+	$D_{s1}(2460)$	D^*K	2499.8	2455.4	2459.6 ± 0.6
1^-	$D^*_{sJ}(2860)$	D_1K	2917.9	2875.0	$2863.2^{+4.0}_{-2.6}$
2^-	$D_{s2}(2910)$	D_2K	2959.1	2916.3	?

Table 3.2: The predictions of the pole position of the kaonic bound states (in units of MeV).

3.2.2.2 Non-Relativistic formulation

According to the heavy quark effective theory, we can do the replacement to the heavy-light meson propagator in the heavy quark limit

$$\frac{1}{l^2 - m_H^2 + i\epsilon} \to \frac{1}{2m_H(v\cdot k - \Delta + i\epsilon)}, \tag{3.17}$$

where v is the velocity of the heavy meson, k the residue momentum with the relation $k^\mu = l^\mu - m_H v^\mu$ and Δ is the mass difference between pseudoscalar and vector heavy mesons which can be dropped here. Treating the heavy meson nonrelativistically, we get an analytic expression for the regularized loop function [86]

$$\begin{aligned} G_{NR}(s) &= i\int \frac{d^4q}{(2\pi)^4 2m_H}\frac{1}{(q^2 - m_K^2 + i\epsilon)(\sqrt{s} - q\cdot v - m_H + i\epsilon)} \\ &= \frac{1}{16\pi^2 m_H}\left\{E_K\left[a(\mu) + \log\left(\frac{m_K^2}{\mu^2}\right)\right] + 2p_{\rm cm}\cosh^{-1}\left(\frac{E_K}{m_K}\right) - i\,2\pi p_{\rm cm}\right\}, \end{aligned} \tag{3.18}$$

where again μ is the regularization scale, $a(\mu)$ is the subtraction constant which is scale-dependent rendering the loop function scale-independent, and $p_{cm} = \lambda(s, m_H^2, m_K^2)/(2\sqrt{s})$ is the center of mass momentum.

3.2.3 Results

In the calculation, we will choose the nonrelativistic loop function for the case with a nonrelativistic heavy meson and a relativistic light meson in the loop, because the relativistic loop function violates spin symmetry [86]. A bound state of the charmed meson and kaon is associated with a pole of the resummed scattering amplitude below threshold on the real axis in the first Riemann sheet of the complex energy plane. We fix the value of subtraction constant $a(\mu)$ to reproduce the mass of the $D^*_{s0}(2317)$ at 2317.8 MeV, and get $a(\mu = 1\ \text{GeV}) = -4.0$ which is a little different from the one in Ref. [65] where the authors consider two coupled channels DK and $D_s\eta$. And we assume that the same subtraction constant can be used in all other channels. Because of renormalization group invariance, a change of the scale μ can be balanced by a corresponding change of the subtraction constant $a(\mu)$. For example, if the scale change from μ to μ', the subtraction constant will change as

$$a(\mu') = a(\mu) + \log\left(\frac{\mu'}{\mu^2}\right). \tag{3.19}$$

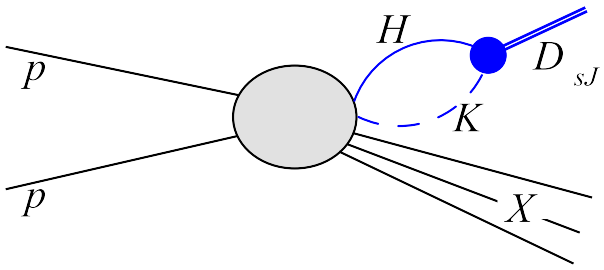

Figure 3.3: The mechanism considered here for the inclusive production of the D_{sJ} as a HK bound state in proton–proton collisions. Here, X denotes all the produced particles other than the H and K in the collision.

We present the results in Tab. 3.2 with the experimental data for comparison, where the central values for the masses of the constituents are used.

For a given scale μ, different values of the subtraction constant correspond to different pole positions in a given channel. This fact allows us to vary the constant to get different binding energies so as to investigate how the cross sections depend on the binding energy later on.

3.3 Hadroproduction of the kaonic molecules

We assume that the production of the D_{sJ} will happen through two steps. The charmed meson kaon pairs will be generated first, and the pairs form the D_{sJ} states afterward. The mechanism is shown in Fig. 4.2. This mechanism is valid only when the binding energy of the bound state is small so that the constituents H and K are only slightly off-shell. However, in principle, the D_{sJ} states can also couple to other components such as the conventional $c\bar{s}$ or a $[cq][\bar{s}\bar{q}]$ tetraquark if they have the required quantum numbers even the dominant component of their wave function is a kaon–charmed meson bound state. All the components contribute to the production of the D_{sJ} states. In general, it is a process-dependent question to conclude which one is more important. Here we assume the bound state component dominants.

3.3.1 Factorization of the near-shreshold production

Before going to the HK case, we will discuss the factorization for the production rate of $X(3872)$ first. In Ref. [59], a factorization formula of the $D^*\bar{D}$ production in the near-threshold region was used. It applys the universal elastic scattering amplitude f to account for the final state interaction (FSI) of $D^{*0}\bar{D}^0$ pair, and reads

$$\begin{aligned} d\sigma[D^{*0}\bar{D}^0(\boldsymbol{k})] &= \frac{1}{\text{flux}}\sum_X \int d\phi_{D^*\bar{D}+X} \left|\frac{\mathcal{T}[D^{*0}\bar{D}^0(\boldsymbol{k})+X]}{f(\boldsymbol{k})}\right|^2 |f(\boldsymbol{k})|^2 \frac{d^3k}{(2\pi)^3 2\mu} \\ &= \frac{1}{\text{flux}}\sum_X \int d\phi_{D^*\bar{D}+X} \left|\frac{\mathcal{T}[D^{*0}\bar{D}^0(0)+X]}{f(0)}\right|^2 |f(\boldsymbol{k})|^2 \frac{d^3k}{(2\pi)^3 2\mu}, \end{aligned} \tag{3.20}$$

where $\boldsymbol{k}$ is the center-of-mass momentum of the constituents, μ is the reduced mass, $\mathcal{T}[D^{*0}\bar{D}^0(\boldsymbol{k})+X]$ is the amplitude for the $D^{*0}\bar{D}^0$ inclusive production, and X means all the other particles in the inclusive process. The phase space integration runs over all the rest particles and the one for the total momentum of the $D^{*0}\bar{D}^0$ pair. The second equality in in Eq. (3.20) holds because of the Migdal-Watson theorem [97, 98]. The dramatic dependence of the amplitude $\mathcal{T}$ on the relative momentum $\boldsymbol{k}$ is mainly given by the

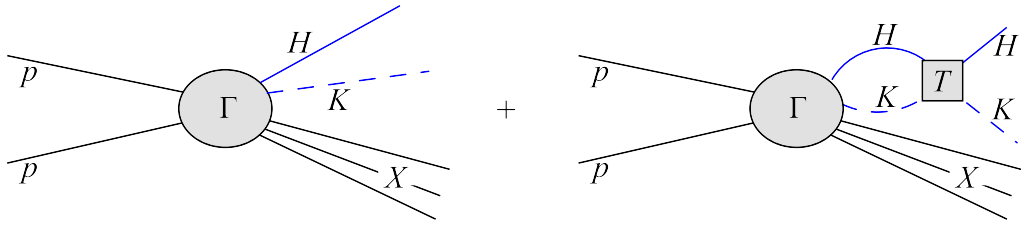

Figure 3.4: Inclusive production of the HK pair in proton–proton collisions. Here Γ denotes the vertex for direct production, T is the resummed HK scattering amplitude, and X denotes all the produced particles other than the HK pair.

universal scattering amplitude f in the near-threshold region. Thus $\mathcal{T}/f$ is insensitive to $\boldsymbol{k}$ and we can take the limit $\boldsymbol{k} \to 0$ in that factor.

In this FSI method, the cross-channel rescattering with other particles comoving with the components is neglected. However, it is argued that the presence of such particles could make the use of the Migdal-Watson theorem invalid and largely affect the so-calculated cross section [61, 99]. In fact, the effect of the comoving hadrons can be treated as perturbations. We will discuss this in more details in Section 4.2.1.

However, in general, it is not clear how the factor $\mathcal{T}/f$ depends on the relative momentum at all. Especially, when the produced particles contain one or more of the lowest-lying pseudoscalar mesons (pions, kaons and the η-meson) which are the pseudo-Goldstone bosons of the spontaneous breaking of chiral symmetry of QCD, the near-threshold production amplitude without the FSI should have a momentum dependence required by chiral symmetry. At first sight, it is not clear whether the universal elastic scattering amplitude is valid to describe the FSI and there exists a factorization formula analogous to Eq. (3.20) or not. As a consequence of chiral symmetry, we will argue that such a factorization formula indeed exists by using the resummed S-wave scattering amplitude in Eq. (3.14) instead of the universal one.

For the inclusive HK production, the general differential cross section formula reads

$$d\sigma[HK(\boldsymbol{k})] \quad = \quad \frac{1}{\text{flux}} \sum_X \int d\phi_{HK+X} |\mathcal{M}[HK(\boldsymbol{k}) + X]|^2 \frac{d^3k}{(2\pi)^3 2\mu}, \tag{3.21}$$

where $\boldsymbol{k}$ is the three-momentum in the center-of-mass frame of the HK pair, μ is the reduced mass, and $\mathcal{M}[HK(\boldsymbol{k}) + X]$ is the production amplitude including the FSI. As depicted in Fig. 3.4, we separate the inclusive production amplitude of the HK pair into two parts: one is that for the direct production denoted by Γ, and the other one includes the FSI described by the scattering amplitude T. Thus, we have an integral equation

$$\mathcal{M}(\boldsymbol{k}; s) = \Gamma(\boldsymbol{k}; s) + i \int \frac{d^4q}{(2\pi)^4} \frac{\Gamma(\boldsymbol{q}; s)\, T(\boldsymbol{q}, \boldsymbol{k}; s)}{(q^2 - m_K^2 + i\epsilon)[(p-q)^2 - m_H^2 + i\epsilon]}. \tag{3.22}$$

If we rewrite this equation in terms of operators, we get

$$\hat{\mathcal{M}} = \hat{\Gamma}(1 + \hat{G}\,\hat{T}), \tag{3.23}$$

where $\hat{G}$ is the operator for the Green's function of the HK system. Similarly, the BSE given in Eq. (3.13) can be written as

$$\hat{T} = \hat{V}(1 + \hat{G}\,\hat{T}). \tag{3.24}$$

Inserting Eq. (3.24) into Eq. (3.23), we obtain

$$\hat{\mathcal{M}} = \hat{\Gamma}\,\hat{V}^{-1}\,\hat{T}. \tag{3.25}$$

The production amplitude should be dominated by the S-wave if we are only considering the production of the HK pair in the near-threshold region. Taking the same on-shell approximation as the resummed scattering amplitude given in Eq. (3.14), in the near-threshold region we have

$$\mathcal{M}(\boldsymbol{k}) \simeq \Gamma_0(\boldsymbol{k})\, V_0(\boldsymbol{k})^{-1}\, T_0(\boldsymbol{k}), \tag{3.26}$$

where we have explicitly presented the dependence of all the functions on the center-of-mass momentum. From Eq. (3.12) we know that the S-wave amplitude is proportional to the energy of kaon, i.e. $V_0(\boldsymbol{k}) \propto E_K = \sqrt{m_K^2 + \boldsymbol{k}^2}$.

But how does the direct production amplitude $\Gamma_0(\boldsymbol{k})$ depend on the momentum? To answer this question, we need to do a chiral symmetry analysis which is applicable in the near-threshold region. Since we are only interested in the HK pair in the process and do not care about the details of the other particles, we may parameterize all the other particles involved in the inclusive production process by an external source field S which has the same quantum numbers as the HK pair. This means that we neglect the cross-channel rescattering of the charmed meson and kaon with other particles in the final state, as it is much smaller than the one between the charmed meson and kaon. Actually, the spirit of this kind of treatment has already been used to investigate the $\pi\pi(K\bar{K})$ system in the decays $J/\psi \to \phi\pi\pi(K\bar{K})$ [100]. In order to ensure that the interaction strength vanishes at threshold as required by the Goldstone theorem, the coupling of the Goldstone bosons (pions, kaons and the eta) to any other fields has to be in a derivative form in the chiral limit when the masses of the up, down and strange quarks are zero. Thus, the Lagrangian for the near-threshold HK production at leading order in the momentum expansion can be written as

$$\mathcal{L}_{\rm prod} = c\, S\, \partial^\mu H\, \partial_\mu K, \tag{3.27}$$

where all the short-distance physics has been parameterized into the coefficient c and the source field S. As a matter of fact, there can be a term of the form $\partial^\mu S\, H\, \partial_\mu K$. However, this term can be recast into the one in Eq. (3.27) modulo a higher order term by using integration by parts. In the Lagrangian, we have made an implicit approximation that in the final states of the inclusive production, there is no other soft chiral particles other than the kaon in the HK pair so that we can neglect the interaction of the kaon with them. Although there are two derivatives in the Lagrangian, it is of order $O(k)$, with k being a momentum much smaller than the typical hadron scale $\Lambda_\chi \sim 1$ GeV. The reason is that the dominant part of the heavy meson four-momentum is the mass of the heavy meson, and thus $\partial^\mu H$ is dominated by its temporal component. An insertion of the light quark masses will give higher order corrections. Therefore, at leading order in the chiral expansion, the direct production amplitude is proportional to the energy of kaon too, i.e. $\Gamma_0(\boldsymbol{k}) \propto E_K$. It is same energy dependence as in $V_0(\boldsymbol{k})$ given in Eq. (3.12). Together with Eq. (3.25), this means that the production amplitude can be factorized into the product of a constant C and the resummed scattering amplitude of HK in the near-threshold region

$$\mathcal{M}(\boldsymbol{k}) = C\, T_0(\boldsymbol{k}). \tag{3.28}$$

Indeed, a factorization formula for the production of the HK pair does exist in the near-threshold region

$$d\sigma[HK(\boldsymbol{k})] \;=\; \frac{1}{\text{flux}} \sum_X \int d\phi_{HK+X}\, |C|^2\, |T_0(\boldsymbol{k})|^2\, \frac{d^3k}{(2\pi)^3 2\mu}, \tag{3.29}$$

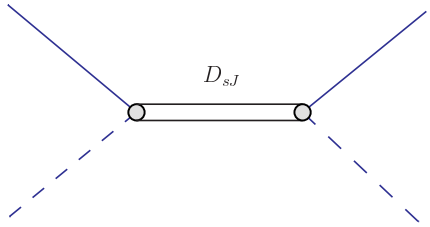

Figure 3.5: The scattering of the charmed meson and kaon through the resonance. The charmed meson and kaon are represented by solid and dashed lines, respectively.

where the constant C may take a value of $\mathcal{M}[HK(\boldsymbol{k}) + X]/T_0(\boldsymbol{k})$ for any $\boldsymbol{k}$ provided that $k \ll \Lambda_\chi$. It is related to the coefficient c in Eq. (3.27) through

$$|C| = \left|\frac{\Gamma(\boldsymbol{k})}{V_0(\boldsymbol{k})}\right| = \frac{|c|F^2}{2}. \tag{3.30}$$

Eq. (3.29) is the analogue of the factorization used in studying the $D\bar{D}^*$ production in Ref. [59], and is applicable to the near-threshold production of a pair of a heavy meson and a pseudo-Goldstone boson. This formula allows for the separation of the long-distance and short-distance contributions in the amplitudes for the production of the molecules. The short-distance one is the same for the processes $pp \to HK$ and $pp \to D_{sJ}$, while the long-distance factor resides in a multiplicative factor of the scattering amplitude given in Eq. (3.14).

3.3.2 Production of the charm-strange hadronic molecules

The cross section for the production of D_{sJ} is

$$\sigma[D_{sJ}] = \frac{1}{\text{flux}} \sum_X \int d\phi_{D_{sJ}+X} \, |\mathcal{M}[D_{sJ} + X]|^2 \, . \tag{3.31}$$

Since the integrated phase space $d\phi_{HK+X}$ in Eq. (4.24) contains the part of the total momentum of the HK pair, the phase space integration in the above equation $d\phi_{D_{sJ}+X}$ is the same as $d\phi_{HK+X}$. Since these D_{sJ} states are the bound state poles of $T_0(s)$, the resummed scattering amplitude $T_0(\boldsymbol{k})$ contains information about the generated hadronic molecules. Therefore, it is straightforward to extend the factorization formula Eq. (3.29) to the case of the inclusive D_{sJ} production provided that these states are produced through intermediate HK pairs. The recipe is to replace the $HK \to HK$ scattering amplitude $T_0(s)$ in Eq. (3.29) by the amplitude for the process $HK \to D_{sJ}$, which is given by the effective coupling constant for the $D_{sJ}HK$ vertex in the vicinity of the D_{sJ} pole. Thue, we have

$$\begin{aligned} \sigma[D_{sJ}] &= \frac{1}{\text{flux}} \sum_X \int d\phi_{D_{sJ}+X} \, |C \, g_{\text{eff}}|^2 \\ &= \left|\frac{F^2}{2} \, g_{\text{eff}}\right|^2 \frac{1}{\text{flux}} \sum_X \int d\phi_{D_{sJ}+X} \, |c|^2 \, , \end{aligned} \tag{3.32}$$

where C is the same constant as that in Eq. (3.29).

The scattering of the heavy charmed meson and kaon with a pole can be depicted as Fig. 3.5, and

around the pole the amplitude can be approximated by

$$T_0(s) = g_{\rm eff}\frac{1}{s - s_{\rm pole}}g_{\rm eff} \tag{3.33}$$

where $s_{\rm pole} = M^2_{D_{sJ}}$ and the effective coupling constant $g_{\rm eff}$ is given by the residue of the transition matrix element at the pole

$$\begin{aligned} g^2_{\rm eff} &= \lim_{s\to s_{\rm pole}}(s - s_{\rm pole})\,T_0(s) \\ &= \frac{1}{d[V_0(s)^{-1} - G(s)]/ds}\Big|_{s=s_{\rm pole}}. \end{aligned} \tag{3.34}$$

We have checked that the same equation will be obtained if we use the approach adopted in Ref. [59] which uses the Migdal-Watson theorem [97, 98] and the unitary relation for the scattering amplitude.

If we vary the subtraction constant in the expression of loop function G, we can get different binding energies. Therefore the cross section for the hadronic molecule in Eq. (3.32) is dependent on the subtraction constant, and indeed on the binding energy. With a smaller binding energy, we found that the production rate of the molecules gets smaller. This conclusion is in agreement with Ref [59]. As we know the scattering length relate to the binding energy E_B as $a = (2\mu E_B)^{-1/2}$, it means that the bound state with a larger scattering length is more difficult to be produced. Yet, this conclusion relies on the assumption that the subtraction constant $a(\mu)$ in the first DK loop attached to the production vertex takes the same value as that in generating the pole.

3.3.3 Estimate the cross section using Monte Carlo event generators

MC event generators have been used in many other processes as a phenomenological and successful tool. They are able to simulate the hadronization of partons produced in QCD processes, and therefore provide an estimate of the $pp \to HK$ inclusive cross sections. Here we will use two commonly adopted programs, Pythia [101] and Herwig [102]. However, the above two event generators do not incorporate the FSI effect which governs the momentum dependence close to threshold as depicted in the scattering amplitude $T_0(s)$ in Eq. (3.14). Therefore, the MC cross section corresponds to the case without near-threshold FSI, and can be approximately expressed in terms of the vertex given in the leading order Lagrangian in Eq. (3.27),

$$\Big(\frac{d\sigma[HK(\boldsymbol{k})]}{dk}\Big)_{\rm MC} = K_{HK}\frac{1}{\rm flux}\sum_X\int d\phi_{HK+X}\,|c\,m_H\,E_K|^2\,\frac{k^2}{4\pi^2\mu}, \tag{3.35}$$

where the factor $K_{HK} \sim O(1)$ is introduced because of the overall difference between MC simulation and the experimental data, while for an order-of-magnitude estimate we can roughly take $K_{HK} \simeq 1$.

Therefore, the coupling constant c can be determined using Eq. (3.35).

$$\frac{1}{\rm flux}\sum_X\int d\phi_{HK+X}\,|c|^2 = \Big(\frac{d\sigma[HK(\boldsymbol{k})]}{dk}\Big)_{\rm MC}\frac{4\pi^2\mu}{k^2E_K^2m_H^2}, \tag{3.36}$$

Substituting the result into the Eq. (3.32), we obtain the cross section for the D_{sJ}:

$$\sigma[D_{sJ}] = \Big|\frac{F^2}{2}\,g_{\rm eff}\Big|^2\Big(\frac{d\sigma[HK(\boldsymbol{k})]}{dk}\Big)_{\rm MC}\frac{4\pi^2\mu}{k^2E_K^2m_H^2}. \tag{3.37}$$

Although the expression contains explicitly a factor of $1/(E_K^2 k^2)$, this factor is completely cancelled by $(d\sigma[HK(\boldsymbol{k})]/dk)_{\rm MC}$ and thus a momentum-independent value is obtained.

3.4 Results

In order to form a molecular state, it is necessary that the constituents move nearly collinearly as a multi-quark system and thus have a small relative momentum. Such configurations can be realized in an inclusive $2 \to 2$ QCD process first, and later the multiquark final states can be produced by soft parton shower radiations. The dominant partonic process for the production of the D_{sJ} states is $gg \to c\bar{c}$ because the gluon density at the LHC energy is much larger than those for quarks. Besides that, the process $q\bar{q} \to c\bar{c}$ will also be included in this analysis.

We have used Pythia and Herwig to generate 10^8 events which contain a pair of the charm and anti-charm quarks. These events are then analyzed by the Rivet library [103] in order to pick out the charmed-meson kaon pair with a small invariant mass. Since the kaons in these events are mostly produced from the soft gluon emission by the heavy charm quarks, they tend to move together with the charmed hadrons. This portion of the events will contribute significantly to the formation of the molecules. To match the capability of the detectors, we have also implemented the cuts on the transverse momentum of the meson pair $p_T > 5$ GeV, and the rapidity $|y| < 2.5$ and $2.0 < y < 4.5$ for the ATLAS/CMS (denoted as LHC for simplicity) and LHCb detectors, respectively. In Fig. 3.6, we show the differential cross sections (histograms in this figure) versus the center-of-mass momentum of the constituent mesons up to 0.35 GeV for the inclusive processes $pp \to DK$, D^*K, D_1K, and D_2K at the LHC with $\sqrt{s} = 8$ TeV. Since the production of charmed mesons D_1 and D_2 is not included in Pythia, we only show the results from Herwig.

As analyzed in Section 3.3.1 and shown in Eq. (3.35), one should be able to approximately describe the production mechanism in the MC calculation using the leading order effective Lagrangian given in Eq. (3.27), and the resulting differential cross section is proportional to $k^2 E_K^2$. To validate this feature, we fit to these distributions with Eq. (3.35) up to 350 MeV for the center-of-mass momentum. The fitted results are shown as curves in Fig. 3.6. Note that the shape of the cross section in Eq. (3.35) is completely fixed, and the fitting procedure only results in a normalization constant, which is proportional to square of the coupling constant $|c|^2$. From this figure, one sees that the MC results can be well described, except the D^*K from Herwig where there exists a clear peak at the bin between 150 MeV and 200 MeV. This peak can be attributed to the resonance $D_{s1}(2536)$ because it decays into $D^{*+}K^0$ and $D^{*0}K^+$ with a center-of-mass momentum of 149 and 167 MeV, respectively. Note that this resonance was included in Herwig but not in Pythia. In principle, this resonating contribution can be built in the scattering amplitudes using a coupled-channel formalism, which will improve the consistency with the MC simulations. However, since we are only interested in an order-of-magnitude estimate, we refrain from doing such an analysis.

With Eq. (4.27) and the differential distributions in Fig. 3.6, we can obtain the production rates of the hadronic D_{sJ} molecules. These results for the cross sections for the inclusive processes $pp \to D_{s0}^*(2317)$, $D_{s1}(2460)$, $D_{sJ}(2860)$ and $D_{s2}(2910)$ (in units of μb) at the LHC with $\sqrt{s} = (7, 8, 14)$ TeV are shown in Table 3.3. Results outside (inside) brackets are obtained using Herwig (Pythia if applicable). Here the rapidity range $|y| < 2.5$ has been assumed for the LHC detectors (ATLAS and CMS), while the rapidity range $2.0 < y < 4.5$ is used for the LHCb. The differences between the values from Pythia and Herwig are caused by the different hadronization mechanisms to form the charmed and kaon mesons. From this table, one sees that the cross sections for the $pp \to D_{sJ}(2860)$ and the $pp \to D_{s2}(2910)$ at the LHC are at the 10^{-1} μb level, while the ones for the $pp \to D_{s0}^*(2317)$ and the $pp \to D_{s1}(2460)$ are

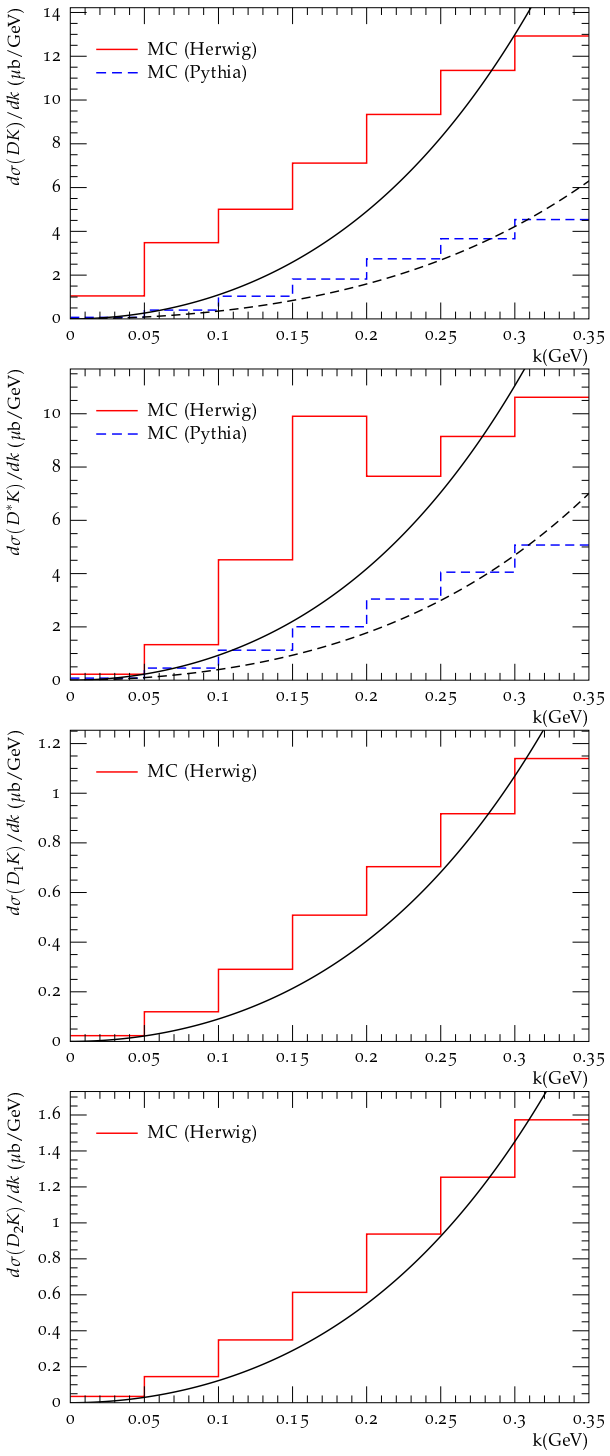

Figure 3.6: Differential cross sections $d\sigma/dk$ (in units of μb/GeV) for the inclusive processes $pp \to DK$, D^*K, D_1K and D_2K at the LHC with $\sqrt{s} = 8$ TeV. The histograms are obtained from the MC simulation (Herwig and Pythia) while the curves are fitted according to the momentum dependence $k^2E_K^2$. In the MC calculation, the kinematic cuts used are $|y| < 2.5$ and $p_T > 5$ GeV, which lie in the phase-space regions of the ATLAS and CMS detectors. Here, we have averaged the events in different charged channels, e.g. D^0K^+ and D^+K^0 for the DK case.

	$D^*_{s0}(2317)$	$D_{s1}(2460)$	$D_{sJ}(2860)$	$D_{s2}(2910)$
LHC 7	2.5(0.83)	2.1(0.91)	0.21(-)	0.27(-)
LHCb 7	0.61(0.15)	0.5(0.17)	0.05(-)	0.06(-)
LHC 8	2.9(0.94)	2.4(1.0)	0.24(-)	0.32(-)
LHCb 8	0.74(0.18)	0.61(0.2)	0.06(-)	0.08(-)
LHC 14	5.5(1.6)	4.7(1.7)	0.5(-)	0.65(-)
LHCb 14	1.6(0.35)	1.3(0.38)	0.13(-)	0.17(-)

Table 3.3: Integrated normalized cross sections (in units of μb) for the inclusive processes $pp \to D^*_{s0}(2317)$, $D_{s1}(2460)$, $D_{sJ}(2860)$ and $D_{s2}(2910)$ at LHC. The results outside (inside) brackets are obtained using Herwig (Pythia). Here the rapidity range $|y| < 2.5$ has been assumed for the LHC experiments (ATLAS and CMS), while the rapidity range $2.0 < y < 4.5$ is used for the LHCb.

larger by roughly one order of magnitude. Such large production rates suggest a promising perspective for searching for these four exotic states at the LHC.

The $D_{s1}(2460)$ has a large decay branching fraction into $D_s\gamma$ and thus can be reconstructed from the $K^+K^-\pi^+\gamma$ final states. With the available decay branching fractions [77], we find that the cross section for the process $pp \to D_{s1}(2460) \to D_s^+\gamma \to K^+K^-\pi^+\gamma$ reaches $O(10^7$ fb), and this would yield $O(10^8)$ events when considering the integrated luminosity of 22 fb^{-1} from ATLAS and CMS in 2012 [104, 105]. The $D_{sJ}(2860)$ mainly decays into DK and D^*K, while the $D_{s2}(2910)$ has a large partial width into D^*K. These two hadrons can be reconstructed in hadronic final states. In particular, based on the 1 fb^{-1} data accumulated in 2011, the LHCb Collaboration has used the DK final state to reconstruct the $D_{sJ}(2860)$ [90], where about 3×10^4 D^0K^+ events from the $D_{sJ}(2860)$ were observed. Using the cross section shown in Table 3.3 and assuming that the $D_{sJ}(2860) \to D^0K^+$ is of $O(10^{-1})$ supported by the Babar data [106], we predict about $O(10^6)$ D^0K^+ events to be generated, which is about two orders of magnitude larger. However, since the detection efficiency of the experiment was not published, a direct comparison is not possible. Currently, we may only conclude that our prediction is not in conflict with the measurement. A more quantitative comparison is expected when the efficiency corrected data is available in the future.

The search for the D_{sJ} states at hadron colliders depends on the non-resonant background contributions. To investigate this issue, we take the $D_{s0}(2317)$ to be constructed in the $D_s\gamma$ final state as an example. To be conservative, we use the cross section $\sigma(pp \to D_s^\pm + \text{anything})$ as an upper bound for the background. The ATLAS collaboration has provided a measurement of this cross section at $\sqrt{s} = 7$ TeV [107]:

$$\sigma(D_s^\pm) = (168 \pm 34^{+27}_{-25} \pm 18 \pm 10)\,\mu\text{b}. \tag{3.38}$$

where the $p_T(D_s^\pm) > 3.5$ GeV and the pseudo-rapitidity $\eta < 2.1$. Our results in Table 3.3 show that the cross section of the $pp \to D_{s0}(2317)$ at $\sqrt{s} = 7$ TeV is about 2 μb. Using the integrated luminosity in 2012, 22 fb^{-1} [104, 105], we have an estimate for the signal/background ratio

$$\frac{S}{\sqrt{B}} \sim \frac{2 \times 22 \times 10^9 \times 5\%}{\sqrt{170 \times 22 \times 10^9}} \sim 1 \times 10^3, \tag{3.39}$$

where 5% is the current upper bound for the branching fraction of the $D_{s0}(2317) \to D_s\gamma$ [77]. It is worthwhile to point out that our theoretical results have to be modified somewhat due to the mismatch in kinematics, however, we believe that the above estimate indicates a great potential for observing the

discussed molecular states at the LHC.

3.5 Discussions

We have explored the hadroproduction of $D^*_{s0}(2317)$, $D_{s1}(2460)$, $D_{sJ}(2860)$ and the predicted $D_{s2}(2910)$ states at the LHC under the assumption that these hadrons are S-wave hadron molecules. We have made use of two MC event generators, Herwig and Pythia, to simulate the production of the charmed-meson kaon pairs. Together with effective field theory to handle the final state interaction among the meson pairs and neglect their interactions with other particles, we have derived an estimate of the production rates for these particles at the order-of-magnitude accuracy. Our results show that the cross sections for the $pp \to D_{sJ}(2860)$ and the $pp \to D_{s2}(2910)$ at the LHC are at the $10^{-1}\mu$b level, while the ones for the $pp \to D^*_{s0}(2317)$ and the $pp \to D_{s1}(2460)$ are larger by roughly one order of magnitude. Thus, these states can be copiously produced at the LHC, and measurements in the future would be able to test the molecular description of the above states and also the production mechanism. Such measurements are very important to gain deeper insights into the hadron interactions, in particular the interactions between heavy and light mesons.

CHAPTER 4

Production of the $X(3872)$ and its bottom analogs and spin partner at hadron colliders

We derived the formula to estimate the cross section of the inclusive production of an S-wave loosely bound states by using the amplitude from heavy hadron chiral perturbation theory (HHChPT) for the heavy-light mesons in Chapter 3. In this chapter, we will study the production of the exotic hadrons with hidden heavy flavor at hadron colliders under the assumption that these particles are S-wave meson-meson molecules. Most of the calculations and discussions presented here are taken from the publication in Ref. [108]. We primarily focus on the production of the X_b which is bottom analogue of the $X(3872)$ with $B\bar{B}^*$ components and its spin partner, a $B^*\bar{B}^*$ molecule with $J^{PC} = 2^{++}$ and denoted as X_{b2}, at the LHC and the Tevatron. Besides, the results on the production of the spin partner of the $X(3872)$, denoted as X_{c2} with $J^{PC} = 2^{++}$, will also be given. According to the heavy quark spin symmetry, the binding energies of the X_{b2} and X_{c2} are similar to those of the X_b and $X(3872)$, respectively. Since the $X(3872)$ has been studied experimentally and theoretically, we will also revisit the production of the $X(3872)$, and compare the obtained results with the experimental data and other theoretical results.

This chapter is organized as follows. We begin in Section 4.1 by revisiting the dynamical generation of all the mentioned candidates of hadronic molecules above, denoted as X in the following. In Section 4.2, we will derive the factorization formula for the production amplitude. In Section 4.3, we will present the production cross section by using the event generators. Finally, the results and discussions will be shown in Section 4.4 and Section 4.5, respectively.

4.1 Charmonium-like XYZ states

Over the last decade or so, many charmonium-like states have been observed but they can not fit into the conventional charmonium spectroscopy predicted by the quark model, in particular these close to or above the open-charm thresholds. One can see this cleary from Fig. 4.1 where we show the spectroscopy of the charmonia which is taken from Ref. [109]. Among them the $X(3872)$ is one of the most interesting states. We will discuss this state as well as its partner in the following.

4.1.1 The $X(3872)$ and its bottom analogs and spin partner

The Belle Collaboration first discovered the $X(3872)$ in B exclusive decay $B \to K\pi\pi J/\psi$ in the $\pi\pi J/\psi$ invariant mass distribution at the e^+e^- collider in 2003 [111], and later the BaBar Collaboration confirmed

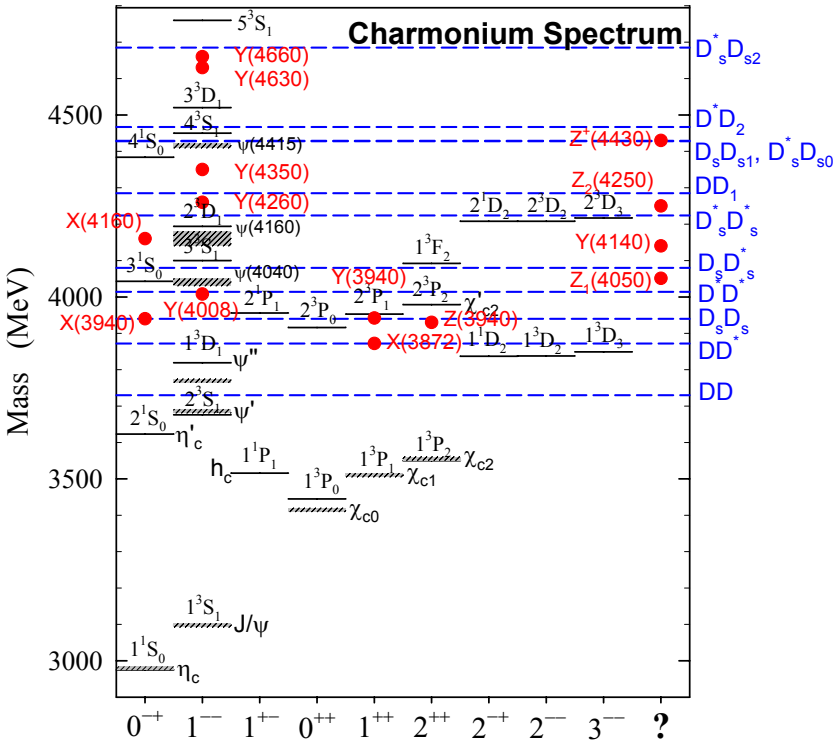

Figure 4.1: Spectroscopy of the charmonia taken from Ref. [109]. The solid lines denote the predictions by quark model [32] while the shaded lines represent the observed conventional charmonium states [110]. The horizontal dashed lines are various $D_s^{(*)}\bar{D}_s^{(*)}$ thresholds, while the red dots are the newly observed charmonium-like states. The states in the last column do not fit the listed spin assignment.

its existence in the same channel [112]. The possible quantum numbers J^{PC} of the $X(3872)$ are 1^{++}, as the analyses of its decays to $J/\psi\pi^+\pi^-$ [113] and $D^0\bar{D}^0\pi^0$ [114] favor 1^+ rather than 2^- and the decay to $J/\psi\gamma$ [115] suggests it is even under charge conjugation. The quantum number was finally determined by the LHCb Collaboration 10 years after the discovery [116]. On the other hand, the isovector hypothesis is excluded by using a likelihood ratio test [117], and also by the fact that it is observed only in the neutral charge state. Until now, its internal structure is under debate. The $X(3872)$ is peculiar in some aspects, for example its total width is so tiny and only the upper bound is known: $\Gamma < 1.2$ MeV and its mass lies extremely close to the $D^0\bar{D}^{*0}$ [77],

$$M_{X(3872)} - M_{D^0} - M_{D^{*0}} = (-0.12 \pm 0.24)\ \text{MeV}. \tag{4.1}$$

Because of the proximity to the threshold, the $X(3872)$ is regarded as one especially promising candidate for a hadronic molecule—either a $D\bar{D}^*$ loosely bound state [118] or a virtual state [119].

The unexpected large ratio of the branching fraction of the two processes $X(3872) \to J/\psi\pi^+\pi^-$ and $X(3872) \to J/\psi\pi^+\pi^-\pi^0$ was reported by the Belle Collaboration for the first time [120]. As the $X(3872)$ is an isosinglet $I = 0$, the process $X(3872) \to J/\psi\pi^+\pi^-$, via a virtual ρ^0, violates the isospin symmetry and should be suppressed. However, the isospin violation is remarkably large, as shown by [77]

$$\frac{\Gamma(X(3872) \to J/\psi\omega)}{\Gamma(X(3872) \to J/\psi\pi^+\pi^-)} = 0.8 \pm 0.3. \tag{4.2}$$

One explanation is that the larger phase space for decay of the $X(3872)$ to $J/\psi\rho$ than $J/\psi\omega$ can contribute to the large ratio [121]. Furthermore, the evidence for different rates of charged and neutral B decays into $X(3872)$ was also found in Ref. [122].

These puzzling facts have stimulated great interest in revealing the underlying structure of the $X(3872)$. One of the important aspects is to discriminate the compact multiquark configuration and the loosely bound hadronic molecule configurations. Although recent calculations of the hadroproduction rates at the LHC based on nonrelativistic QCD indicate that the $X(3872)$ could hardly be an ordinary charmonium $\chi_{c1}(2P)$ [123], the disagreements in theoretical predictions in the molecule picture is also sizable [14, 59–61, 124].

On one hand, it is important to study the $X(3872)$ itself. However, a possible analogue of the $X(3872)$ in the bottom sector may exist due to the heavy flavor symmetry. In Ref. [125], it was referred to X_b, and we follow the notation here. Actually, such a state was predicted to exist in both the tetraquark model [126] and hadronic molecular calculations [13, 127, 128]. But the mass of the $B\bar{B}^*$ molecule based on the mass of the $X(3872)$ is a few tens of MeV higher than the one predicted in the tetraquark model. For example, the mass of the lowest-lying 1^{++} $\bar{b}\bar{q}bq$ tetraquark was predicted to be 10504 MeV [126], while in Ref. [13] the mass was predicted to be (10580^{+9}_{-8}) MeV based on the molecule assumption. Therefore, it is also expedient to search for the X_b on the other hand. The measurements of its properties would help us to understand the underlying interaction in the formation of the $X(3872)$ in addition to the X_b.

It is unlikely to discover X_b at the current electron-positron colliders, as its mass is larger than 10 GeV and its quantum numbers J^{PC} are 1^{++}. But at the Super-KEKB, large data sets are expected in future, of order 50 ab^{-1} [129]. This makes the prospect for the observation of the X_b bright through the $\Upsilon(5S, 6S)$ radiative decays.

4.1.2 Dynamical generation

The heavy quark spin symmetry (HQSS) has been widely adopted to predict new hadronic molecules [73, 130–134], as well as the heavy flavor symmetry (HFS) [13, 135]. By exploring the consequences of heavy quark symmetries on the $X(3872)$ within the framework of effective field theory, Ref. [13] made predictions on the bottom analogues and the spin partner of $X(3872)$. In this section, we will explore the consequences of the heavy quark symmetries for the hadronic molecules mentioned above and discuss the dynamical generation of them.

The Lippmann-Schwinger equation (LSE) in terms of the operators reads

$$\hat{T} = \hat{V} + \hat{V}\hat{G}\hat{T}. \tag{4.3}$$

In the momentum space, the LSE is an integral equation. One can solve the integral equation numerically. However, as discussed in Section 3.2, the integral equation turns out to be an algebric equation after taking the on-shell approximation. We can iterate the on-shell S-wave $V_0(E)$ infinite times and get the resummed S-wave amplitude as

$$T_0(E) = V_0(E)\,[1 - G(E)V_0(E)]^{-1}\,, \tag{4.4}$$

where $G(E)$ is the two-point loop integral

$$G(E) = i\int \frac{d^4q}{(2\pi)^4}\frac{1}{(q^2 - m_H^2 + i\epsilon)[(P-q)^2 - m_{H'}^2 + i\epsilon]}, \tag{4.5}$$

where $E = \sqrt{P^2}$, and m_H and $m_{H'}$ are the masses of two charmed mesons. The loop integral is obviously divergent, but can be regularized by various methods, for example using a sharp cut-off parameter or form factors are shown in the Appendix D. Here we will choose the same Gaussian form factor used in Ref. [13] to regularize the loop function, as we study the production of the hadronic molecules predicted there. Then the regularized loop function reads

$$G(E,\Lambda) = -\frac{\mu}{\pi^2}\left[\sqrt{2\pi}\,\frac{\Lambda}{4} + \frac{\pi}{2}\,k\,e^{2\,k^2/\Lambda^2}\left(\text{erfi}\left(\frac{\sqrt{2}\,k}{\Lambda}\right) - 1\right)\right], \tag{4.6}$$

where Λ is the cutoff, μ is the reduced mass of the heavy mesons and $\text{erfi}(z) = (2/\sqrt{\pi})\int_0^z e^{t^2}dt$. The regularized loop integral is dependent on the cutoff Λ. We will use the range of $[0.5, 1.0]$ GeV for the cutoff Λ following Ref. [13]. This range is a reasonable choice as the following considerations. On one hand the cutoff of the effective theory Λ should be larger than the typical momentum scale we are concerning, i.e. the wave number of the bound states. On the other hand, it should be as small as possible in order to make the heavy quark symmetry valid.

The Lagrangian describing the strong interactions of heavy mesons and antimesons which contain one heavy quark (Q) or antiquark ($\bar{Q}$) includes two contributions at the leading order (LO) in the effective field theory (EFT) expansion, and can be written as

$$\mathcal{L}^{(0)} = \mathcal{L}^{(0)}_{4H} + \mathcal{L}^{(0)}_{\pi HH}, \tag{4.7}$$

where $\mathcal{L}^{(0)}_{4H}$ is the 4-meson interaction vertex while $\mathcal{L}^{(0)}_{\pi HH}$ is for the interaction vertex with one pion exchanged. The contact range Lagrangian for the 4-meson interaction, which is consistent with the HQSS and chiral symmetry, can be written as [133, 136]

$$\begin{aligned}
\mathcal{L}^{(0)}_{4H} &= D_{0a}\,\text{Tr}\left[\bar{H}^{(Q)a}H^{(Q)}_a\gamma_\mu\right]\text{Tr}\left[H^{(\bar{Q})b}\bar{H}^{(\bar{Q})}_b\gamma^\mu\right] + D_{0b}\,\text{Tr}\left[\bar{H}^{(Q)a}H^{(Q)}_a\gamma_\mu\gamma_5\right]\text{Tr}\left[H^{(\bar{Q})b}\bar{H}^{(\bar{Q})}_b\gamma^\mu\gamma_5\right] \\
&+ E_{0a}\,\text{Tr}\left[\bar{H}^{(Q)a}\,\vec{\tau}^{\,b}_a\,H^{(Q)}_b\gamma_\mu\right]\text{Tr}\left[H^{(\bar{Q})r}\,\vec{\tau}^{\,s}_r\,\bar{H}^{(\bar{Q})}_s\gamma^\mu\right] \\
&+ E_{0b}\,\text{Tr}\left[\bar{H}^{(Q)a}\,\vec{\tau}^{\,b}_a\,H^{(Q)}_b\gamma_\mu\gamma_5\right]\text{Tr}\left[H^{(\bar{Q})r}\,\vec{\tau}^{\,s}_r\,\bar{H}^{(\bar{Q})}_s\gamma^\mu\gamma_5\right],
\end{aligned} \tag{4.8}$$

and the Lagrangian for the one pion exchange is [137]

$$\mathcal{L}^{(0)}_{\pi HH} = -\frac{g}{\sqrt{2}F_\pi}\left\{\text{Tr}\left[\bar{H}^{(Q)b}H^{(Q)}_a\gamma_\mu\gamma_5\right] + \text{Tr}\left[H^{(\bar{Q})b}\bar{H}^{(\bar{Q})}_a\gamma^\mu\gamma_5\right]\right\}(\vec{\tau}\cdot\partial_\mu\vec{\pi})^a_b + O(\pi^2), \tag{4.9}$$

where τ^{ab} are the Pauli matrices, a, b, r, s are the isospin indices, and $\vec{\pi}$ are the pion fields. F_π is the pion decay constant, while g is a coupling constant which can be determined from the charmed meson decay $D^* \to D\pi$.

With the leading order Lagrangian, the potential is quite simple because the pion exchanges and coupled-channel effects can be considered subleading [133, 138]. It only contains the energy-independent contact range interactions between the considered heavy meson pair. Therefore, at very low energies, the interaction between heavy mesons and antimesons ($D^{(*)}\bar{D}^{(*)}$ or $B^{(*)}\bar{B}^{(*)}$) can be described solely in terms of the contact-range potential.

We use the matrix field $H^{(Q)}$ ($H^{(\bar{Q})}$) to denote the doublets of pseudoscalar and vector heavy-meson

(antimeson)

$$H_a^{(Q)} = \frac{1+\not{v}}{2}[P_{a\mu}^{*(Q)}\gamma^\mu - P_a^{(Q)}\gamma_5], \tag{4.10}$$

$$H^{(\bar{Q})a} = [P_\mu^{*(\bar{Q})a}\gamma^\mu - P^{(\bar{Q})}\gamma_5]\frac{1-\not{v}}{2}, \tag{4.11}$$

where the pseudoscalar meson (antimeson) fields are represented by $P_a^{(Q)}$ ($P_a^{(\bar{Q})}$) and their vector HQSS partners are $P_a^{*(Q)}$ ($P_a^{*(\bar{Q})}$). Thus we have the relation

$$C_0^{D\bar{D}^*}(1^{++}) = C_0^{D^*\bar{D}^*}(2^{++}), \tag{4.12}$$

which is the consequence of HQSS. On the other hand, assuming HFS for the contact term[1], we have

$$C_0^{D\bar{D}^*}(1^{++}) = C_0^{B\bar{B}^*}(1^{++}), \tag{4.13}$$

$$C_0^{D^*\bar{D}^*}(2^{++}) = C_0^{B^*\bar{B}^*}(2^{++}). \tag{4.14}$$

Thus, the four leading order low energy constants are equivalent and we denote them as C_0. The value of the constant C_0 is unknown, but it satisfies the equation

$$1 - C_0\, G[E, \Lambda] = 0, \tag{4.15}$$

at the pole of the bound state $E = E_{\rm pole}$. This equation can be used to determine the constant C_0. However, as shown above the loop function G is dependent on the cutoff Λ, C_0 should depend on Λ as well. This is required by the renormalization group invariance, and at the end the physical observables are cutoff independent. We first take the observed $X(3872)$ mass as input to determine the constant C_0, and then use the value to predict the partners of the $X(3872)$. To take the heavy quark symmetry breaking into account, we can expect the counter term C_0 to deviate from the heavy quark limit by the order of Λ_{QCD}/m_Q, that is [133]

$$C_0^{m_Q} = C_0^{m_Q\to\infty}\left(1 + O\left(\frac{\Lambda_{QCD}}{m_Q}\right)\right), \tag{4.16}$$

where we take $\Lambda_{QCD} = 300$ MeV, and $m_Q = 1.5$ GeV for the charm quark and $m_Q = 4.5$ GeV for the bottom quark. Thus a relative uncertainty of 20% in charm sector and 7% in bottom sector will be introduced. In the calculation, we use the central values for the masses of the constituents. The values of the predicted masses together with uncertainties are listed in Tab. 4.1.

One may notice that there is one big difference between the predicted X_b and the $X(3872)$, that is we expect that the isospin breaking effects would be much smaller for the X_b than that for the $X(3872)$. For the $X(3872)$, the distance of its mass to the $D^0\bar{D}^{*0}$ threshold is much smaller than the distance to the D^+D^{*-} threshold, which leaves its imprint in the wave function at short distances through the charmed meson loops so that a sizable isospin breaking effect is expected. But the mass difference between the charged and neutral B mesons is only (0.32 ± 0.06) MeV [77], moreover the binding energy of the $B\bar{B}^*$ system may be larger than that in the charmed sector due to a larger reduced mass. Besides, although the isospin breaking observed in the $X(3872)$ decays into J/ψ and two/three pions can be largely explained by the phase space difference between the $X(3872) \to J/\psi\rho$ and the $X(3872) \to J/\psi\omega$ [121], the phase space difference between the $\Upsilon\rho$ and $\Upsilon\omega$ systems is negligible since the mass splitting between the X_b

[1] This assumption is reasonable: considering resonance saturation for the contact terms, they will not depend on M_Q. However, there is another point of view, see Ref. [136]

J^{PC}	state	Thresholds	$\Lambda = 0.5$ GeV	$\Lambda = 1$ GeV	Experiment
1^{++}	$\frac{1}{\sqrt{2}}(D\bar{D}^* - D^*\bar{D})$	3875.84	3871.69 (input)	3871.69 (input)	3871.69 ± 0.17 [77]
2^{++}	$D^*\bar{D}^*$	4017.2	4012^{+1}_{-2}	4012^{+3}_{-4}	?
1^{++}	$\frac{1}{\sqrt{2}}(B\bar{B}^* - B^*\bar{B})$	10604.6	10581^{+8}_{-9}	10539^{+25}_{-27}	?
2^{++}	$B^*\bar{B}^*$	10650.4	10626^{+8}_{-9}	10584^{+25}_{-27}	?

Table 4.1: The predictions of the pole position of the bound states in units of MeV. The uncertainties are caused by the heavy quark symmetry breaking.

and the $\Upsilon(1S)$ is definitely larger than 1 GeV. Therefore, to a very good approximation, the X_b should be an isosinglet state, which is in line with the predictions in Refs. [13, 127, 128].

4.2 Factorization formula

To derive the factorized formula for the prompt production cross section, we start with the scattering amplitude. The inclusive amplitude can be written in terms of its wave function in the momentum representation $\tilde{\psi}_X(\boldsymbol{k})$ as

$$\mathcal{M}[X] = \int \frac{d^3k}{(2\pi)^3\sqrt{2\mu}} \mathcal{M}[HH'(\boldsymbol{k}) + \text{all}]\, \tilde{\psi}_X(\boldsymbol{k}), \tag{4.17}$$

where the X stands for $X(3872)$, X_b, X_{b2} or X_{c2}, μ is the reduced mass of the heavy mesons H and H' and $\mathcal{M}[HH' + \text{all}]$ is the amplitude for the inclusive production of heavy mesons H and H'.

4.2.1 The rescattering effect

The squared amplitude is written as

$$\begin{aligned} |\mathcal{M}[X]|^2 &= \left| \int \frac{d^3k}{(2\pi)^3\sqrt{2\mu}} \mathcal{M}[HH'(\boldsymbol{k}) + \text{all}]\, \tilde{\psi}_X(\boldsymbol{k}) \right|^2 \\ &\leq \int \frac{d^3k}{(2\pi)^3 2\mu} \left|\mathcal{M}[HH'(\boldsymbol{k}) + \text{all}]\right|^2 \int \frac{d^3k}{(2\pi)^3} \left|\tilde{\psi}_X(\boldsymbol{k})\right|^2, \end{aligned} \tag{4.18}$$

where the Schwartz inequality has been applied and the last factor is the normalization integral for the wave function. In order to estimate the upper bound for the production cross section of $X(3872)$, Ref. [14] used a sharp cutoff $k_{\max}$ for the integral over $\boldsymbol{k}$, where $k_{\max}$ is the momentum scale set by the binding momentum $\sqrt{2\mu E_X}$, with E_X the energy of $X(3872)$ relative to the threshold, i.e. the binding energy. After applying the uncertinty principle relation, the authors of Ref. [14] got $k_{\max} = 35$ MeV. While after inserting the phase integral, the amplitude squared $|\mathcal{M}[HH'(\boldsymbol{k}) + \text{all}]|^2$ for the prompt charmed meson pairs was simulated by the Monte Carlo event generators like Pythia and Herwig. However, in the event generators, the amplitude squared is independent of the relative momentum $\boldsymbol{k}$, and we will discuss this later in more detail. They obtained 0.11 nb and 0.071 nb for the Fermilab Tevatron by using Pythia and Herwig, respectively. The results are smaller by orders of magnitude than the lower bound on the experimental one, (3.1 ± 0.7) nb, which is extracted from the CDF data. Therefore, they concluded that

the expectation of the $X(3872)$ being a charmed meson molecule is unlikely.

However, in Ref. [59], the authors argued that the upper limit of the integral $k_{\max}$ should not be set by the binding momentum, but set by the typical momentum scale associated with the range of interaction between the charmed mesons. The final state interaction between the charmed mesons can play an important role in the region of small relative momentum. The effect can make the charmed mesons which are created with a large relative momentum to rescatter into the small region. Therefore the integral region in Eq. (4.18) should be extended. As a result, the upper bound on the cross section estimated in Ref. [14] will increase significantly, and the large discrepancy with the lower bound on experimental result will be resolved.

In order to take the rescattering effect into account, Ref. [59] used the universal elastic scattering amplitude to account for the dramatic energy dependence of the matrix element according to the Migdal-Watson theorem [97, 98], then derived the factorized formula of the production rate.

However, one may doubt the use of the Migdal-Watson approach, because of a huge numbers of hadrons comoving with the molecular components. The hadrons near the constituent mesons with a small relative momentum can be investigated by using the event generators. In Ref. [99], it was shown that effect of the hadrons is significant and do necessarily interfere the charmed mesons to rescatter into the bound state in an unknown way. Thus the hadrons could significantly change the prompt production cross section estimated in Ref. [59]. While the authors of Ref. [60] argued that the interaction strength between a hadron with a constituent of the would-be loosely bound S-wave molecule is much smaller than the one between the two constituents. Hence the effect of the comoving hadrons can be treated as perturbations, and the use of Migdal-Watson theorem is valid.

4.2.2 Factorization of the amplitude

By using the Schrödinger equation for the bound state

$$\langle \boldsymbol{k}| \hat{H} |\psi\rangle = -E_B \langle \boldsymbol{k}|\psi\rangle \tag{4.19}$$

where $\hat{H} = \hat{\boldsymbol{k}}^2/2\mu + V$ is the Hamiltonian for the system, with V the potential for the two-body scattering and E_B is the binding energy. The wave function can be expressed as

$$\tilde{\psi}_X(\boldsymbol{k}) \quad = \quad -\frac{2\mu}{\boldsymbol{k}^2 + 2\mu E_B} T_X(\boldsymbol{k}), \tag{4.20}$$

where $T_X(\boldsymbol{k}) = \langle \boldsymbol{k}| V |\psi\rangle$ is amplitude for the coupling of the bound state to the two-body channel, i.e. $HH' \to X$. In the case that the hadronic molecule is a loosely bound state, T_X can be approximated by the

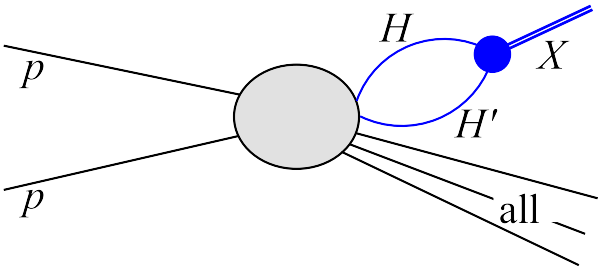

Figure 4.2: The mechanism considered here for the inclusive production of the X as a HH' bound state in proton–proton collisions. Here, *all* denotes all the produced particles other than the H and H' in the collision.

nonrelativistic coupling constant g_{NR} of the X to its constituents and independent of the momentum. The nonrelativistic coupling constant has the relation to the relativistic one as $g = g_{NR}\sqrt{2m_H}\sqrt{2m_{H'}}\sqrt{2m_X}$. As m_X is the mass of X and extremely close the threshold, thus $m_X \approx m_H + m_{H'}$. Then the wave function is

$$\begin{aligned}\tilde{\psi}_X(\boldsymbol{k}) &= 4m_H m_{H'} \frac{g}{\sqrt{2m_H}\sqrt{2m_{H'}}\sqrt{2m_X}} \int \frac{dk^0}{2\pi} G(k) \\ &= g\sqrt{2\mu} \int \frac{dk^0}{2\pi} G(k), \end{aligned} \tag{4.21}$$

where $G(k)$ is the Green function of the heavy meson pair. After inserting the wave function into Eq. (4.17), we can obtain

$$\mathcal{M}[X] = g \int \frac{d^4k}{(2\pi)^4} \mathcal{M}[HH'(\boldsymbol{k}) + \text{all}]\, G(k). \tag{4.22}$$

Or alternatively, when the binding energy of a bound state is small, we can assume that the formation of the hadronic molecule, which is a long-distance process, would occur after the production of its constituents, which is of short-distance nature. The mechanism is shown in Fig. 4.2. In general, the scattering amplitude is an integral equation over the momentum of the intermediate mesons, and we can get the same formula as above.

As argued in Ref. [59], one should be able to approximate the production amplitude $\mathcal{M}[HH' + \text{all}]$, which does not take into account the FSI carrying a strong momentum dependence near threshold, by a constant. According to the Migdal-Watson theorem [97, 98], which is valid when coupled channels and cross-channel FSI are neglected, the FSI in the production is described by the elastic scattering amplitude. Thus, both $\mathcal{M}[HH' + \text{all}]$ and g can be taken outside the momentum integral, while the integral of the Green function $G(k)$ turns out to be the divergent two-point scalar loop function. Therefore, the amplitude for the production of the hadronic molecule can be written as [58]

$$\mathcal{M}[X] = \mathcal{M}[HH' + \text{all}]\; G\; g, \tag{4.23}$$

where G is the two-point loop integral.

4.3 The cross section using event generators

To derive the cross section for the production of the hadronic molecules, the starting point is the general differential Monte Carlo (MC) cross section formula for the inclusive production of the constituents

$$d\sigma[HH'(\boldsymbol{k})]_{\text{MC}} = K_{HH'} \frac{1}{\text{flux}} \sum_{\text{all}} \int d\phi_{HH'+\text{all}} |\mathcal{M}[HH'(\boldsymbol{k}) + \text{all}]|^2 \frac{d^3k}{(2\pi)^3 2\mu}. \tag{4.24}$$

where $\boldsymbol{k}$ is the three-momentum in the center-of-mass frame of the HH' pair, μ is the reduced mass of the HH' pair. As we know the event generators have been tuned in many high energy experiments to reproduce the distributions of one charmed meson, but to our knowledge no distribution of charmed meson pairs has been reproduced to be tuned in the event generators. Thus the factor $K_{HH'}$ is introduced for the overall difference between MC simulation and the experimental data. Generally this factor is of $O(1)$, for example Ref. [14] tuned the MC tools on the $D^0 D^{*-}$ pair production cross section distributions

on the CDF data [139] and the factors were 0.74 and 1.8 for Pythia and Herwig, respectively. Therefore, we can roughly take $K_{HH'} \simeq 1$ for an order-of-magnitude estimate.

The event generators like Pythia and Herwig do not include the information of the final state interaction between the mesons, and the matrix element $\mathcal{M}[HH'(\boldsymbol{k}) + \text{all}]$ is independent of the relative momentum approximately in the low relative momentum region. Thus in the region where the relative momentum is small, we have the relation

$$\frac{d\sigma[HH'(\boldsymbol{k})]_{\text{MC}}}{dk} \approx \boldsymbol{k}^2. \tag{4.25}$$

On the other side, the cross section for the production of the hadronic molecule is written as

$$\sigma[X] = \frac{1}{\text{flux}} \sum_{\text{all}} \int d\phi_{X+\text{all}} \left|\mathcal{M}[X + \text{all}]\right|^2, \tag{4.26}$$

where the phase space integration is the same as the one in Eq. (4.24). Finally we can deduce the cross section of X based on the Eqs. (4.23) and (4.24) as

$$\sigma[X] = \frac{1}{4m_H m_{H'}} g_{\text{eff}}^2 |G|^2 \left(\frac{d\sigma[HH'(\boldsymbol{k})]}{dk}\right)_{\text{MC}} \frac{4\pi^2\mu}{\boldsymbol{k}^2}. \tag{4.27}$$

The divergent loop integral G is regularized and expressed in Eq. (D.5). As for the coupling constant g_{eff}, the same as Eq. (3.34), it is related to the residue of the bound state pole by

$$\begin{aligned} g_{\text{eff}}^2 &= \lim_{s \to s_{\text{pole}}} (s - M_X^2) \frac{C_0(\Lambda)}{1 - C_0(\Lambda)\, G(\sqrt{s}, \Lambda)} \\ &= \frac{C_0(\Lambda)}{d[1 - C_0(\Lambda)\, G(\sqrt{s}, \Lambda)]/ds}\bigg|_{s=M_X^2}, \end{aligned} \tag{4.28}$$

where s is the center-of-mass energy squared and the parameter Λ comes from the Gaussian form factor used to regularize the loop integral G. Thus the loop integral and the coupling constant will be dependent on Λ. In principle, the Λ-dependence should be absorbed by a counterterm parameterizing short distance physics. However, without any knowledge of the counterterm, we allow Λ to choose a value in the range of [0.5, 1] GeV [13] and the resulting different cross section values indicate the intrinsic uncertainty.

4.4 Results

As illustrated in Fig. 4.2, the mesonic constituents must be produced at first, and in order to form the molecule the constituents have to collinearly move with a small relative momentum. This configurations can be generated from the inclusive QCD process containing a heavy quark pair $Q\bar{Q}$ with a similar relative momentum in the final state. However, there must be a third parton produced in the recoil direction. Thus the process is a $2 \to 3$ one.

In the explicit realization of the $2 \to 3$ parton process, we generate it initially through the hard scattering, and more quarks will be produced via soft radiations. Madgraph [140] is used to generate the $2 \to 3$ partonic events which contain a pair of heavy quark and antiquark ($\bar{b}b$ or $\bar{c}c$) in the final states, and later on are passed to the MC event generators for the hadronization. In the hadronization stage, we use Herwig [102] and Pythia [101]. Finally, the outputs from the event generator are analyzed by using the Rivet library [103].

In order to improve the efficiency of the simulation, we apply the partonic cuts for the transverse momentum $p_T > 2$ GeV for heavy quarks and light jets, $m_{c\bar{c}} < 4.5$ GeV ($k_{D\bar{D}^*} = 1.14$ GeV and $k_{D^*\bar{D}^*} = 1.02$ GeV), $m_{b\bar{b}} < 10.7$ GeV ($k_{B\bar{B}^*} = 715$ MeV and $k_{B^*\bar{B}^*} = 517$ MeV at the hadron level), and $\Delta R(c,\bar{c}) < 1 (\Delta R(b,\bar{b}) < 1)$ where $\Delta R = \sqrt{\Delta\eta^2 + \Delta\phi^2}$ ($\Delta\phi$ is the azimuthal angle difference and $\Delta\eta$ is the pseudo-rapidity difference of the $b\bar{b}$).

As one can see from Eq. (4.27), we need to calculate the differential cross section of the charmed meson pair from the event generators. As the $X(3872)$ and its spin partner and bottom analogs, X_c, X_b, X_{b2}, are the bound state of $D\bar{D}^*$, $D^*\bar{D}^*$, $B\bar{B}^*$, $B^*\bar{B}^*$, respectively. Thus we will simulate the 4 distributions correspondingly based on 10^7 partonic events generated by Madgraph. Here we show the differential cross sections $d\sigma/dk$ (in units of nb/GeV) for the process $pp \to B^0\bar{B}^{*0}$ in Fig. 4.3, and the ones for the reaction $pp \to B^{*0}\bar{B}^{*0}$ in Fig. 4.4 at the LHC with the center-of-mass energy $\sqrt{s} = 8$ TeV and at the Tevatron with $\sqrt{s} = 1.96$ TeV for example. The kinematic cuts are $|y| < 2.5$ and $p_T > 5$ GeV, where y and p_T are the rapidity and the transverse momentum of the bottom mesons, respectively. The cuts lie in the phase space regions of the ATLAS and CMS detectors. While for the Tevatron experiments (CDF and D0) at 1.96 TeV, we use $|y| < 0.6$; the rapidity range $2.0 < y < 4.5$ is used for the LHCb detector. The solid and dashed lines in the plots are from Herwig and Pythia generators, respectively. Before we extract the factor $1/k^2 d\sigma/dk$ from the differential distributions, we have checked that $d\sigma/dk$ is approximately proportional to k^2, cf. Eq. (4.25).

4.4.1 The $X(3872)$

Before we move to predict the producion rate for the bottom analogs and the spin partner of the $X(3872)$, it is important to compare our results with the experimental ones of the $X(3872)$. To do such a comparison, we need to estimate the range for the branching ratio $\mathcal{B}(X(3872) \to J/\psi\pi^+\pi^-)$. First, we shall revisit the production of the $X(3872)$ from the experimental data. On one hand, by making use of the Babar upper limit for $\mathcal{B}(B^+ \to X(3872)K^+)$ [141] and the most recent Belle measurement of $\mathcal{B}(B^+ \to X(3872)K^+) \times \mathcal{B}(X(3872) \to J/\psi\pi^+\pi^-)$ [142],

$$\begin{aligned} \mathcal{B}(B^+ \to X(3872)K^+) &< 3.2 \times 10^{-4}, \\ \mathcal{B}(B^+ \to X(3872)K^+) \times \mathcal{B}(X(3872) \to J/\psi\pi^+\pi^-) &= (8.63 \pm 0.82 \pm 0.52) \times 10^{-6}, \end{aligned} \tag{4.29}$$

we can derive the lower bound:

$$\mathcal{B}(X(3872) \to J/\psi\pi^+\pi^-) > 0.027. \tag{4.30}$$

On the other hand, in addition to the $J/\psi\pi^+\pi^-$ channel [142], if we sum over the branching fractions of all measured channels of the $X(3872)$, for example $D^0\bar{D}^{*0} + c.c.$ [143], $J/\psi\omega$ [144], $\psi'\gamma$ and $J/\psi\gamma$ [145, 146], we can derive the upper bound for the branching fraction of the $X(3872) \to J/\psi\pi^+\pi^-$:

$$\mathcal{B}(X(3872) \to J/\psi\pi^+\pi^-) < 0.083 \tag{4.31}$$

Together with the experimental measurements about the production cross section of the $X(3872)$ with subsequently decaying to $J/\psi\pi^+\pi^-$ final states, like the measurements by the CDF Collaboration [147]

$$\sigma(p\bar{p} \to X) \times \mathcal{B}(X(3872) \to J/\psi\pi^+\pi^-) = (3.1 \pm 0.7) \text{ nb}, \tag{4.32}$$

$\sigma(pp/p\bar{p} \to X(3872))$	Ref. [14]	Ref. [59]	Λ = 0.5 GeV	Λ = 1 GeV	Experiment
Tevatron	< 0.085	1.5–23	10(7)	47(33)	37–115 [147]
LHC7	–	45–100	16(7)	72(32)	13–39 [148]

Table 4.2: Integrated cross sections (in units of nb) for $pp/\bar{p} \to X(3872)$ compared with previous theoretical estimates [14, 59] in which the LHC7 result is estimated based on non-relativistic QCD, and experimental measurements by CDF [147] and CMS [148]. Results outside (inside) brackets are obtained using Herwig (Pythia). Kinematical cuts used are: $p_T > 5$ GeV and $|y| < 0.6$ at Tevatron and 10 GeV $< p_T <$ 50GeV and $|y| < 1.2$ at LHC with $\sqrt{s} = 7$ TeV. We have converted the experimental data $\sigma(p\bar{p} \to X) \times \mathcal{B}(X(3872) \to J/\psi\pi^+\pi^-) = (3.1 \pm 0.7)$nb [147] and $\sigma(pp \to X) \times \mathcal{B}(X(3872) \to J/\psi\pi^+\pi^-) = (1.06 \pm 0.11 \pm 0.15)$nb [148] into cross sections using $\mathcal{B}(X(3872) \to J/\psi\pi^+\pi^-) \in [0.027, 0.083]$ as discussed in the text.

and by the CMS Collaboration [148]

$$\sigma(pp \to X) \times \mathcal{B}(X(3872) \to J/\psi\pi^+\pi^-) = (1.06 \pm 0.11 \pm 0.15)\ \text{nb}, \tag{4.33}$$

we can obtain a range of values of $\sigma(p\bar{p}/pp \to X(3872))$.

We show the integrated cross sections (in units of nb) for the $pp/\bar{p} \to X(3872)$ in Tab. 4.2, and compare with previous theoretical estimates [14, 59] and the experimental results. Results outside (inside) brackets are obtained using Herwig (Pythia). In this table, we have converted the experimental data of the CDF and CMS Collaborations to $\sigma(p\bar{p}/pp \to X(3872))$. And we use the same kinematical cuts on the transverse momentum and rapidity as those in the experimental analyses: $p_T > 5$ GeV and $|y| < 1.2$ at the Tevatron and 10GeV $< p_T <$ 50GeV and $|y| < 0.6$ at the LHC with $\sqrt{s} = 7$ TeV.

As we can see from the table, the upper bound derived for $\sigma(p\bar{p}/pp \to X)$ at Tevatron by Ref. [14] is quite small, while the values predicted by Ref. [59] increased significantly after taking into account the final state interaction by using the universal scattering amplitude but still can not fit the experiments. Our results agree with the experimental measurements quite well, which validates our estimate based on an effective field theory treatment of the rescattering effect.

In summary, our estimates for the cross section at the Tevatron are given as

$$\sigma(p\bar{p} \to X(3872)) = \begin{cases} (10, 47)\ \text{nb} & \text{for Herwig} \\ (7, 33)\ \text{nb} & \text{for Pythia} \end{cases}, \tag{4.34}$$

and at the LHC with $\sqrt{s} = 7$ TeV

$$\sigma(pp \to X(3872)) = \begin{cases} (16, 72)\ \text{nb} & \text{for Herwig} \\ (7, 32)\ \text{nb} & \text{for Pythia} \end{cases}. \tag{4.35}$$

4.4.2 The bottom analogs and the spin partner of the X(3872)

As for the partners of the $X(3872)$, we collect the integrated cross sections (in units of nb) for the $pp \to X_b$, and $pp \to X_{b2,c2}$ in Tab. 4.3, in which the results outside (inside) brackets are obtained using Herwig (Pythia). From the table, one sees that the cross sections for the X_{b2} is similar to those for the X_b, and the ones for the X_{c2} are of the same order as those for the $X(3872)$ given in Table 4.2 but are two orders of magnitude larger than those for their bottom analogues.

The CMS Collaboration recently presented some results of the first search for new bottomonium states

X_b	E_{X_b} = 24 MeV(Λ = 0.5 GeV)	E_{X_b} = 66 MeV(Λ = 1 GeV)
Tevatron	0.08(0.18)	0.61(1.4)
LHC 7	1.5(3.1)	12(23)
LHCb 7	0.25(0.49)	1.9(3.7)
LHC 8	1.8(3.6)	14(27)
LHCb 8	0.3(0.62)	2.2(4.7)
LHC 14	3.2(6.8)	24(51)
LHCb 14	0.65(1.3)	4.9(9.7)
X_{b2}	$E_{X_{b2}}$ = 24 MeV(Λ = 0.5 GeV)	$E_{X_{b2}}$ = 66 MeV(Λ = 1 GeV)
Tevatron	0.05(0.13)	0.36(1.)
LHC 7	0.92(2.3)	6.9(17)
LHCb 7	0.14(0.36)	1.1(2.7)
LHC 8	1.1(2.7)	8.1(20)
LHCb 8	0.19(0.46)	1.4(3.5)
LHC 14	1.9(5.)	15(37)
LHCb 14	0.38(0.96)	2.9(7.2)
X_{c2}	$E_{X_{c2}}$ = 4.8 MeV(Λ = 0.5 GeV)	$E_{X_{c2}}$ = 5.6 MeV(Λ = 1 GeV)
Tevatron	4.4(3.)	22(15)
LHC 7	66(44)	327(216)
LHCb 7	14(8.5)	71(42)
LHC 8	74(52)	369(256)
LHCb 8	17(10)	83(50)
LHC 14	135(90)	672(446)
LHCb 14	35(19)	174(92)

Table 4.3: Integrated cross sections (in units of nb) for the $pp/\bar{p} \to X_b$, and $pp/\bar{p} \to X_{b2}$ at the LHC and Tevatron. Results out of (in) brackets are obtained using Herwig(Pythia). The rapidity range $|y| < 2.5$ has been assumed for the LHC experiments (ATLAS and CMS) at 7, 8 and 14 TeV; for the Tevatron experiments (CDF and D0) at 1.96 TeV, we use $|y| < 0.6$; the rapidity range $2.0 < y < 4.5$ is used for the LHCb.

based on a data sample corresponding to an integrated luminosity of 20.7 fb^{-1} at $\sqrt{s} = 8$ TeV [149]. The search mainly focused on the X_b decaying to $\Upsilon(1S)\pi^+\pi^-$. Unfortunately, no evidence for the X_b was found. Nevertheless, the upper limit at a confidence level of 95% on the product of the production cross section of the X_b and the decay branching fraction of $X_b \to \Upsilon(1S)\pi^+\pi^-$ has been set to be

$$\frac{\sigma(pp \to X_b \to \Upsilon(1S)\pi^+\pi^-)}{\sigma(pp \to \Upsilon(2S) \to \Upsilon(1S)\pi^+\pi^-)} < (0.009, 0.054)\,, \tag{4.36}$$

where the range corresponds to the variation of the X_b mass from 10 to 11 GeV.

Using the current experimental data on the $\sigma(pp \to \Upsilon(2S))$, it is easy to convert the above ratio into the cross section which can be directly used to compare with our results. Since the masses of the $\Upsilon(2S)$ and X_b are not very different, it may be a good approximation to assume that the ratio given in Eq. (4.36)

is insensitive to kinematic cuts. Using the CMS measurement in Ref. [150]:

$$\sigma(pp \to \Upsilon(2S))\mathcal{B}(\Upsilon(2S) \to \mu^+\mu^-) = (2.21 \pm 0.03^{+0.16}_{-0.14} \pm 0.09)\ \text{nb}, \tag{4.37}$$

with the cuts p_T <50 GeV and $|y| < 2.4$ for the $\Upsilon(2S)$, and the branch ratios $\mathcal{B}(\Upsilon(2S) \to \mu^+\mu^-) = (1.93 \pm 0.17)\%$ and $\mathcal{B}(\Upsilon(2S) \to \Upsilon(1S)\pi^+\pi^-) = (17.85 \pm 0.26)\%$ [77], we get

$$\sigma(pp \to X_b)\mathcal{B}(X_b \to \Upsilon(1S)\pi^+\pi^-) < (0.18, 1.11)\ \text{nb}. \tag{4.38}$$

Taking into account theoretical uncertainty caused by Λ, our estimate for the cross section $\sigma(pp \to X_b)$ is

$$\sigma(pp \to X_b) \sim \begin{cases} (1.8, 14)\ \text{nb} & \text{for Herwig} \\ (3.6, 27)\ \text{nb} & \text{for Pythia} \end{cases}. \tag{4.39}$$

However, after considering the branching ratio $\mathcal{B}(X_b \to \Upsilon(1S)\pi^+\pi^-)$ which is expected to be tiny because of isospin breaking (we will discuss this later), our result given in Eq. (4.39) is consistent with the CMS upper bound in Eq. (4.38).

4.5 Discussions

Our numerical results may only be regarded as an order-of-magnitude estimate. This is because the short-distance physics of the production was only estimated by varying Λ in the range of [0.5, 1] GeV, as well as other effects such as the cross-channel FSI were completely neglected and so on.

As we have discussed above, the X_b and X_{b2} are isosinglets and their isospin breaking decays will be heavily suppressed in sharp contrast to the $X(3872)$. As a consequence, we can not simply draw an analogy to the decay $X(3872) \to J/\psi\pi^+\pi^-$ and attempt to search for its partner X_b in the similar $\Upsilon(1S, 2S, 3S)\pi^+\pi^-$ channels, because the isospin of the $\Upsilon(1S, 2S, 3S)\pi^+\pi^-$ systems is one when the quantum numbers are $J^{PC} = 1^{++}$. This explains why the CMS Collaboration got the negative search result [151]. The possible channels that can be used to search for the X_b and X_{b2} include the $\Upsilon(nS)\gamma$ ($n = 1, 2, 3$), $\Upsilon(1S)\pi^+\pi^-\pi^0$ and $\chi_{bJ}\pi^+\pi^-$. In addition, the X_{b2} can also decay into $B\bar{B}$ in a D-wave, and the decays of the X_{c2} are similar to those of the X_{b2} with the bottom being replaced by its charm analogue. Since the mass of the X_{c2} is about 140 MeV larger than that of the $X(3872)$, therefore the phase space difference between the $J/\psi\rho$ and $J/\psi\omega$ becomes negligible. As a result, the isospin breaking decay $X_{c2} \to J/\psi\pi^+\pi^-$ through an intermediate ρ meson should be largely suppressed compared with the decay of the $X(3872)$ into the same particles.

The $\Upsilon(nS)\gamma$ ($n = 1, 2, 3$) final states are advantageous compared with the pionic decays, because no pion needs to be disentangled from the combinatorial background. However, the disadvantage is also obvious, that is the low efficiency in reconstructing a photon at hadron colliders. The $X(3872)$ meson has a sizable partial decay width into the $J/\psi\gamma$ channel [77]

$$\mathcal{B}(X(3872) \to \gamma J/\psi) > 6 \times 10^{-3}, \tag{4.40}$$

which is expected to be comparable with the branching ratio for the $X_b \to \gamma\Upsilon$, see Ref. [152] for an estimate. If the estimate is reasonable, the cross section for the $pp \to X_b \to \gamma\Upsilon(1S) \to \gamma\mu^+\mu^-$ is of $O(10\ \text{fb})$ or even larger when summing up the $\Upsilon(1S, 2S, 3S)$. Consequently, we can expect at least a few hundred events according to the fact that the CMS and ATLAS Collaborations have accumulated more than 20 fb^{-1} data [104, 105]. At the LHCb detector, less events will be collected, about $O(3\ \text{fb}^{-1})$ [153],

due to the smaller integrated luminosity. However, a data sample of about 3000 fb^{-1} will be collected, for instance by ATLAS after the upgrade [154], and the future prospect is bright for the production.

As we know a signal could be buried by a huge background. Thus the background contributions from nonresonant can also play an important role in the search for these molecular states apart from the production rates at hadron colliders. In order to investigate this issue, let us take the X_b as an example. The X_b will be reconstructed in the $\Upsilon + \gamma$ final states. In this process, the inclusive cross section $\sigma(pp \to \Upsilon)$ can serve as an upper bound for the background. From the ATLAS Collaboration, it has been measured at $\sqrt{s} = 7$ TeV as [155]

$$\sigma(pp \to \Upsilon(1S)(\to \mu^+\mu^-)) = (8.01 \pm 0.02 \pm 0.36 \pm 0.31)\ \text{nb}, \tag{4.41}$$

with the kinematic cuts $p_T < 70$ GeV and $|y| < 2.25$. Our results in Tab. 4.3 show that the corresponding cross section for the $pp \to X_b$ is about 1 nb at $\sqrt{s} = 7$ TeV. And it is noteworthy to point out that our kinematic cuts in p_T are more stringent compared to the ones set by the ATLAS Collaboration. If we use the integrated luminosity in 2012, 22 fb^{-1} [104], we can estimate the lower bound for the signal/background ratio

$$\frac{S}{\sqrt{B}} \gtrsim \frac{1 \times 22 \times 10^6 \times 2.48\% \times 10^{-2}}{\sqrt{8 \times 22 \times 10^6}} \simeq 0.4, \tag{4.42}$$

where 2.48% is the branching fraction of the $\Upsilon(1S) \to \mu^+\mu^-$ [77], and 10^{-2} is a rough estimate for the branching fraction of the $X_b \to \Upsilon(1S)\gamma$. The value of the signal/background ratio can be significantly enhanced in the data analysis by employing suitable kinematic cuts which can greatly suppress the background, and accumulating many more events based on the upcoming 3000 fb^{-1} data [154].

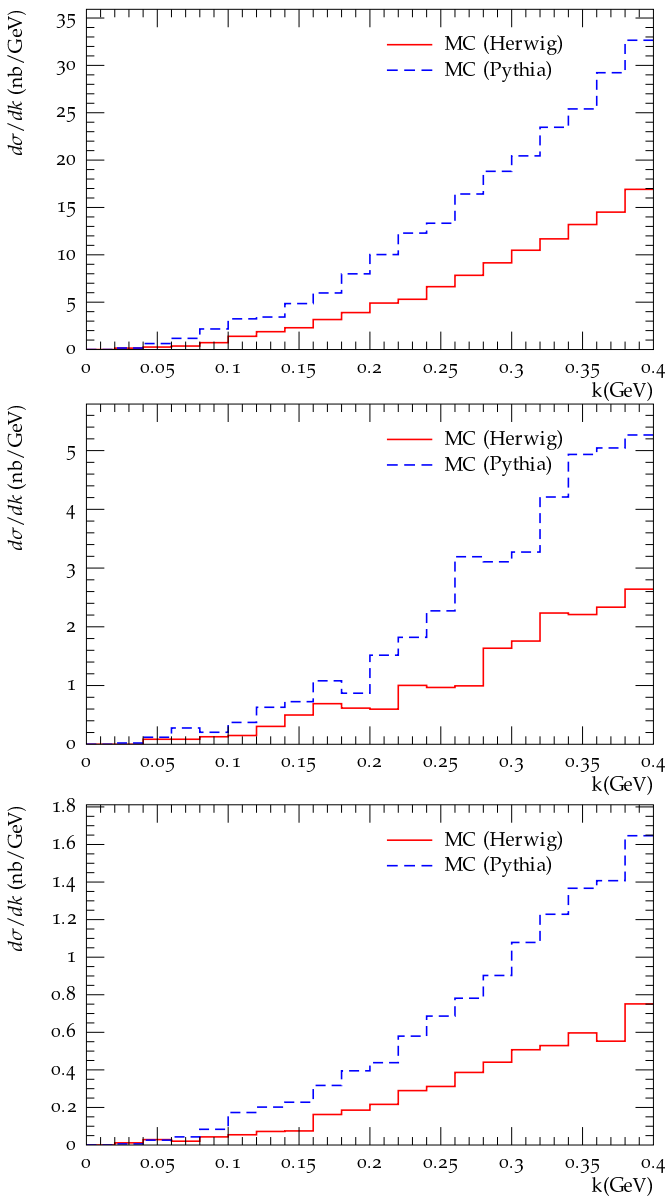

Figure 4.3: Differential cross sections $d\sigma/dk$ (in units of nb/GeV) for the process $pp \to B^0\bar{B}^{*0}$ at the LHC with $\sqrt{s}$ = 8 TeV (the first and second panels) and at the Tevatron with $\sqrt{s}$ = 1.96 TeV (the third panel). The kinematic cuts for the first panel are used as $|y| < 2.5$ and $p_T > 5$ GeV, which lie in the phase-space regions of the ATLAS and CMS detectors, for the Tevatron experiments (CDF and D0) at 1.96 TeV (the third panel), we use $|y| < 0.6$; the rapidity range $2.0 < y < 4.5$ is used for LHCb (the second panel). The solid and dashed lines are from Herwig and Pythia generators, respectively.

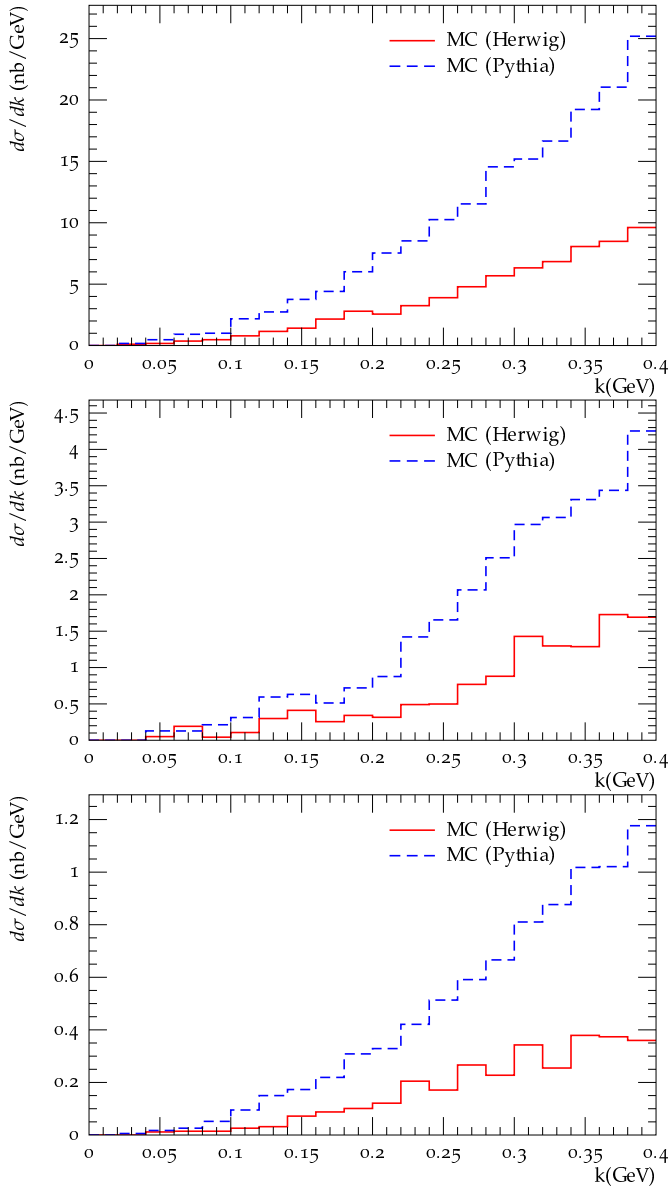

Figure 4.4: Differential cross sections $d\sigma/dk$ (in units of nb/GeV) for the process $pp \to B^{*0}\bar{B}^{*0}$ at the LHC with $\sqrt{s}$ = 8 TeV (the first and second panels) and at the Tevatron with $\sqrt{s}$ = 1.96 TeV (the third panel). The kinematic cuts for the first panel are used as $|y| < 2.5$ and $p_T > 5$ GeV, which lie in the phase-space regions of the ATLAS and CMS detectors, for the Tevatron experiments (CDF and D0) at 1.96 TeV (the third panel), we use $|y| < 0.6$; the rapidity range $2.0 < y < 4.5$ is used for LHCb (the second panel). The solid and dashed lines are from Herwig and Pythia generators, respectively.

Part II

Rescattering of final states in heavy hadron decays

CHAPTER 5

Production of the spin partner of $X(3872)$ through charmonium decay

Although the $X(3872)$ has been observed by many other experiments after its discovery [112, 116, 148, 156–158], no evidence for the existence of its spin partner has been reported. In Chapter 4, we investigated the prompt production of the $X(3872)$ and its spin partner denoted as X_{c2} there, based on the hadronic molecular assumption. It was shown that there is a significant potential for the discovery of these states.

On the other hand, Ref. [8] reported the study on the production of the $X(3872)$ as a $D\bar{D}^*$ molecule in charmonia radiative transitions. In that paper, it was shown that the favorite energy regions for the $X(3872)\gamma$ production are around the $Y(4260)$ mass and 4.45 GeV. Later on, the BESIII Collaboration observed events for the process $Y(4260) \to X(3872)\gamma$ [7], which may be regarded as a support of the dominantly molecular nature of the $X(3872)$. The existence of the $D^*\bar{D}^*$ bound state is the consequence of the heavy quark spin symmetry of the molecular nature of the $X(3872)$, its mass can be derived later by heavy quark spin symmetry as around 4012 MeV. Thus we denote the spin partner as $X_2(4012)$ in this chapter. In this chapter, we will investigate the production of the $X_2(4012)$ associated with the photon radiation in electron–positron collisions as an extension of Ref. [8]. The production of the $X_2(4012)$ in e^+e^- collisions in the energy range of the BESIII experiment [159] thus provides an opportunity to search for new charmonium-like states on the one hand and can offer useful information towards understanding the $X(3872)$ on the other hand. The main calculations and discussions of this part are taken from our published paper in Refs. [160].

We will organize this chapter as follows. We first give a brief Introduction in Section 5.1. Then, we will illustrate the production mechanism and give the effective Lagrangians in Section 5.2. After that, we will give the results with a simple treatment of the width of the intermediate meson in Section 5.3, followed by the momentum-dependent width in Section 5.4. The last section serves as a summary.

5.1 Introduction

In the heavy quarkonium mass region, the so called XYZ states have been observed, and many of these quarkonium-like states defy a conventional quark model interpretation. They are therefore suggested to be exotic. The $X(3872)$, discovered by the Belle Collaboration [111], is the one of the most interesting exotic states. As the mass of the $X(3872)$ is extremely close to the $D^0\bar{D}^{*0}$ threshold, it is regarded as one especially promising candidate for a hadronic molecule.

Effective field theory (EFT) can cope with the interaction between heavy mesons in bound state systems at low energies. For such a kind of systems, heavy quark symmetry is relevant due to the presence of the heavy quark/antiquark in the meson/antimeson. This fact leads to predictions of new states as partners of the observed XYZ states in the hadron spectrum. For example, with an EFT description of the heavy mesonic molecules, the heavy quark symmetry can be used to predict the existence of the spin and bottom partners of the $X(3872)$ [13, 133].

The spin partner of the $X(3872)$, called $X_2(4012)$ hereafter, is predicted to exist as the S-wave bound state of $D^*\bar{D}^*$ with quantum numbers 2^{++} [133]. Such a state was also expected to exist in other models, see Refs. [127, 161–164]. It is different from the $X(3872)$ in several aspects: first, being an isoscalar state it should decay into the $J/\psi\pi\pi\pi$ with a branching fraction much larger than that for the $J/\psi\pi\pi$ because the $J/\psi\rho$ and $J/\psi\omega$ thresholds are far below the mass of the $X_2(4012)$ (very different to the case of the $X(3872)$); second, it is expected to decay dominantly into open charm mesons, $D\bar{D}$, $D\bar{D}^*$ and $D^*\bar{D}$, in a D-wave with a width of the order of a few MeV [165]; third, its mass as set by the $D^*\bar{D}^*$ threshold is higher than the quark model prediction for the first radially excited χ_{c2} [32].

The significance of the $X_2(4012)$ state is that its mass should be approximately given by the

$$M_{X_2(4012)} \approx M_{X(3872)} + M_{D^*} - M_D \approx 4012 \text{ MeV} \tag{5.1}$$

as dictated by heavy quark spin symmetry for heavy-flavor hadronic molecules [13, 73]. One also can derive its mass with explicit calculation as shown in Section. 4.1, and get the same value predicted in Tab. 4.1. Notice that a state with the same quantum numbers 2^{++} was also predicted in the tetraquark model [166]. However, the fine splitting between the 2^{++} and 1^{++} tetraquarks, which was predicted to be 70 MeV in Ref. [166], is not locked to that between the D^* and D. Similarly, the splitting between the $2P$ $c\bar{c}$ states in the Godfrey–Isgur quark model is 30 MeV [32], also much smaller than $M_{D^*} - M_D$. Therefore, if a 2^{++} state will be observed in experiments with a mass around 4012 MeV, the mass by itself would already be a strong support for the hadronic molecular nature of both the $X(3872)$ and the tensor state. As a result, searching for a 2^{++} state with a mass around 4012 MeV is very important even for understanding the nature of the $X(3872)$.

5.2 Production mechanism

The production of the $X(3872)$ through the radiative decay of the $\psi(4160)$ charmonium is considered in Ref. [167] using heavy hadron chiral perturbation theory along with the X-EFT [168]. Then, Ref. [8] studied the $X(3872)$ production by considering the contribution from intermediate charmed meson loops, and it was argued that the dominant mechanism is as follows: the initial charmonium is coupled to a pair of charmed mesons with one being S-wave with $s_\ell^P = \frac{1}{2}^-$, where s_ℓ is the total angular momentum of the light-flavor cloud in the charmed meson, and the other being P-wave with $s_\ell^P = \frac{3}{2}^+$, and the P-wave charmed meson radiatively transits to a $D(D^*)$ which coalesces with the other S-wave charmed meson, $\bar{D}^*(\bar{D})$, into the $X(3872)$. The spin partner of $X(3872)$, the $X_2(4012)$, can be produced by a similar mechanism as shown in Fig. 5.1.

In the triangle loop, all the heavy-light mesons can be considered as nonrelativistic. Thus the three-point

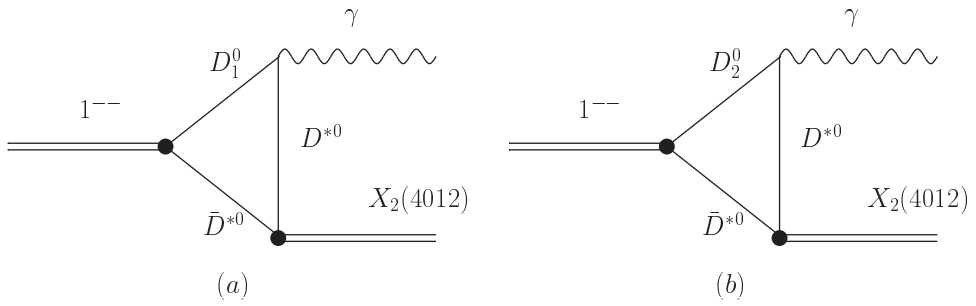

Figure 5.1: Relevant triangle diagrams for the production of the $X_2(4012)$ in vector charmonia radiative decays. The charge-conjugated diagrams are not shown here.

loop function can be evaluated simply

$$\begin{aligned} I(m_1,m_2,m_3) &= i\int \frac{d^dl}{(2\pi)^d}\frac{1}{(l^2-m_1^2+im_1\Gamma_1)[(P-l)^2-m_2^2+i\epsilon][(l-q)^2-m_3^2+i\epsilon]} \\ &= \frac{\mu_{12}\mu_{23}}{16\pi m_1 m_2 m_3}\frac{1}{\sqrt{a}}\Bigg[\tan^{-1}\left(\frac{c_{23}-c_{12}+i\mu_{12}\Gamma_1}{2\sqrt{a(c_{12}-i\mu_{12}\Gamma_1)}}\right) \\ &\quad +\tan^{-1}\left(\frac{2a+c_{12}-i\mu_{12}\Gamma_1-c_{23}}{2\sqrt{a(c_{23}-a)}}\right)\Bigg], \end{aligned} \tag{5.2}$$

where m_1, m_2 and m_3 are the masses of the intermediate heavy mesons. Γ_1 is the width of first meson, here we take it as a constant. Generally, the width is momentum-dependent and we will discuss later. And $a=\left(\frac{\mu_{23}}{m_3}\right)^2\vec{q}^{\,2}$, $b_{12}=m_1+m_2-M$, $b_{23}=b_{12}+m_3-M+q^0$, $c_{12}=2\mu_{12}b_{12}$, $c_{23}=2\mu_{23}(b_{23}+\frac{\vec{q}^2}{2m_3})$ and $\mu_{ij}=m_im_j/(m_i+m_j)$ are the reduced mass. More details can be found in the Appendix D.2.

Notice that the $X_2(4012)$ couples to $D^*\bar{D}^*$ instead of $D\bar{D}^*+c.c.$, as it is in the case of the $X(3872)$. We will only consider the neutral charmed mesons in the loops because the photonic coupling between the P-wave and S-wave charmed mesons for the neutral ones is much larger than that for the charged ones. This is due to cancellation of contributions from the charm and down quarks in the charged mesons, see, e.g. [169]. In the loops, the $X_2(4012)$ couples to the $D^{*0}\bar{D}^{*0}$ pair in an S-wave. With the quantum numbers being 1^{--}, the initial charmonium can couple to one P-wave and one S-wave charmed meson in either S- or D-wave. Since both the initial charmonium and the $X_2(4012)$ in the final state are close to the corresponding thresholds of the charmed-meson pairs, we are able to use a power counting in velocity of the intermediate mesons. Following the power counting rules as detailed in Ref. [170] and presented in the case of interest in Refs. [8, 171], the dominant contribution comes from the case when the coupling of the initial charmonium to the charmed mesons is in an S-wave. In this case, the initial charmonium should be a D-wave state in the heavy quark limit $m_c\to\infty$ as a consequence of heavy quark spin symmetry [172].

As a result of the approximate heavy quark spin symmetry, one can classify the heavy-light charmed mesons according to the total angular momentum of the light degrees of freedom s_ℓ and collect them in doublet s_ℓ^P with total spin $J=s_\ell\pm\frac{1}{2}$ where the parity $P=(-1)^{l+1}$ and orbital angular momentum l. In

the nonrelativistic limit, the superfields for the $\frac{1}{2}^-$ and $\frac{3}{2}^+$ multiplets using 2×2 matrices are written as

$$H_a = \vec{P}_a^* \cdot \vec{\sigma} + P_a \tag{5.3}$$

$$T_a^i = P_{2a}^{ij}\sigma^j + \sqrt{\frac{2}{3}}\, P_{1a}^i + i\sqrt{\frac{1}{6}}\,\epsilon_{ijk}P_{1a}^j\sigma^k, \tag{5.4}$$

where $\vec{\sigma}$ are the Pauli matrices, P_a, P_a^*, P_{1a} and P_{2a} annihilate the pseudoscalar, vector, axial vector and 2^+ tensor charmed mesons, respectively. More details are shown in Section 2.2.3. Besides, the field for the D-wave 1^{--} charmonium state can be written as

$$J^{ij} = \frac{1}{2}\sqrt{\frac{3}{5}}\left(\psi^i\sigma^j + \psi^j\sigma^i\right) - \frac{1}{\sqrt{15}}\delta^{ij}\,\vec{\psi}\cdot\vec{\sigma}, \tag{5.5}$$

where ψ annihilates the D-wave vector charmonium. The general nonrelativistic formula for the orbital angular momentum $L = 2$ multiplet is shown in Eq. (2.65). Here the spin-2 and spin-3 states are irrelevant for our study and they are not shown above. In order to calculate the triangle diagrams in Fig. 5.1, we need the Lagrangian for coupling the D-wave charmonia to the $\frac{1}{2}^-$-$\frac{3}{2}^+$ charmed-meson pair as well as that for the E1 radiative transitions between the charmed mesons [8]

$$\mathcal{L} = \frac{g_4}{2}\mathrm{Tr}\left[\left(\bar{T}_a^{j\,\dagger}\,\sigma^i H_a^\dagger - \bar{H}_a^\dagger\,\sigma^i T_a^{j\,\dagger}\right)J^{ij}\right] + \sum_a \frac{c_a}{2}\,\mathrm{Tr}\left[T_a^i H_a^\dagger\right]E^i + \mathrm{H.c.}, \tag{5.6}$$

where E^i is the electronic field, c_a is the coefficients dependent on the light flavor and in the first term the Einstein summation convention is used while for the latter we distinguish the coupling constants for different light flavors because there is no isospin symmetry in the electromagnetic interaction. Moreover, we parametrize the coupling of the $X_2(4012)$ to the pair of vector charm and anticharm mesons as

$$\mathcal{L}_{X_2} = \frac{x_2}{\sqrt{2}}X_2^{ij\,\dagger}\left(D^{*0\,i}\bar{D}^{*0\,j} + D^{*+\,i}D^{*-\,j}\right) + \mathrm{H.c.}. \tag{5.7}$$

In order to quantify the relative production rate of the $\gamma X_2(4012)$ with respect to the $\gamma X(3872)$, we require the $Y(4260)$ to couple to the $\frac{1}{2}^-$-$\frac{3}{2}^+$ meson pair as follows

$$\begin{aligned}\mathcal{L}_Y = {}& \frac{y}{\sqrt{2}}Y^{i\,\dagger}\left(D_{1a}^i\bar{D}_a - D_a\bar{D}_{1a}^i\right) + i\frac{y'}{\sqrt{2}}\epsilon^{ijk}Y^{i\,\dagger}\left(D_{1a}^j\bar{D}_a^{*\,k} - D_a^{*\,k}\bar{D}_{1a}^j\right)\\ & + \frac{y''}{\sqrt{2}}Y^{i\,\dagger}\left(D_{2a}^{ij}\bar{D}_a^{*\,j} - D_a^{*\,j}\bar{D}_{2a}^{ij}\right) + \mathrm{H.c.},\end{aligned} \tag{5.8}$$

where we have assumed isospin symmetry in the couplings and the flavor index a runs over up and down quarks. Notice that if the $Y(4260)$ is a pure $D_1\bar{D}$ (here and in the following the charge conjugated channels are dropped for simplicity) molecule [173, 174], it would not couple to the $D_1\bar{D}^*$ and $D_2\bar{D}^*$ as given by the y' and y'' terms, and thus cannot decay into the $\gamma X_2(4012)$. These two terms are included to allow the decay to occur. Actually, the $Y(4260)$ may have $D_1\bar{D}^*$ and $D_2\bar{D}^*$ components, and the possibility was discussed in Ref. [175]. Because the $X_2(4012)$ is the spin partner of the $X(3872)$, for a rough estimate, we can assume that x_2 takes the same value as the coupling constant of the $X(3872)$ to the $D\bar{D}^*$. We also assume that the values of y' and y'' are related to y by a spin symmetry relation for D-wave charmonia. Their relation to y can be obtained by comparing the coupling of D-wave charmoinium to the corresponding charmed mesons in Eq. (5.6) with Eq. (5.8), and we get $y' = -y/2$ and $y'' = \sqrt{6}y/10$.

5.3 Results

As we mentioned we take the assumption that the $X_2(4012)$ and $Y(4260)$ are pure hadronic molecules. Since the $X_2(4012)$ and $Y(4260)$ are slightly below the corresponding S-wave threshold, the effective coupling to the constituents can be written as [176]

$$g^2_{\rm NR} = \frac{16\pi}{\mu}\sqrt{\frac{2\epsilon}{\mu}}\left[1 + O\left(\sqrt{2\mu\epsilon}\, r\right)\right] \tag{5.9}$$

under the nonrelativistic normalization. In this equation, $\mu = m_1 m_2/(m_1 + m_2)$ is the reduced mass, the binding energy $\epsilon = m_1 + m_2 - M$ and r is the range of forces. Thus the coupling constants y and x_2 in Eq. (5.7) and Eq. (5.8) can be given by the above equation [177].

By taking the PDG [77] data for the corresponding masses, we get that the threshold of D^0 and D^{*0} is (3871.80 ± 0.12) MeV and the mass of the $X(3872)$ is (3871.69 ± 0.17) MeV [77]. With $M_Y = (4251 \pm 9)$ MeV, and the isospin averaged masses of the D and D_1 mesons, we derive the mass differences between the $X(3872)$ and $Y(4260)$ and their corresponding thresholds, respectively,

$$M_{D^0} + M_{D^{*0}} - M_X = (0.11 \pm 0.21)\ \text{MeV}, \qquad M_D + M_{D_1(2420)} - M_Y = (38.38 \pm 9.09)\ \text{MeV}. \tag{5.10}$$

Since the $X_2(4012)$ has a similar binding energy to that of the $X(3872)$ due to the heavy quark spin symmetry [133], we take the binding energy of $X_2(4012)$ to be 0.11 MeV. Then, we obtain

$$|x_2| = 0.86\ \text{GeV}^{-1/2}, \qquad |y| = 3.59^{+0.20}_{-0.23} \pm 1.87\ \text{GeV}^{-1/2}\,, \tag{5.11}$$

where the first errors above are due to the uncertainties of the binding energies of $Y(4260)$, and the second ones are from the approximate nature of Eq. (5.9). The range of forces is estimated by $r^{-1} \sim \sqrt{2\,\mu\,\Delta_{\rm th}}$ where $\Delta_{\rm th}$ is the difference between the threshold of the components and the next close one, which is $M_{D_1} + M_{D^*} - M_{D_1} - M_D$ for the $Y(4260)$.

With the Lagrangians and the loop function shown in last section, we can now proceed to calculate quantitatively the production of the $\gamma X_2(4012)$ in electron–positron collisions. The amplitude for the Feynman diagrams in Fig. 5.1 is written as

$$\mathcal{M} = -\frac{ic_u g_4}{2\sqrt{15}} E_\gamma x_2 \varepsilon^i(\psi)\varepsilon^j(\gamma)\varepsilon^{ij}(X_2)\left(5I[D_1^0, \bar{D}^{*0}, D^{*0}] - I[D_2^0, \bar{D}^{*0}, D^{*0}]\right), \tag{5.12}$$

where E_γ is the energy of the photon and $\varepsilon(\psi)$, $\varepsilon(\gamma)$ and $\varepsilon(X_2)$ are the corresponding polarization vectors.

Although in the heavy quark limit the production of the D-wave vector heavy quarkonium or the pair of $\frac{1}{2}^-$ and $\frac{3}{2}^+$ heavy mesons are suppressed due to the heavy quark spin symmetry [172], we can expect a large spin symmetry breaking in the charmonium mass region above 4 GeV. This may be seen from similar values of electronic widths of the excited vector charmonia. Thus, we will assume that the production of the $\gamma X_2(4012)$ occurs through the D-wave charmonia or the D-wave components of excited vector charmonia.

We have made a quantitative estimation for coupling constant $|x_2|$, while g_4 is still unknown. Without any detailed information about the values of the coupling constants, we can predict the energy regions with the maximal production cross sections. In Fig. 5.2, we show the dependence of the decay width of a D-wave charmonium into the $\gamma X_2(4012)$, divided by $(g_4 x_2)^2$, on the mass of the D-wave charmonium or the center-of-mass energy of the e^+e^- collisions. The value of the photonic coupling c_u does not

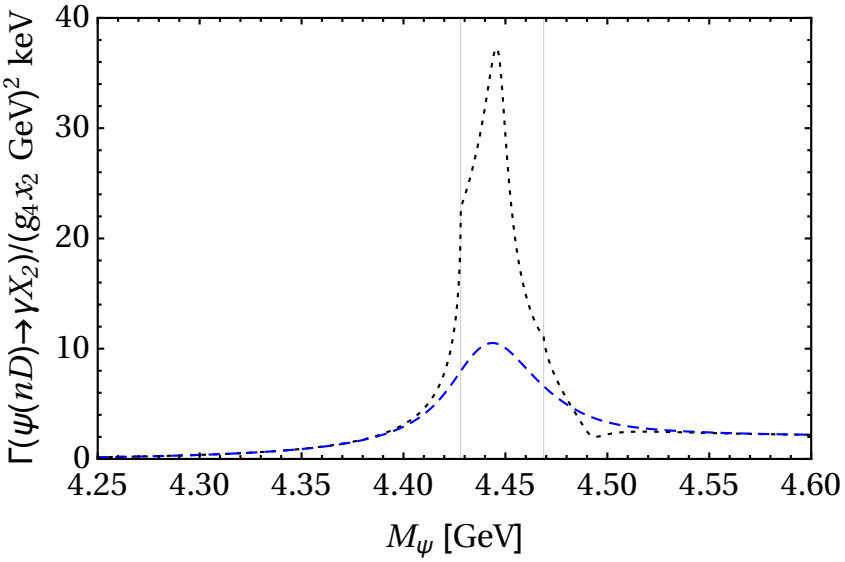

Figure 5.2: Dependence of the partial decay width of a D-wave charmonium into $\gamma X_2(4012)$ on the mass of the charmonium. The dashed and dotted curves are obtained with and without taking into account the widths of the $D_1(2420)$ and $D_2(2460)$, respectively. The left and right solid lines are the $D_1\bar{D}^*$ and $D_2\bar{D}^*$ thresholds, respectively. Here, $c_u = 0.4$ is used.

affect the shape of the dependence either. Nevertheless, we took $c_u = 0.4$ which is a typical value evaluated from various quark model predictions for the decay widths $\Gamma(D_1^0 \to \gamma D^{(*)0})$ [178–180]. In the figure, the dashed curve is obtained neglecting the widths of the D_1 and D_2 states, and the dashed curve is the result of evaluating the triangle loop integrals with constant widths for the D_1 and D_2. The left and right solid lines corresponds to the $D_1\bar{D}^*$ and $D_2\bar{D}^*$ thresholds, respectively. The maximum around 4.447 GeV and the local minimum around 4.492 GeV of the dotted curve are due to the presence of Landau singularities [181] of triangle diagrams in the complex plane at $(4.447 \pm i\,0.003)$ GeV (for the D_1 loop) and $(4.492 \pm i\,0.003)$ GeV (for the D_2 loop), respectively (for a discussion of the Landau singularities in the triangle diagrams of heavy quarkonium transitions, we refer to Ref. [171]). The two cusps on both sides of the shoulders of the peak show up at the thresholds of the $D_1\bar{D}^*$ and $D_2\bar{D}^*$.

From the figure, it is clear that the ideal energy regions for producing the $\gamma X_2(4012)$ in e^+e^- collisions are around the $D_1\bar{D}^*$ and $D_2\bar{D}^*$ thresholds, i.e. between 4.4 GeV and 4.5 GeV. It is also clear that the mass region of the $Y(4260)$ is not good for the production of the $\gamma X_2(4012)$, contrary to the case of the $\gamma X(3872)$. The ratio of the partial decay widths of the $Y(4260)$ to the $\gamma X_2(4012)$ and the $\gamma X(3872)$ can be estimated parameter-free, and is

$$\frac{\Gamma(Y(4260) \to \gamma X_2(4012))}{\Gamma(Y(4260) \to \gamma X(3872))} \approx 10^{-2}\,. \tag{5.13}$$

In the above ratio, whether or not one takes into account the finite widths of the P-wave charmed mesons only results in a minor change of 2%. It is clear that unless the $Y(4260)$ couples to the $D_1\bar{D}^*$ and/or $D_2\bar{D}^*$ with a coupling much larger than that for the $D_1\bar{D}$, which is less possible, the branching fraction of the $Y(4260) \to \gamma X_2(4012)$ is much smaller than that of the $Y(4260) \to \gamma X(3872)$. Given that the number of events for the latter process as observed at BESIII is the order of 10 [7], it is unlikely to make an observation of the $\gamma X_2(4012)$ at an energy 4.26 GeV at BESIII.

5.4 Momentum-dependent width

In last section, we have obtained the results when the width of the first intermediate meson is taken to be a constant. Here only one meson in the triangle diagram is allowed to have finite width, otherwise there would be not apparent threshold effect. Generally, in momentum space, the propagator of intermediate meson with infinitesimal width can be written as

$$B(s) = \frac{1}{s - m^2 + i\epsilon},$$

where m is the mass of the intermediate meson and s is the square of the momentum. This is for the case of scalar and pseudoscalar mesons, while for the vector and axial vector mesons we can get the same formula if we take the nonrelativistic approximation. If the width can not be neglected, we can make the replacement $\epsilon \to m\,\Gamma$. The naive way of dealing the width Γ is to set it as a constant, that is what we do in last section. However, the width should be dependent on the momentum square s. This effect may be included using the spectral function of the intermediate resonance. For instance, whenever it appears in an amplitude, such as $B(s)A(s)$, we replace the expression by

$$B(s)A(s) \to \frac{1}{\mathcal{W}} \int_{s_{thr}}^{\infty} ds' \frac{\rho(s')A(s')}{s' - s - i\epsilon}, \tag{5.14}$$

where $\rho(s)$ is the spectral function, $\mathcal{W}$ is the normalization factor

$$\mathcal{W} = \int_{s_{thr}}^{\infty} \rho(s')ds'. \tag{5.15}$$

and s_{thr} is the square of threshold of the decay channel. Therefore we can replace the loop function in Eq. (5.2) neglecting the constant width of the intermediate meson with a new one.

- For the D_1 in the first diagram of Fig. 5.1, its dominant decay channel is $D^*\pi$ in a D-wave coupling. One can easily find that $\Gamma_{D_1}(s) = g^2 p_{cm}^5/(8\pi f_\pi M_{D_1}\sqrt{s})$, where $p_{cm} = \lambda(s, m_D^2, m_\pi^2)/(2\sqrt{s})$ is the center of mass momentum with $\lambda(x, y, z) = x^2 + y^2 + z^2 - 2xy - 2yz - 2xz$. Thus we can make the replacement

$$I(m_{D_1}, m_{D^*}, m_{D^*}) \to \frac{1}{\mathcal{W}_1} \int_{s_{thr}}^{\infty} ds'\rho(s')I(\sqrt{s'}, m_2, m_3) \tag{5.16}$$

  with the spectral function

$$\rho(s) = -\frac{1}{\pi}\mathrm{Im}\left[\frac{1}{s - m_{D_1}^2 + i m_{D_1}\Gamma_{D_1}}\right] = \frac{1}{\pi}\frac{m_{D_1}\Gamma_{D_1}}{(s - m_{D_1}^2)^2 + m_{D_1}^2\Gamma_{D_1}^2} \tag{5.17}$$

  and the normalization factor

$$\mathcal{W}_1 = \int_{s_{thr}}^{\infty} \rho(s)ds. \tag{5.18}$$

  where $s_{thr} = (m_{D^*} + m_\pi)^2$.

- For the D_2 in the second diagram of Fig. 5.1, it has D-wave coupling to $D\pi$ and $D^*\pi$ channels. Thus $\Gamma_{D\pi}(s) = g^2 p_{cm}^5/(8\pi f_\pi M_{D_2}\sqrt{s})$ and $\Gamma_{D^*\pi}(s) = 3g^2 p_{cm}^5/(4\pi f_\pi M_{D_2}\sqrt{s})$. Thus we can make the

replacement

$$I(m_{D_2}, m_{D^*}, m_{D^*}) \to \frac{1}{\mathcal{W}_2}\left[\int_{s_{thr1}}^{\infty} ds'\rho_1(s')I(\sqrt{s'}, m_2, m_3) + \int_{s_{thr2}}^{\infty} ds'\rho_2(s')I(\sqrt{s'}, m_2, m_3)\right] \quad (5.19)$$

with the spectral functions

$$\rho_1(s) = \frac{1}{\pi}\frac{m_{D_1}\Gamma_{D\pi}}{(s-m_{D_2}^2)^2 + m_{D_2}^2(\Gamma_{D\pi}+\Gamma_{D^*\pi})^2}, \quad (5.20)$$

$$\rho_2(s) = \frac{1}{\pi}\frac{m_{D_2}\Gamma_{D^*\pi}}{(s-m_{D_2}^2)^2 + m_{D_1}^2(\Gamma_{D\pi}+\Gamma_{D^*\pi})^2} \quad (5.21)$$

and the normalization factor

$$\mathcal{W}_2 = \int_{s_{thr1}}^{\infty}\rho_1(s)ds + \int_{s_{thr2}}^{\infty}\rho_2(s)ds, \quad (5.22)$$

where $s_{thr1} = (m_D + m_\pi)^2$, $s_{thr2} = (m_{D^*} + m_\pi)^2$.

In the above formulae, the coupling constant g can be estimated by using the value $\Gamma_{D_1}(M_{D_1}) = 27.1$ MeV.

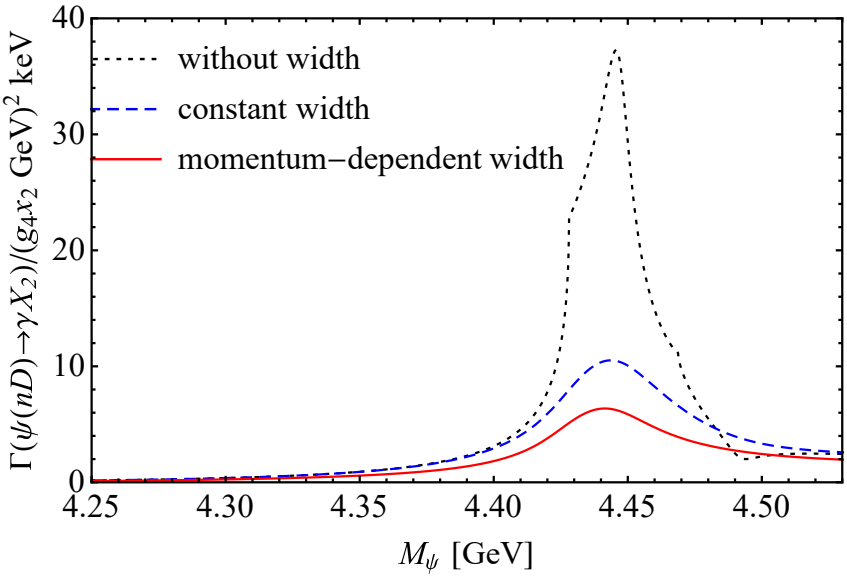

Figure 5.3: The partial decay width as Fig. 5.2, but with the width of intermediate meson considered. The dashed line is the result of a constant width, while the solid line is from the momentum-dependent width.

The partial decay width with momentum-dependent width is shown in Fig. 5.3 as the solid line, where the results without width and with a constant width are shown as dotted and dashed lines, respectively. One finds that the enhancement due to the triangle diagram with either a constant or momentum-dependent width is much smaller than the one without any width. The enhancement is related to the kinematical triangle singularity to be discussed in Chapter 7. However, our conclusion made above that the ideal energy regions for producing the $\gamma X_2(4012)$ in e^+e^- collisions are between the $D_1\bar{D}^*$ and $D_2\bar{D}^*$ thresholds remains the same.

5.5 Summary

To summarize, it is generally expected that the $X(3872)$ as a hadronic molecule has a spin partner close to the $D^*\bar{D}^*$ threshold. In this chapter, we have investigated the production of the $\gamma X_2(4012)$ in e^+e^- collisions. According to our calculation, we strongly suggest to search for the $X_2(4012)$ associated with a photon in the energy region between 4.4 GeV and 4.5 GeV in e^+e^- collisions. Besides, the width ratio of the $Y(4260)$ decaying to $\gamma X_2(4012)$ and $\gamma X(3872)$ is quite small, at the order of 10^{-2}. Thus observing the $\gamma X_2(4012)$ at an energy around 4.26 GeV would be unlikely in the BESIII experiment according to the current result for $Y(4260) \to \gamma X(3872)$.

CHAPTER 6

Hindered $M1$ transition between two bottomia

We have seen in the previous chapters that meson loops are the driving force for producing hadronic molecules. In fact, they may also play a significant role in certain heavy quarkonium processes, for instance the ones to be discussed in this chapter.

The effects of intermediate mesons can enhance the transitions compared to the corresponding tree-level contributions. For example, the charmed meson loops can play an important role in the transitions between two charmonia with one emitted light pseudoscalar meson [170]. In the hindered magnetic dipole transitions of heavy quarkonia, the coupled-channel effects originate from the coupling of quarkonia to a pair of heavy and anti-heavy mesons. In this chapter, we will study the hindered magnetic dipole transitions between two P-wave bottomonia, $\chi_b(nP)$ and $h_b(n'P)$, with $n \neq n'$. In these processes the coupled-channel effects are expected to lead to partial widths much larger than the quark model predictions. The main calculations and discussions of this chapter are taken from our paper in Ref. [182].

We will organize this chapter as follows. We first give a short introduction in Section 6.1. And then we will analyze the power counting of the transition amplitudes of tree-level diagrams in the quark model, as well as one-loop and two-loop diagrams in the nonrelativistic effective field theory in Section 6.2. In Section 6.3, we will give the relevant effective Lagrangians we need for calculating the triangle diagram. Then the results are given in Section 6.4. The last section serves as a summary.

6.1 Introduction

In recent years, several new bottomonia were discovered. One of the most interesting discoveries is the $h_b(1P)$ found in the puzzling π^0 transition $\Upsilon(3S) \to \pi^0 h_b(1P)$ with a subsequent electric dipole (E1) transition to the $\eta_b(1S)$ by the Babar collaboration [183]. This finding is consistent with the prediction that such a transition is a promising way to produce the h_b [184, 185]. The isospin violating decay channel has the same final states, $\gamma\gamma h_b$, as the one in the electromagnetic cascades $\Upsilon(3S) \to \gamma\chi_{bJ}(2P)\,(J = 0, 1, 2)$ and $\chi_{bJ}(2P) \to \gamma h_b$. The branching fractions for the E1 transitions $\Upsilon(3S) \to \gamma\chi_{bJ}(2P)$ are well measured to be of the order of 10%, but no experimental result for the hindered magnetic dipole (M1) transition $\chi_{bJ}(2P) \to \gamma h_b$ is available. Thus, it is important to investigate the decay channel $\chi_{bJ}(2P) \to \gamma h_b$. The $h_b(1P)$ later on was also observed in the isospin conserving decay process $\Upsilon(4S) \to \eta h_b$ [186] with a branching fraction $(2.18 \pm 0.21) \times 10^{-3}$, consistent with the estimate of the order 10^{-3} in Ref. [187], where this channel was suggested to be used to search for the h_b.

The quark model has been used to study the spectrum and decay properties of the excited bottomonia without the coupled-channel effects from intermediate open-bottom mesons [188]. The spectrum was

also calculated with the inclusion of coupled-channel effects [189]. More generally, we remark that coupled-channel effects due virtual hadronic loops are of recent interest in heavy quarkonium physics. In the quenched quark model, the mixture between the bare hadron states and the two-meson continuum is not taken into account. When the coupled-channel effects are considered, the quarkonium spectrum gets shifted (the values of these mass shifts depend on the specific models, see, e.g., Refs. [189–198]). In addition to the impact on the mass spectrum, the coupled-channel effects are expected to be important in some transitions between heavy quarkonia [51, 170, 199–207]. In particular, they are expected to dominate the hindered M1 transitions between the P-wave quarkonia because of two reasons: first, the hindered M1 transitions break heavy quark spin symmetry and their widths in the quark model come from relativistic corrections; second, the coupled-channel contribution has an enhancement due to the S-wave couplings of the two vertices involving heavy quarkonia [208]. For instance, the partial width of $\chi_{c2}(2P) \to \gamma h_c(1P)$ from the coupled-channel effects is two orders of magnitude larger than the prediction from the quark model as shown in Ref. [208]. Hindered M1 transitions between bottomonia may be measured at Belle-II [209]. However, so far, only few predictions on the hindered M1 transitions in the bottomonium sector have been given, and all of them are based on quark model calculations [188]. Since in bottomonium systems the relativistic corrections are small, the quark model predictions on these partial widths are tiny, in the range from sub-eV to eV. Yet, similar to the charmonia case, the coupled-channel effects due to virtual bottom mesons could enhance the decay widths to values that make an observation possible. This motivates us to study here the hindered M1 transitions between P-wave bottomonia by considering the coupled-channel effects through the coupling to virtual bottom and anti-bottom mesons. An additional important motivation for us to study these processes is the fact that experimentalists plan to study them at the coming Belle-II experiment [209].

6.2 Power counting analysis

We first consider the decay amplitude for an $M1$ transition between two heavy quarkonia in quark models. It is proportional to the overlap of the wave functions of the two quarkonia [188]

$$\Gamma_1 \propto |\langle \psi_f | \psi_i \rangle|^2 E_\gamma^3 , \tag{6.1}$$

where ψ_i and ψ_f are the wave functions of the initial and final heavy quarkonia, respectively, and E_γ is the energy of photon in the rest frame of the initial quarkonium. As discussed in Ref. [208], the transition amplitude starts from $E_\gamma v_b/m_b$ for the process of $2P$ to $1P$, where v_b and m_b are the bottom quark velocity and mass, respectively, and the factor $1/m_b$ is due to the spin-flip of the heavy quark in M1 transitions. Therefore in quark models the transition rates are very small, and only come from relativistic correction.

On the other hand, due to the fact that the bottomonia are close to the open bottom thresholds so that the intermediate bottom mesons in the triangle diagram are nonrelativistic, we can use the nonrelativistic effective field theory (NREFT) suitable for investigating such coupled-channel effects in heavy quarkonia transitions [51, 170, 210]. A P-wave bottomonium couples to a pair of ground state bottom and anti-bottom mesons in an S-wave. At leading order, the coupling is described by a constant which does not contribute any power to the velocity counting. Thus, according to the velocity counting in Section 2.2.3 the triangle diagram in Fig. 6.1 scales as [208]

$$\mathcal{A}_{\text{triangle}} \propto \frac{v^5}{(v^2)^3} \frac{E_\gamma}{m_b} = \frac{E_\gamma}{v m_b}, \tag{6.2}$$

where the factor E_γ accounts for the P-wave coupling of the photon to the bottom mesons. One thus

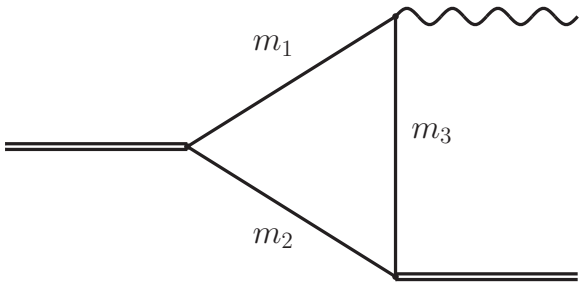

Figure 6.1: Triangle diagram where the double, solid and wavy lines represent the bottomonium, bottomed meson and the photon, respectively.

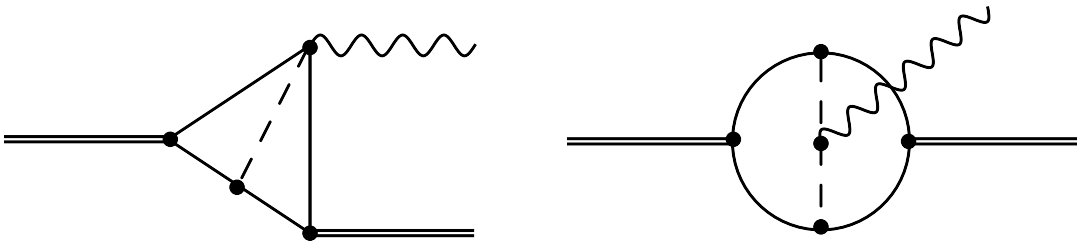

Figure 6.2: Two typical two-loop diagrams where the double, solid and wavy lines are the same as in Fig. 6.1 and the dashed lines represent the exchanged pions.

sees that the closer the bottomnia to the bottom-meson thresholds, the larger the coupled-channel effects. One remark is in order: v in the power counting is in fact the average of two velocities. This can be estimated as $v = (v_i + v_f)/2$ with $v_i = \sqrt{|m_1 + m_2 - M_i|/\bar{m}_{12}}$ and $v_f = \sqrt{|m_2 + m_3 - M_f|/\bar{m}_{23}}$, where $m_{1,2,3}$ are masses of intermediate mesons as labelled in Fig. 6.1, $M_{i(f)}$ is the mass for the initial (final) bottomonium, and $\bar{m}_{jk}$ is the averaged value of m_j and m_k.

However, unlike the case of charmonium hindered M1 transitions, the two-loop diagrams with a pion exchanged between two intermediate bottom mesons are not highly suppressed for the bottomonium transitions. From the power counting analysis in Ref. [208], the photon vertex in the left diagram of Fig. 6.2 does not contribute to the velocity counting, but contribute a factor g/F_π with F_π the pion decay constant and $g \simeq 0.5$ the axial coupling constant for bottom mesons [211–213], which comes from the axial coupling between the bottom-meson with pion, and the vertex scales as $E_\gamma g/F_\pi$. As a result, the two-loop diagram in the left of Fig. 6.2 scales as

$$\begin{aligned} \mathcal{A}_{\text{2-loop}} &\propto \frac{(v^5)^2}{(v^2)^5}\frac{g^2}{(4\pi)^2 F_\pi}\frac{E_\gamma}{m_b}M_B^2 \\ &= \frac{E_\gamma}{m_b}\left(\frac{gM_B}{\Lambda_\chi}\right)^2, \end{aligned} \tag{6.3}$$

where the factor $1/(4\pi)^2$ is taken into account as there is one more loop than in the one-loop case, $\Lambda_\chi = 4\pi F_\pi$ is the chiral symmetry breaking scale, M_B is the bottom meson mass and the factor M_B^2 is introduced in order to make the scaling have the same dimension as $\mathcal{A}_{\text{triangle}}$. One can easily see that the

right diagram in Fig. 6.2 has the same scaling as the left one as the one more propagator in the left one is balanced by two more P-wave vertices. Hence the relative importance of the two-loop diagrams shown in Fig. 6.2 in comparison with the triangle diagram given in Fig. 6.1 can be described by a factor

$$\frac{\mathcal{A}_{\text{2-loop}}}{\mathcal{A}_{\text{triangle}}} \sim v\frac{g^2 M_B^2}{\Lambda_\chi^2}. \tag{6.4}$$

Taking the masses of the $1P$, $2P$ and $3P$ bottomonia from Refs. [77, 214], the velocity in the power counting may be estimated to be 0.31, 0.23 and 0.18 for the $2P \to 1P$, $3P \to 1P$ and $3P \to 2P$ radiative transitions, respectively. One then finds that the relative factor given in Eq. (6.4) is of order one, which means that the contribution of two-loop diagrams like the ones shown in Fig. 6.2 should be of similar size as the one-loop triangle diagram in Fig. 6.1. This is different from the charmonium case studied in Ref. [208] where M_B^2 is replaced by the much smaller M_D^2 and thus leads to a suppression. Nevertheless, we will only calculate the triangle diagram, and keep in mind that given the power counting of the two-loop diagrams such a calculation can only be regarded as an estimate, rather than a precise calculation, with a quantitative uncertainty analysis out of reach.

6.3 Effective Lagrangians

As shown in Section 2.2.3, the heavy meson fields are collected in doublets due to the heavy quark spin symmetry, and can be written in a two-component notation as it is convenient for nonrelativistic calculation. The explicit forms of the doublet H_a and $\bar{H}_a$ read

$$H_a = \vec{P}_a^* \cdot \vec{\sigma} + P_a, \tag{6.5}$$

$$\bar{H}_a = -\vec{\bar{P}}_a^* \cdot \vec{\sigma} + \bar{P}_a, \tag{6.6}$$

where $\vec{\sigma}$ are the Pauli matrices, P_a and P_a^* annihilate the pseudoscalar and vector bottom mesons, respectively. On the other hand, the P-wave spin singlet h_b and triplet χ_{bJ} bottomonia can be collected in a multiplet as

$$\chi^i = \sigma^j \left(\chi_{b2}^{ij} - \frac{1}{\sqrt{2}} \epsilon^{ijk} \chi_{b1}^k + \frac{1}{\sqrt{3}} \delta^{ij} \chi_{b0} \right) + h_b^i \,, \tag{6.7}$$

which is taken from the general nonrelativistic formula for the orbital angular momentum $L = 1$ multiplet shown in Eq. (2.64).

As mentioned above, the leading order coupling of the P-wave bottomonium to the bottom and anti-bottom mesons is in an S-wave, and thus the effective Lagrangian is given by [210, 215]

$$\mathcal{L}_\chi = i\frac{g_1}{2} \text{Tr}[\chi^{\dagger i} H_a \sigma^i \bar{H}_a] + h.c., \tag{6.8}$$

where g_1 is the coupling constant and Tr denotes the trace in the spinor space.

We also need the magnetic coupling of the photon to the S-wave heavy mesons in the two-component notation [52, 206, 216]

$$\mathcal{L}_\gamma = \frac{e\beta}{2} \text{Tr}\left[H_a^\dagger H_b \, \vec{\sigma} \cdot \vec{B} \, Q_{ab} \right] + \frac{e\,Q'}{2m_Q} \text{Tr}\left[H_a^\dagger \, \vec{\sigma} \cdot \vec{B} \, H_a \right], \tag{6.9}$$

where $B^k = \epsilon^{ijk} \partial^i A^j$ is the magnetic field, $Q_{ab} = \text{diag}(2/3, -1/3, -1/3)$ is the light quark electric charge

$\chi_{b0} \to h_b\gamma$	$[B^*, \bar{B}^*, B]$, $[B^*, \bar{B}^*, B^*]$, $[B, \bar{B}, B^*]$
$\chi_{b1} \to h_b\gamma$	$[B^*, \bar{B}, B^*]$, $[B, \bar{B}^*, B^*]$
$\chi_{b2} \to h_b\gamma$	$[B^*, \bar{B}^*, B]$, $[B^*, \bar{B}^*, B^*]$
$h_b \to \chi_{b0}\gamma$	$[B^*, \bar{B}, B]$, $[B, \bar{B}^*, B^*]$, $[B^*, \bar{B}^*, B^*]$
$h_b \to \chi_{b1}\gamma$	$[B^*, \bar{B}, B^*]$, $[B^*, \bar{B}^*, B]$
$h_b \to \chi_{b2}\gamma$	$[B, \bar{B}^*, B^*]$, $[B^*, \bar{B}^*, B^*]$

Table 6.1: Triangle loops contributing to each transition, where the mesons are listed as $[m_1, m_2, m_3]$ corresponding to the notations in Fig. 6.1. For simplicity, the charge conjugation modes and the light flavor labels are not shown here.

matrix, Q' is the heavy quark electric charge (for a bottom quark, $Q' = -1/3$) and m_Q is the mass of the heavy quark. β is a unknown parameter introduced in Ref. [216]. If we compare the tree level predictions for the electromagnetic decay widths of the vector heavy mesons, i.e. $\Gamma(P_a^* \to P_a\gamma)$, with these in the quark model, we can get $\beta = 1/m_q$, where m_q is the light constituent quark mass. One can also fit the parameter β to the experimental results of the electromagnetic decay widths to obtain its value. The first term in the above Lagrangian is the magnetic moment coupling of the light degrees of freedom, which preserves heavy quark spin symmetry. The second term is the magnetic moment coupling of the heavy quark and suppressed by $1/m_Q$.

6.4 Results and discussion

We specify the intermediate mesons in the list $[m_1, m_2, m_3]$, as denoted in Fig. 6.1. All the possible loops with the intermediate pseudoscalar and vector bottomed mesons are listed in Table 6.1 for the corresponding transitions. With the effective Lagrangians given in last section and the loop integral in Eq. (5.2), we can proceed to calculate quantitatively the transition rates. The pertinent amplitudes for the hindered magnetic dipole transitions from $\chi_b(nP)$ to $h_b(n'P)$ are of the form expressed in terms of the triangle loop function

$$\begin{aligned}
\mathcal{M}_{\chi_{b0}\to\gamma h_b} &= -\frac{2iegg'}{\sqrt{3}} q^i \varepsilon^j(\gamma)\epsilon_{ijk}\varepsilon^k(h_b) \sum_{a=u,d,s} \Big\{ 2\left(\beta Q_a + \frac{1}{3m_b}\right) I(B_a^*, \bar{B}_a^*, B_a^*) \\
&\quad + \left(\beta Q_a - \frac{1}{3m_b}\right)\Big[I(B_a^*, \bar{B}_a^*, B_a) - 3I(B_a, \bar{B}_a, B_a^*)\Big]\Big\}, \qquad (6.10) \\
\mathcal{M}_{\chi_{b1}\to\gamma h_b} &= 2i\sqrt{2}egg' \left[\vec{q}\cdot\vec{\varepsilon}(\chi_{b1})\vec{\varepsilon}(\gamma)\cdot\vec{\varepsilon}(h_b) - \vec{q}\cdot\vec{\varepsilon}(h_b)\vec{\varepsilon}(\gamma)\cdot\vec{\varepsilon}(\chi_{b1})\right] \\
&\quad \times \sum_{a=u,d,s} \left[\left(\beta Q_a + \frac{1}{3m_b}\right) I(B_a^*, \bar{B}_a, B_a^*) - \left(\beta Q_a - \frac{1}{3m_b}\right) I(B_a, \bar{B}_a^*, B_a^*)\right], \qquad (6.11) \\
\mathcal{M}_{\chi_{b2}\to\gamma h_b} &= 4iegg'\epsilon_{ijk}\varepsilon^{kl}(\chi_{b2}) \sum_{a=u,d,s} \Big\{ -q^i\varepsilon^j(\gamma)\varepsilon^l(h_b)\left(\beta Q_a - \frac{1}{3m_b}\right) I(B_a^*, \bar{B}_a^*, B_a) \\
&\quad + \varepsilon^i(h_b)\Big[q^l\varepsilon^j(\gamma) - q^j\varepsilon^l(\gamma)\Big]\left(\beta Q_a + \frac{1}{3m_b}\right) I(B_a^*, \bar{B}_a^*, B_a^*)\Big\}. \qquad (6.12)
\end{aligned}$$

The transition amplitudes for the hindered magnetic dipole transitions from $h_b(nP)$ to $\chi_b(n'P)$ are of the form

$$\begin{aligned}
\mathcal{M}_{h_b\to\gamma\chi_{b0}} &= -\frac{2iegg'}{\sqrt{3}} q^i \varepsilon^j(\gamma)\varepsilon^k(h_b)\epsilon_{ijk} \sum_{a=u,d,s} \Big\{ 2\left(\beta Q_a + \frac{1}{3m_b}\right) I(B_a^*, \bar{B}_a^*, B_a^*) \\
&\quad + \left(\beta Q_a - \frac{1}{3m_b}\right)\Big[I(B_a, \bar{B}_a^*, B_a^*) - 3I(B_a^*, \bar{B}_a, B_a)\Big]\Big\}, \qquad (6.13) \\
\mathcal{M}_{h_b\to\gamma\chi_{b1}} &= 2i\sqrt{2}egg' \left[\vec{q}\cdot\vec{\varepsilon}(\chi_{b1})\vec{\varepsilon}(\gamma)\cdot\vec{\varepsilon}(h_b) - \vec{q}\cdot\vec{\varepsilon}(h_b)\vec{\varepsilon}(\gamma)\cdot\vec{\varepsilon}(\chi_{b1})\right] \\
&\quad \times \sum_{a=u,d,s} \left[\left(\beta Q_a + \frac{1}{3m_b}\right) I(B_a^*, \bar{B}_a, B_a^*) - \left(\beta Q_a - \frac{1}{3m_b}\right) I(B_a^*, \bar{B}_a^*, B_a)\right], \qquad (6.14) \\
\mathcal{M}_{h_b\to\gamma\chi_{b2}} &= 4iegg'\epsilon_{ijk}\varepsilon^{kl}(\chi_{b2}) \sum_{a=u,d,s} \Big\{ -q^i\varepsilon^j(\gamma)\varepsilon^l(h_b)\left(\beta Q_a - \frac{1}{3m_b}\right) I(B_a, \bar{B}_a^*, B_a^*) \\
&\quad + \varepsilon^i(h_b)\Big[q^l\varepsilon^j(\gamma) - q^j\varepsilon^l(\gamma)\Big]\left(\beta Q_a + \frac{1}{3m_b}\right) I(B_a^*, \bar{B}_a^*, B_a^*)\Big\}, \qquad (6.15)
\end{aligned}$$

where the initial bottomonium should be understood to be of higher excitation then the final one, $\varepsilon^i(\gamma)$, $\varepsilon^i(h_b)$ and $\varepsilon^i(\chi_{b1})$ are the polarization vectors for the photon, h_b and χ_{b1}, respectively, and $\varepsilon^{ij}(\chi_{b2})$ is the symmetric polarization tensor for the χ_{b2}. One also needs to notice that a factor $\sqrt{M_i M_f}$, with $M_{i,f}$ denoting the masses of the initial and final bottomonia, should be multiplied to each of the amplitudes to account for the nonrelativistic normalizations of the heavy quarkonium fields (similar factors for the intermediate heavy mesons have been absorbed in the definition of the loop function).

From these amplitudes, one clearly sees two sources of spin symmetry breaking: the terms from the bottom quark magnetic moment are explicitly proportional to $1/m_b$, and the sum of β-terms in each amplitude vanishes if the vector and pseudoscalar bottom mesons are taken to be degenerate. For Eqs. ((6.10), (6.11), (6.13), (6.14)) given above, this point is apparent, for Eqs. ((6.12), (6.15)), one can see this after taking the absolute value squared of the amplitude and summing up the polarizations.

The loops involved here are convergent, which means that the coupled-channel effects for the processes of interest are dominated by long-distance physics described in our NREFT. We do not need to introduce a counterterm here. The situation is different for the case of E1 transitions. The loop integrals involved there are divergent, and thus the contact term considered in Ref. [206] also serves as the counterterm and is necessary for renormalization.

Using the masses of the mesons given by the Particle Data Group [77], it is easy to get numerical results for the partial decay widths. As for the masses of the $3P$ bottomonia, we choose the quark model values from Ref. [188], which were obtained based on the measured $\chi_{bJ}(3P)$ mass by the LHCb Collaboration [214] with the predicted multiplet mass splittings, i.e. $M_{h_b(3P)} = 10.519$ GeV, $M_{\chi_{b0}(3P)} = 10.500$ GeV, $M_{\chi_{b1}(3P)} = 10.518$ GeV and $M_{\chi_{b2}(3P)} = 10.528$ GeV. These masses are very close to the ones in Ref. [189], where the coupled-channel effects are taken into account in a nonrelativistic quark model. We also take $\beta = 1/276\ \text{MeV}^{-1}$ [52], and $m_b = 4.9$ GeV.

The decay amplitudes are proportional to the product squared of the coupling constants of the bottom and anti-bottom mesons to the $1P$, $2P$ and $3P$ bottomonia, denoted as g_1, g_1' and g_1'', respectively. As the mass of the $\chi_{bJ}(1P, 2P, 3P)$ and $h_b(1P, 2P, 3P)$ are below the bottom and anti-bottom meson threshold, the coupling constants cannot be measured directly. Here, we show the decay width of the hindered M1 transitions between two P-wave bottomonia in units of the coupling constants in the Table 6.2. The unknown parameters will get cancelled if we calculate ratios of the decay widths which are proportional to the same product squared of coupling constants. Furthermore, we also expect that these ratios are

	$J=0$	$J=1$	$J=2$	units
$\chi_{bJ}(3P) \to h_b(2P)\gamma$	0.3	1.8	1.4	$(g_1' g_1'')^2$ keV
$h_b(3P) \to \chi_{bJ}(2P)\gamma$	0.3	2.2	1.6	$(g_1' g_1'')^2$ keV
$\chi_{bJ}(3P) \to h_b(1P)\gamma$	4.9	13.4	11.9	$(g_1 g_1'')^2$ keV
$h_b(3P) \to \chi_{bJ}(1P)\gamma$	3.3	15.8	15.4	$(g_1 g_1'')^2$ keV
$\chi_{bJ}(2P) \to h_b(1P)\gamma$	1.2	1.8	1.8	$(g_1 g_1')^2$ keV
$h_b(2P) \to \chi_{bJ}(1P)\gamma$	0.7	2.0	2.5	$(g_1 g_1')^2$ keV

Table 6.2: Decay widths for the hindered M1 transitions between $\chi_{bJ}(nP)$ and $h_b(n'P)$, where the coupling constants take values in units of $\text{GeV}^{-1/2}$.

	$J=0$		$J=1$		$J=2$	
	ours	RQM	ours	RQM	ours	RQM
$\frac{\Gamma_{h_b(2P)\to\chi_{bJ}(1P)\gamma}}{\Gamma_{\chi_{bJ}(2P)\to h_b(1P)\gamma}}$	0.59	0.03	1.1	0.5	1.4	9.2

Table 6.3: Comparison of the ratios of the decay widths for the $2P$ to $1P$ bottomonia with the ones from the RQM [188].

less sensitive to the two-loop diagrams in Fig. 6.2 as the numerator and denominator in the ratio, being related to each other via spin symmetry, would get a similar correction. The ratios in our calculation can be easily obtained from Table 6.2. In order to show that the coupled-channel effects lead to very different values for some of these ratios, we show a comparison of ratios for selected decay widths of the hindered M1 transitions between the $2P$ to $1P$ bottomonia with those obtained in the quenched quark model of Ref. [188] in Table 6.3. These predictions can be tested in the future from experiments or lattice QCD calculations. In fact, radiative transitions of S-wave bottomonia, including the hindered M1 ones, have been studied by using lattice QCD [217–219]. As suggested in Ref. [208], one can check the coupled-channel effects directly in lattice QCD by comparing results in full and quenched calculations — the former includes the coupled-channel effects intrinsically while the latter does not.

As mentioned in Ref. [188], the numerical results of these hindered transitions in the quark model are very sensitive to relativistic corrections (these transitions do not vanish only when relativistic corrections are accounted for in the quenched quark model). Nevertheless, they are tiny because the M1 transitions break heavy quark spin symmetry as well, and are in the ballpark of sub-eV to eV in Ref. [188]. If the partial widths really take such small values, an experimental observation of the bottomonium hindered M1 transitions would be impossible in the foreseeable future. In turn, this means that once such transitions are observed, the mechanism would be different from that in the quenched quark model, and would be caused by coupled-channel effects. Then, the measured partial widths can be used to estimate the involved coupling constants.

Unfortunately, the values of the coupling constants g_1, g_1' and g_1'' cannot be estimated reliably. If one takes the model estimate made in Ref. [215],[1] $g_1 = -2\sqrt{m_{\chi_{b0}}/3}/f_{\chi_{b0}}$ and uses the value $f_{\chi_{b0}} \approx 175$ MeV

[1] Here we have replaced the charmonium quantities by the corresponding bottomonium ones, and there is a factor of 2 difference for g_1 in the definition of the Lagrangian in (6.9) and that in Ref. [215].

from a QCD sum rule calculation [220], then one gets $g_1 \sim -20\ \text{GeV}^{-1/2}$. This value is so large that if the χ_{b0} is located only 1 MeV above the $B^0\bar{B}^0$ threshold it would have a huge width of 21 GeV. However, the quark model predictions for the open-bottom partial decay widths of the $4P$ bottomonia leads to $|g_1(4P)| \sim 0.2\ \text{GeV}^{-1/2}$ (the one for the $5P$ states is slightly smaller), which, although it is for the $4P$ states, is two orders of magnitude smaller than that from the former estimate. In Ref. [208], the product of the coupling constants $(g_1 g_1')^2$ is estimated to be of order $O(10\ \text{GeV}^{-2})$ in the charm sector, where the difference between the model estimate for g_1 [215] and the extracted value from quark model predictions of the $2P$ charmonium decay widths is much smaller. If we naively take the same estimate here, despite that there is no simple flavor symmetry between charmonia and bottomonia, then the partial decay widths of $O\left(1 \sim 10^2\right)$ keV could be large enough for a possible measurement in the future.

In principle, we can also calculate the decay widths for the isospin breaking transitions between the $\chi_{bJ}(nP)$ states with the emission of one pion. They would be proportional to the same combination of unknown coupling constants. The charmonium analogues from the coupled-channel effects have been analyzed in details in Ref. [170]. However, we refrain from such a calculation because the isospin breaking between the charged and neutral bottom mesons is one order of magnitude smaller than that in the charmed sector because of the destructive interference between the contributions from the up and down quark mass difference and the electromagnetic effect [221].

6.5 Summary

In summary, we studied the hindered M1 transitions between two P-wave bottomonia, $\chi_b(nP)$ and $h_b(n'P)$ $(n \neq n')$ assuming the mechanism is dominated by coupled-channel effects. Because of the suppression from heavy quark spin breaking and small relativistic corrections, such transitions have tiny partial widths from sub-eV to eV in the quark model. In the mechanism underlying coupled-channel effects, the breaking of heavy quark spin symmetry can come from the different masses of bottom mesons within the same spin multiplet, and the problem of tiny matrix elements for transitions between bottomonia of different principal quantum numbers in the quark model does not exist as well. Therefore, it is natural to expect that the coupled-channel effects lead to much larger widths for such transitions than those predicted in the quark model. A future observation of such transitions at, e.g., Belle-II [209] may be regarded as a clear signal of the coupled-channel effects, and the measured widths could then be used to extract a rough value of the product of the so-far unknown coupling constants, e.g. $g_1 g_1'$. Such information would be useful for other transitions where intermediate bottom mesons play an important role, such as the decays of the $Z_b(10610)$ and $Z_b(10650)$ into $h_b\pi$ and $h_b(2P)\pi$.

At last, we want to emphasize again that the coupled-channel effects in heavy quarkonium transitions can be checked directly in lattice QCD by comparing results from quenched and fully dynamical simulations as we already suggested in Ref. [208]. A better understanding of coupled-channel effects would lead to new insights into the dynamics of heavy quarkonia.

CHAPTER 7

Kinematical effect in the narrow P_c structure

In 2015, the LHCb Collaboration announced that two pentaquark-like structures were observed in the $J/\psi\, p$ invariant mass distribution in the $\Lambda_b^0 \to J/\psi\, K^-\, p$ decays. In this chapter, we will show that the current information on the narrow structure at 4.45 GeV is compatible with kinematical effects of the rescattering from $\chi_{c1}\, p$ to $J/\psi\, p$. The main results and discussions presented here are taken from our published paper in Ref. [222]. In that paper, we observe the following:

- First, it is located exactly at the $\chi_{c1}\, p$ threshold.
- Second, the mass of the four-star well-established $\Lambda(1890)$ is such that a leading Landau singularity from a triangle diagram can coincidentally appear at the $\chi_{c1}\, p$ threshold.
- Third, there is a narrow structure at the $\chi_{c1}\, p$ threshold but not at the $\chi_{c0}\, p$ and $\chi_{c2}\, p$ thresholds.

In order to check whether that structure corresponds to a real exotic resonance, one can measure the process $\Lambda_b^0 \to K^-\chi_{c1}\, p$. If the $P_c(4450)$ structure exists in the $\chi_{c1}\, p$ invariant mass distribution as well, then the structure cannot be just a kinematical effect but is a real resonance, otherwise, one cannot conclude that the $P_c(4450)$ is another exotic hadron. In addition, it is also worthwhile to the J/ψ invariant mass distribution of processes with a completely different kinematics, such as the photoproduction processes [223–226] or pion induced reactions [227, 228].

This chapter is organized as follows. We will first give a brief introduction to the background in Section 7.1. Then we will discuss the two-point loop diagram for the $\chi_{c1}p$ rescattering in Section 7.2. After that we will briefly introduce the Landau equation and discuss the three-point loop diagram and the motion of the singularity in Section 7.3. The last section is devoted as a summary.

7.1 Introduction

The observation of many different hadrons half a century ago stimulated the proposal of the quark model as a classification scheme [2], and helped to establish quantum chromodynamics (QCD) as the fundamental theory of the strong interactions. Since then, hundreds of more hadrons were discovered. A renaissance of hadron spectroscopy studies started in 2003, and since then a central topic is the identification of the so-called exotic hadrons. These are states beyond the naive quark model scheme, in which mesons and baryons are composed of a quark–antiquark pair $q\bar{q}$ and three quarks qqq, respectively. Most of the new interesting structures were observed in the mass region of heavy quarkonium, and are

called XYZ states (for a list of these particles and a review up to 2014, see Ref. [77]). In particular, the $X(3872)$ [111] extremely close to the $D^0\bar{D}^{*0}$ threshold is widely regarded as an exotic meson, and the charged structures with a hidden pair of heavy quark and heavy antiquark such as the $Z_c(4430)$ [229, 230], $Z_c^{\pm}(3900)$ [231, 232], $Z_c^{\pm}(4020)$ [233], and $Z_b^{\pm}(10610, 10650)$ [5] would be explicitly exotic were they really resonances, i.e. poles of the S-matrix.

Candidates for explicitly exotic hadrons were extended to the pentaquark sector by the new LHCb observations of two structures, denoted as P_c, in the $J/\psi\, p$ invariant mass distribution [18]:

- $P_c(4380)$: $m = (4380 \pm 8 \pm 29)$ MeV, $\Gamma = (205 \pm 18 \pm 86)$ MeV,
- $P_c(4450)$: $m = (4449.8 \pm 1.7 \pm 2.5)$ MeV, $\Gamma = (39 \pm 5 \pm 19)$ MeV.

In the experimental fit, an amplitude analysis of three-body final state $J/\psi pK$ reproduces the two-body mass distributions of m_{Kp} and $m_{J/\psi p}$. Many known Λ^* baryons are introduced because they decay to Kp, and they serve as a background in the $J/\psi p$ invariant mass distribution. In order to obtain a satisfactory fit in this distribution, two additional Breit–Wigner amplitudes were introduced, these are the two structures $P_c(4380)$ and $P_c(4450)$. Moreover, the best fit solution for the quantum numbers are spin-parity J^P values of $(3/2^-, 5/2^+)$, while almost equally acceptable solutions could be either $(3/2^+, 5/2^-)$ or $(5/2^+, 3/2^-)$.

For the nature of this two structures, there have been some explanations. For example, they were suggested to be hadronic molecules composed of an anticharm meson and a charmed baryon [234–236] the existence of which were already predicted in Refs. [237–240]. They were also discussed as a pentaquark doublet in Ref. [241]. Besides, the pentaquark states of diquark-diquark-antiquark as the internal structure was proposed in Refs. [242, 243].

Normally, when people observe a peak in an invariant mass distribution of certain final states, they fit the peak by using the Breit–Wigner parameterization to extract the masses and widths, and claim that a new resonance is discovered. This is exactly the same procedure for the observation of the two pentaquark-like structures as we stated above. However, such a procedure is problematic. On the one hand, many of these structures are very close to certain thresholds to which they couple strongly. In this case, the use of Breit–Wigner is questionable and one needs to account for the thresholds. This can be achieved using the Flatté parameterization [244] (a method in this spirit for near-threshold states with coupled channels and unitarity was recently proposed in Ref. [245]). On the other hand, not every peak should be attributed to the existence of a resonance. In particular, kinematical effects may also show up as peaks. Such kinematical effects correspond to singularities of the S-matrix as well, but they are not poles. In general, they are the so-called Landau singularities including branch points at thresholds and more complicated ones such as the triangle singularity, also called anomalous threshold (detailed discussions of these singularities can be found in the textbooks [246, 247]). The observability of the triangle singularity was extensively discussed in 1960s (see Refs. [248–250] and references therein), and recently was used to explain some structures including the $\eta(1405)$, $a_1(1420)$ and $\phi(2170)$ [251–256]. In fact, there were suggestions that some of the Z_c and Z_b states were threshold effects [257–261] and the threshold effects might be enhanced by triangle singularities [262]. For a general discussion of S-wave threshold effects, see also Ref. [263]. Therefore, in order to establish a structure as a resonance, one has to discriminate it from such kinematical effects. Indeed, this is possible. As discussed in Ref. [264], a resonance can be distinguished from threshold kinematical effects only in the elastic channel which is the channel with that threshold. The purpose of this chapter is to discuss the possible kinematical effects for the narrower structure at 4.45 GeV in the LHCb observations and suggest measurements to check whether it is a real exotic resonance or not.

We first notice that the $P_c(4450)$ structure is exactly located at the threshold of a pair of χ_{c1} and proton,

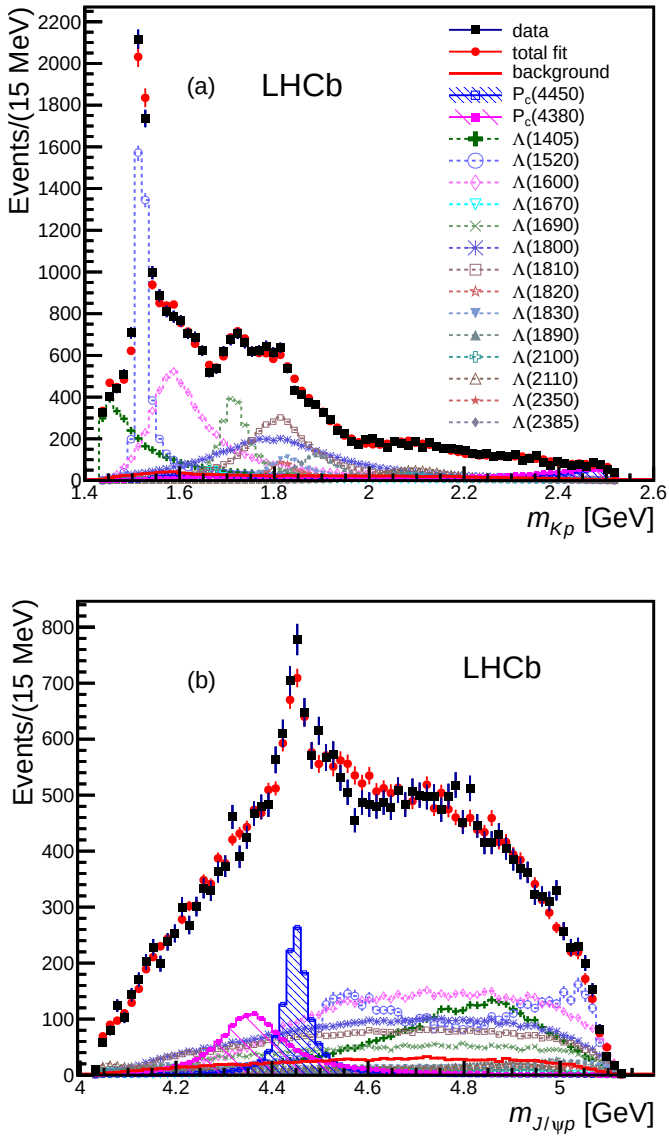

Figure 7.1: The fit projections for the invariant mass distributions (a) m_{Kp} and (b) $m_{J/\psi p}$ for many Λ^* with two P_c^+ states. This two figures are taken from Ref. [18]. In the fit, the amplitude analysis of three-body final state $J/\psi p\pi$ is used to reproduce the two-body mass distributions of m_{Kp} and $m_{J/\psi p}$.

(4448.93 ± 0.07) MeV, and

$$M_{P_c(4450)} - M_{\chi_{c1}} - M_p = (0.9 \pm 3.1)\ \text{MeV}. \tag{7.1}$$

If the angular momentum between the χ_{c1} and proton is a P-wave, then the two-body system can have quantum numbers $J^P = (1/2, 3/2, 5/2)^-$, compatible with the favored possibilities $5/2^+, 5/2^-$ and $3/2^-$ [18]. The $\chi_{c1}\ p$ can rescatter into the observed $J/\psi\ p$ by exchanging soft gluons. Two possible diagrams for such a mechanism will be shown later, and we will discuss them subsequently.

It is worthwhile to notice that the χ_{c1} can be produced in the weak decays of the Λ_b with a similar

magnitude as that for the J/ψ. In the bottom quark decays, the charm quark is produced via the mediation of a W-boson. After integrating out the off-shell mediators, one arrives at two effective operators for the $b \to c\bar{c}s$ transition:

$$O_1 = [\bar{c}^\alpha \gamma^\mu (1-\gamma_5) c^\alpha][\bar{s}^\beta \gamma_\mu (1-\gamma_5) b^\beta], \tag{7.2}$$
$$O_2 = [\bar{c}^\alpha \gamma^\mu (1-\gamma_5) c^\beta][\bar{s}^\beta \gamma_\mu (1-\gamma_5) b^\alpha] , \tag{7.3}$$

where one-loop QCD corrections have been taken into account to form O_1. Here, α, β are color indices, and they should be set to be the same in O_2 in order to form a color-singlet charmonium state. The quark fields, $[\bar{c}\gamma^\mu(1-\gamma_5)c]$, will directly generate the charmonium state. A charmonium with $J^{PC} = 1^{--}$ like the J/ψ is produced by the vector current, while the axial-vector current tends to produce the χ_{c1} with $J^{PC} = 1^{++}$ and the η_c state with $J^{PC} = 0^{+-}$. Since the vector and axial-vector currents have the same strength in the weak operators, one would expect the production rates for the J/ψ and χ_{c1} are of the same order in b quark decays. Corrections to this expectation come from higher-order QCD contributions but are sub-leading [265]. In fact, such an expectation is supported by the B meson decay data [77]:

$$\mathcal{B}(B^+ \to J/\psi K^+) = (10.27 \pm 0.31) \times 10^{-4}, \tag{7.4}$$
$$\mathcal{B}(B^+ \to \chi_{c1} K^+) = (4.79 \pm 0.23) \times 10^{-4}. \tag{7.5}$$

7.2 The $\chi_{c1}p$ inelastic rescattering in two-point loop

Having made the above general observations, we now return to the discussion of the Λ_b^0 decays measured by LHCb. As we already discussed above, the $\chi_{c1}\, p$ can rescatter into the observed $J/\psi\, p$. And there are two possible diagrams for such a mechanism, one is the two-point loop diagram shown in Fig. 7.2 with a prompt three-body production $\Lambda_b^0 \to K^- \chi_{c1}\, p$ followed by the inelastic rescattering process $\chi_{c1}\, p \to J/\psi\, p$.

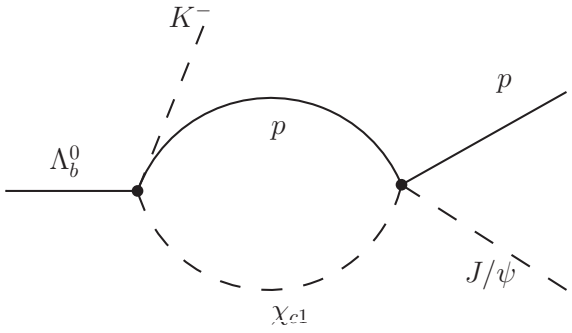

Figure 7.2: The two-point loop diagram illustrating the mechanism of the $\chi_{c1}\, p \to J/\psi\, p$ inelastic rescattering in the decay $\Lambda_b^0 \to K^- J/\psi\, p$.

We will first focus on the two-point loop diagram whose singularity is a branch point at the $\chi_{c1}\, p$ threshold on the real axis of the complex s plane, where and in the following $\sqrt{s}$ denotes the invariant mass of the $J/\psi\, p$ or $\chi_{c1}\, p$ system. It manifests itself as a cusp at the threshold if the $\chi_{c1}\, p$ is in an S-wave. For higher partial waves, the threshold behavior of the amplitude is more smooth and a cusp becomes evident in derivatives of the amplitude with respect to s. Since we are only interested in the near-threshold region, both of the χ_{c1} and the proton are nonrelativistic. Thus, the amplitude for Fig. 7.2

is proportional to the nonrelativistic two-point loop integral

$$G_\Lambda(E) = \int \frac{d^3q}{(2\pi)^3} \frac{\vec{q}^{\,2}\, f_\Lambda(\vec{q}^{\,2})}{E - m_1 - m_2 - \vec{q}^{\,2}/(2\mu)} \,, \tag{7.6}$$

where $m_{1,2}$ denote the masses of the intermediate states in the loop, μ is the reduced mass, E is the total energy and Λ is the cut-off paramter. Here, we consider the case for the P-wave $\chi_{c1}\, p$ which has quantum numbers compatible with the possibilities of the $P_c(4450)$ reported by the LHCb Collaboration, though one should be conservative to take these determinations for granted as none of the singularities discussed here was taken into account in the LHCb amplitude analysis. If we take a Gaussian form factor, $f_\Lambda(\vec{q}^{\,2}) = \exp\left(-2\vec{q}^{\,2}/\Lambda^2\right)$, to regularize the loop integral, the analytic expression for the loop integral is then given by

$$G_\Lambda(E) = -\frac{\mu\,\Lambda}{(2\pi)^{3/2}}\left(k^2 + \frac{\Lambda^2}{4}\right) + \frac{\mu\, k^3}{2\pi} e^{-2k^2/\Lambda^2}\left[\mathrm{erfi}\left(\frac{\sqrt{2}k}{\Lambda}\right) - i\right], \tag{7.7}$$

with $k = \sqrt{2\mu(E - m_1 - m_2 + i\epsilon)}$, and the imaginary error function $\mathrm{erfi}(z) = (2/\sqrt{\pi})\int_0^z e^{t^2} dt$. A better regularization method should be applied in the future, but for our present study such an approach is fine.

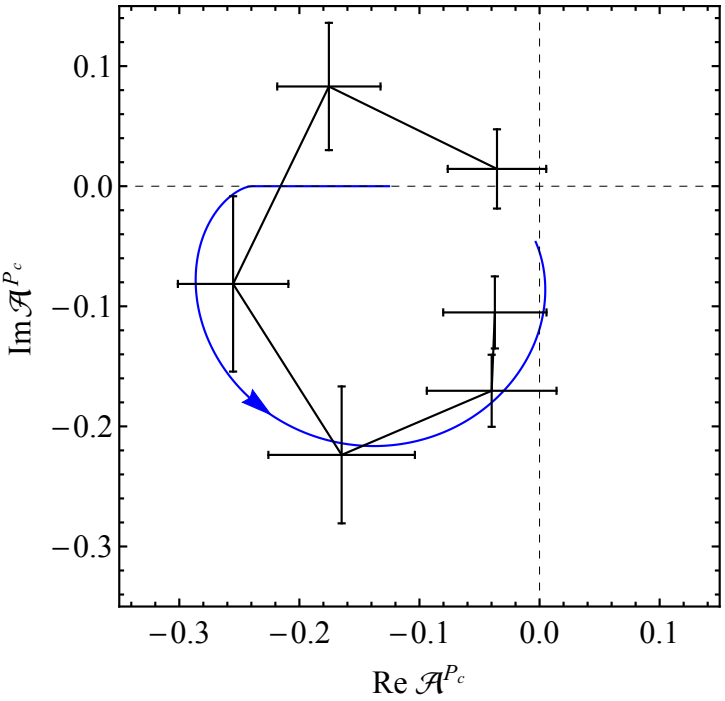

Figure 7.3: Fit to the real and imaginary parts of the $P_c(4450)$ amplitude shown in Fig. 9 in Ref. [18] with Eq. (7.8). The blue curve represents the best fit. It is counterclockwise with increasing the $J\psi\, p$ invariant mass from 4.41 GeV to 4.49 GeV, the same range as for the LHCb diagram.

Using an amplitude with the loop function given in Eq. (D.5), one can get a peak around the $\chi_{c1}\, p$ threshold. In order to have a more quantitative description of the effect of Fig. 7.2, we fit to the Argand plot for the $P_c(4450)$ amplitude depicted in Fig. 9 (a) in Ref. [18] with an amplitude

$$\mathcal{A} = N\,[b + G_\Lambda(E)]\,, \tag{7.8}$$

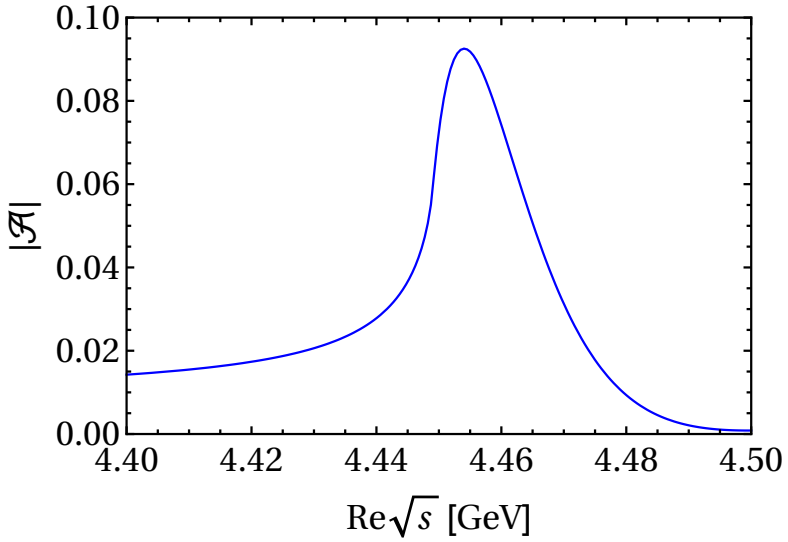

Figure 7.4: Absolute values of the amplitude in Eq. (7.8) which includes the two-point loop integral and is used to fit to the Argand plot in arbitrary units.

where b is a constant background term which may originate from a direct production of the $K^- J/\psi\, p$, and N is an overall normalization. We fit to both the real and imaginary parts of the $P_c(4450)$ amplitude by minimizing the sum of the chi-squared values for both the real and imaginary parts. The best fit with a real background term has $\chi^2/\text{d.o.f.} = 1.75$ and is given by $N = 3144$, $b = -2.9 \times 10^{-4}$ GeV^4 and $\Lambda = 0.16$ GeV. With a real background term, the amplitude in Eq. (7.8) can only be complex when the energy is larger than the $\chi_{c1}\, p$ threshold, as is evident in Fig. 7.3. The background is in general complex as a result of the fact that the $K, J/\psi$ and p can go on shell and many Λ resonances can contribute to the $K\, p$ state. One sees from the figure that the counterclockwise feature of the LHCb amplitude is reproduced, and the overall agreement is good. The absolute value of the amplitude in Eq. (7.8) with these determined parameters has a narrow peak around the $\chi_{c1}\, p$ threshold as shown in Fig. 7.4.

We have checked that using a different form factor $\Lambda^4/\left(\vec{q}^{\,2} + \Lambda^2\right)^2$ gives a similar result. In both cases, the peak is asymmetric unlike the Breit–Wigner form.

7.3 The $\chi_{c1}p$ inelastic rescattering in three-point loop

The second diagram for the $\chi_{c1}\, p$ rescattering into the observed $J/\psi\, p$ final state is a three-point loop diagram shown in Fig. 7.5 with the $K^- p$ pair produced from an intermediate Λ^* state and the proton rescattering with the χ_{c1} into the $J/\psi\, p$.

7.3.1 Landau equation

Before we continue, we will first give a brief introduction to the Landau rules for kinematical singularities [181]. The Landau rule is a useful tool to study analytic properties of the singularities in the Feynman integral. The main contents presented here are following the textbook [266].

First, let us consider the Feynman integral for the triangle diagram shown in Fig. 7.6, where the external particles have momenta p_1, p_2 and p_3 and corresponding masses μ_1, μ_2 and μ_3, i.e. $p_i^2 = \mu_i^2$ $(i = 1, 2, 3)$.

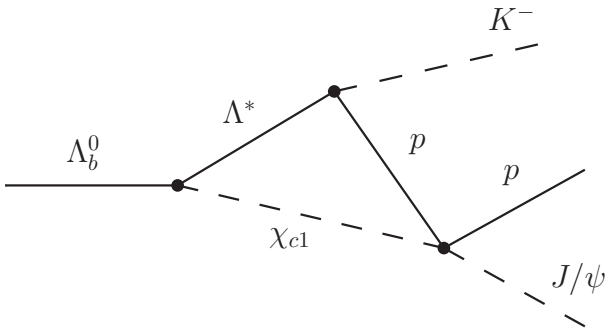

Figure 7.5: The three-point loop diagram illustrating the mechanism of the $\chi_{c1}\, p \to J/\psi\, p$ inelastic rescattering in the decay $\Lambda_b^0 \to K^- J/\psi\, p$.

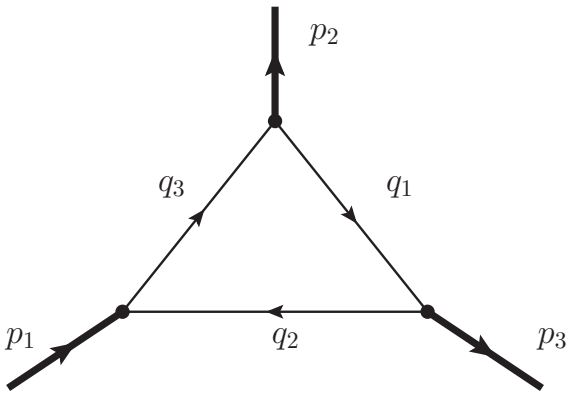

Figure 7.6: The triangle diagram for illustration of the Landau rules.

Momentum conservation requires $p_1 + p_2 + p_3 = 0$. For the internal particles, their momenta are denoted as q_1, q_2 and q_3 with masses m_1, m_2 and m_3, respectively, and generally they are not on shell, i.e. $q_i^2 \neq m_i^2$.

Since the numerator of a tensor integral would not change the singularity, we can consider only the scalar integral for simplicity. The scalar Feynman integral for Fig. 7.6 is of the form

$$I = \int \frac{d^4q_1}{(2\pi)^4} \frac{i}{(q_1^2 - m_1^2 + i\epsilon)(q_2^2 - m_2^2 + i\epsilon)(q_3^2 - m_3^2 + i\epsilon)}. \tag{7.9}$$

From the diagram we have the relations $q_2 = q_1 - p_3$ and $q_3 = q_1 + p_2$, thus there are six poles for the integrand in the complex q_{10} plane

$$q_{10} = \pm\sqrt{\vec{q}_1^2 + m_1^2} \mp i\epsilon, \tag{7.10}$$

$$q_{20} = \pm\sqrt{\vec{q}_2^2 + m_2^2} \mp i\epsilon, \quad \text{i.e.} \quad q_{10} = p_{30} \pm \sqrt{(\vec{q}_1 - \vec{p}_3)^2 + m_2^2} \mp i\epsilon, \tag{7.11}$$

$$q_{30} = \pm\sqrt{\vec{q}_3^2 + m_3^2} \mp i\epsilon, \quad \text{i.e.} \quad q_{10} = -p_{20} \pm \sqrt{(\vec{q}_1 + \vec{p}_2)^2 + m_3^2} \mp i\epsilon. \tag{7.12}$$

The integral can have a singularity only when the poles in the complex q_{10} plane pinch the integral contour. In other words, the condition that the integral has a singularity will be fulfilled when two of the

three denominators in the integral are zero at the same time

$$q_i^2 = m_i^2 \ (i = 1, 2 \text{ or } i = 1, 3, \text{ or } i = 2, 3), \tag{7.13}$$

or all of the three are zero at the same time

$$q_i^2 = m_i^2 \ (i = 1, 2, 3). \tag{7.14}$$

If only two denominators are simultaneously zero, it is essentially the condition to find the singularities of a simpler two-point loop diagram as one of the internal line can be shrunk to a point. In this case, the singularity is called the lower-order singularity of the diagram. We can deal with this as in the last section. Here we consider the case that three denominators are zero simultaneously. The singularity in this case is called the leading order singularity.

Just from Eq. (7.14), we can not get an equation that fulfils the condition of a singularity, and is in terms of the external momentum at the same time. We need the relation of all q_i first. Here we have two strategies:

1. Let us introduce three positive numbers α_1, α_2 and α_3, which are essentially the Feynman parameters as can be seen later and a four-dimensional vector

   $$\alpha_1 q_1 + \alpha_2 q_2 + \alpha_3 q_3.$$

   The spatial components of the vector can be zero by choosing appropriate coordinates. On the other hand, we know that one of the quantities q_{i0} can have a sign opposite to that of the other two. Then we can always find α_1, α_2 and α_3 to make the temporal component of the vector satisfy $\alpha_1 q_{10} + \alpha_2 q_{20} + \alpha_3 q_{30} = 0$. In total, the four-dimensional vector fulfils

   $$\sum_{i=1}^{3} \alpha_i q_i = 0. \tag{7.15}$$

2. We can also introduce integrals over Feynman parameters to combine the denominators of propagators as

   $$I = \int \frac{d^4 q_1}{(2\pi)^4} \left(\prod_{i=1}^{3} d\beta_i \right) \delta \left(\sum_{i=1}^{3} \beta_i - 1 \right) \frac{i}{D}, \tag{7.16}$$

   with D defined by

   $$D = \sum_{i=1}^{3} \beta_i (q_i^2 - m_i^2), \tag{7.17}$$

   where β_i are the Feynman parameters. The condition for the poles pinching the integral contour, i.e. a singularity, is equivalent to [246]

   $$D = 0 = \frac{\partial D}{\partial q_1}. \tag{7.18}$$

   Hence with the partial derivative we can get the similar equation as Eq. (7.15) with α replaced by

β as the q_i depend linearly on the loop momentum q_1, that is

$$\sum_{i=1}^{3} \beta_i q_i = 0. \tag{7.19}$$

It is obvious that α_i are essentially the Feynman parameters.

If we multiply the Eq. (7.15) by q_1, q_2 and q_3, we can obtain

$$\begin{cases} \alpha_1 q_1^2 + \alpha_2 (q_1 q_2) + \alpha_3 (q_1 q_3) = 0 \\ \alpha_1 (q_1 q_2) + \alpha_2 q_2^2 + \alpha_3 (q_2 q_3) = 0 \\ \alpha_1 (q_1 q_3) + \alpha_2 (q_2 q_3) + \alpha_3 q_3^2 = 0 \end{cases} . \tag{7.20}$$

With Eq. (7.20), we know that there is a non-trivial solution for the α_i if and only if the determinant of the 3×3 matrix satisfies

$$\begin{vmatrix} q_1^2 & (q_1 q_2) & (q_1 q_3) \\ (q_1 q_2) & q_2^2 & (q_2 q_3) \\ (q_1 q_3) & (q_2 q_3) & q_3^2 \end{vmatrix} = 0$$

As a result of Eq. (7.14), we can define the parameters $y_{ij} = (m_i^2 + m_j^2 - q_{ij}^2)/(2\, m_i\, m_j)$, where $q_{ij} = q_i + q_j$ being the four momentum of the ij pair. Eventually, the above determinant can be rewritten as the Landau equation

$$1 + 2\, y_{12}\, y_{23}\, y_{13} = y_{12}^2 + y_{23}^2 + y_{13}^2, \tag{7.21}$$

which will be used in the following.

7.3.2 Motion of the singularity

The above discussed leading Landau singularities of the diagram, Fig. 7.5, can cause further enhancement around the $\chi_{c1}\, p$ threshold as we will discuss now.

The leading Landau singularities for a triangle diagram are solutions of the Landau equation in Eq. (7.21). To be specific, we let m_1, m_2 and m_3 correspond to the masses of the Λ^*, χ_{c1} and proton, respectively. Then, $q_{12}^2 = M_{\Lambda_b}^2$, $q_{13}^2 = M_{K^-}^2$ and $q_{23}^2 = s$ is the invariant mass squared of the $J/\psi\, p$ pair. It is easy to solve this equation for any given variable. We solve it as an equation of s, and it has two solutions of the form

$$\begin{aligned} s^{\pm} \;=\; & (m_2 + m_3)^2 + \frac{1}{2m_1^2}\Big[(m_1^2 + m_2^2 - q_{12}^2)(q_{13}^2 - m_1^2 - m_3^2) - 4m_1^2 m_2 m_3 \\ & \pm \lambda^{1/2}(q_{13}^2, m_1^2, m_3^2)\lambda^{1/2}(q_{12}^2, m_1^2, m_2^2)\Big], \end{aligned} \tag{7.22}$$

where $\lambda(x, y, z) = x^2 + y^2 + z^2 - 2xy - 2yz - 2xz$ is the Källén function. The α_i or β_i are Feynman parameters, thus they must be positive. It can be shown that only one solution s^- leads to positive α_i or β_i.

For an easy visualization, we plot in Fig. 7.7 the motion of the solutions in the complex $\sqrt{s}$ plane. The solid line corresponds to the solution s^-, while the dashed line corresponds to the other one s^+. Meanwhile in order to give an easy visualization of the kinematical region between A and B, we also

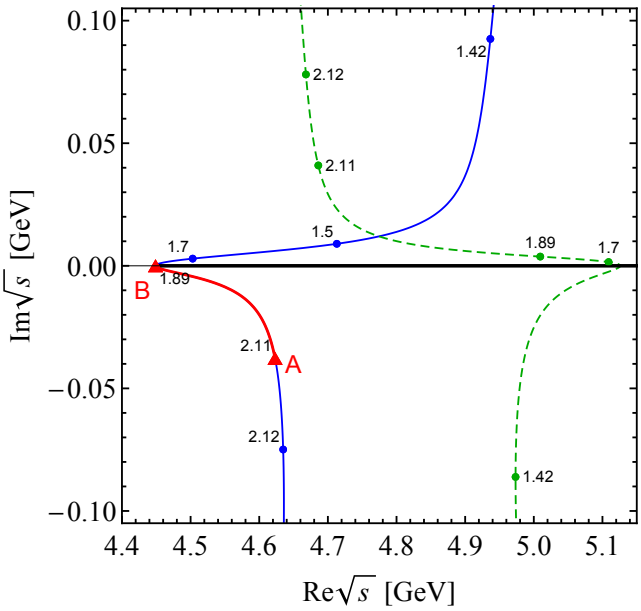

Figure 7.7: Motion of the two triangle singularities in the complex plane of $\sqrt{s} = M_{\chi_{c1}p} = M_{J/\psi p}$ with respect to changing the mass of the exchanged Λ^* baryon (several values are labeled in the plot in units of GeV). The solid line corresponds to the solution s^- in Eq. (7.22), while the dashed line corresponds to the other one s^+. In order to distinguish the trajectories from the real axis, we put a small imaginary part, −5 MeV corresponding to a width of 10 MeV, to M_{Λ^*}. Only the part between the two filled triangles, labelled as A and B, has a large impact on the physical amplitude. The thick solid straight line represents the unitary cut starting from the $\chi_{c1}\,p$ threshold.

show the corresponding Dalitz plot in Fig. 7.8. As discussed in 1960s, see e.g. Ref. [248], only one of the singularities can have an impact on the amplitude in the physical region defined on the upper edge of the real axis on the first Riemann sheet of the complex s-plane, and it is effective only in a limited region of one of these variables. Here we want to investigate in which values the Λ^* mass can take so that there can be an evident singularity effect in the $J/\psi\,p$ invariant mass, $\sqrt{s}$. According to the Coleman–Norton theorem [267], the singularity is in the physical region only when the process can happen classically, which means that all the intermediate states are on shell, and the proton emitted from the decay of the Λ^* moves along the same direction as the χ_{c1} and can catch up with it to rescatter. Let us start from a very large mass for the Λ^* so that it cannot go on shell in Fig. 7.5. Decreasing this mass, when it has a value

$$m_{1,\text{high}} = \sqrt{q_{12}^2} - m_2\,, \tag{7.23}$$

it can go on shell. At this point, the χ_{c1} is at rest in the rest frame of the decaying particle Λ_b, and the proton emitted from the decay $\Lambda^* \to K^- p$ can definitely rescatter with the χ_{c1} classically. This is the point shown as a filled triangle with $M_{\Lambda^*} = 2.11$ GeV, labelled as A, on the solid curves in Fig. 7.7. One can also see the kinematics clearly from the point A in Fig. 7.8. If we decrease m_1 further, the χ_{c1} will speed up and the proton will slow down. Thus, the lower bound of m_1 for the rescattering process that happens classically is given by the case when the χ_{c1} and the proton are at a relative rest as shown by the point B in Fig. 7.8, i.e. when the $\chi_{c1}\,p$ invariant mass is equal to their threshold. Thus, at this point the triangle singularity coincides with the normal threshold, and

$$s^- = (m_2 + m_3)^2. \tag{7.24}$$

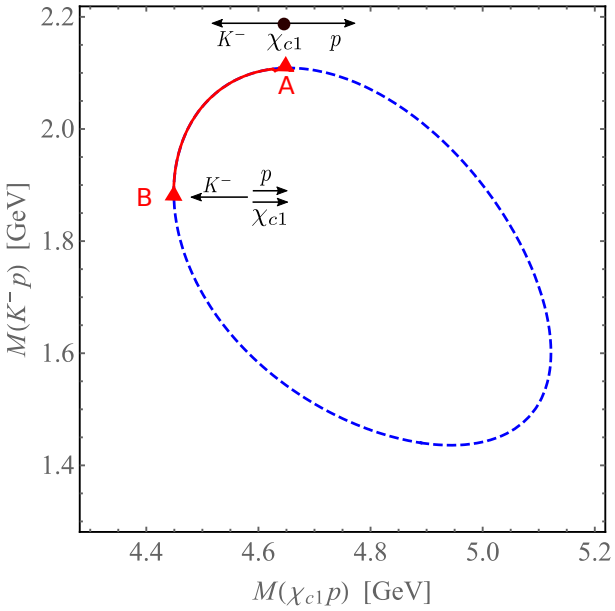

Figure 7.8: The corresponding Dalitz plot which shows the region between A and B in Fig. 7.7.

With Eq. (7.22), one gets

$$m_{1,\text{low}} = \sqrt{\frac{q_{12}^2 m_3 + q_{13}^2 m_2}{m_2 + m_3} - m_2 m_3}\,. \tag{7.25}$$

If m_1 is smaller than $m_{1,\text{low}}$, the proton would not be able to catch up with the χ_{c1} and the triangle diagram can only be a quantum process. For the case of Fig. 7.5, $m_{1,\text{low}}$ is given by $M_{\Lambda^*} = 1.89$ GeV, labelled as B and also shown as a filled triangle in Fig. 7.5. In Fig. 7.7, in order to move the singularity trajectories away from the real axis, we give a 10 MeV width to the Λ^*. For a vanishing width, the solid and dashed trajectories would pinch the real axis at $m_1 = m_{1,\text{high}}$. We can now know on which Riemann sheet of the complex s-plane the singularities are located. Since only when m_1 is between $m_{1,\text{low}}$ and $m_{1,\text{high}}$ (the part between the two filled triangles in the figure), the process can happen classically and the singularity can be on the physical boundary (if the Λ^* width vanishes), we conclude that the singularity shown as the solid curve is always on the second Riemann sheet. On the contrary, the singularity whose trajectory is shown as the dashed curve in Fig. 7.7 is on the second Riemann sheet when it is above the real axis, and it moves into the lower half plane of the first Riemann sheet otherwise. Thus, it is always far away from the physical boundary, and does not have any visible impact on the physical amplitude.

An intriguing observation for the case of interest is that within the range between 1.89 GeV and 2.11 GeV, there is a four-star baryon $\Lambda(1890)$ with $3/2^+$. Taking $M_{\Lambda^*} = 1.89$ GeV, the triangle singularity is just at the $\chi_{c1}\,p$ threshold which can provide a further threshold enhancement. The mechanism of enhanced threshold effect due to the triangle singularity was recently discussed for the case of Z_c and Z_b states [262]. Giving a finite width to the $\Lambda(1890)$, the singularity moves away from the real axis into the lower half plane of the second Riemann sheet (it is located at $(4447 - i\,0.2)$ MeV for $M_{\Lambda^*} = (1.89 - i\,0.03)$ GeV), and the enhancement is reduced. The $\Lambda(1890)$ has a relatively small width (60 to 100 MeV [77]) so that there can still be an important enhancement. In Fig. 7.9, we show the absolute value of the triangle loop integral with the $\chi_{c1}\,p$ in a P-wave for three different widths (for a discussion of the triangle singularities in nonrelativistic triangle loop integral, see Ref. [171]). There is clearly an enhancement nearby 4.45 GeV even when the width is taken to be 100 MeV.

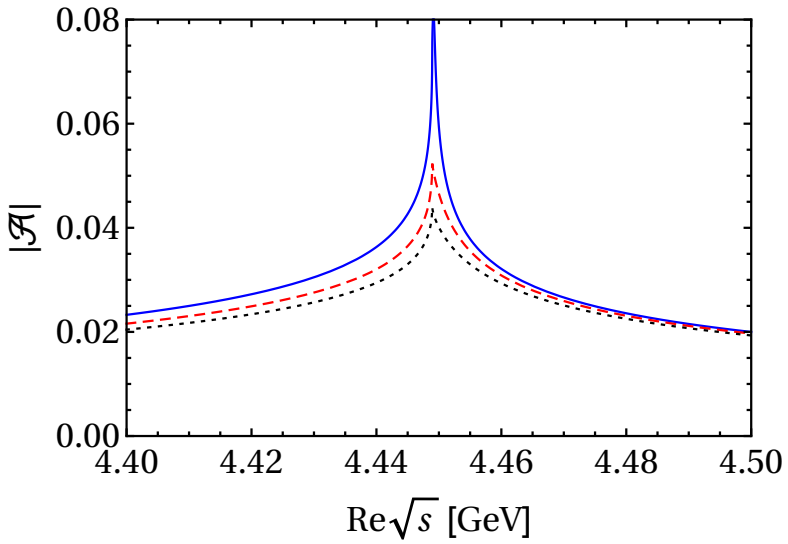

Figure 7.9: Absolute values of amplitudes for the triangle loop integral with the $\chi_{c1}\,p$ vertex in a P-wave in arbitrary units. We assume the $\Lambda(1890)$ with a mass of 1.89 GeV is exchanged in the triangle diagram. The solid, dashed and dotted lines correspond to a width of the $\Lambda(1890)$ of 10, 60 and 100 MeV, in order.

In the above, we have shown that kinematical effects can result in a narrow structure around the $\chi_{c1}\,p$ threshold in the $J/\psi\,p$ invariant mass of the $\Lambda_b^0 \to K^- J/\psi\,p$ decay. Consequently, a natural question is whether such an effect happens at other thresholds, in particular those related to the $\chi_{c1}\,p$ through heavy quark spin symmetry (HQSS). As a result of the HQSS, the operator for annihilating a χ_{c1} and creating a J/ψ is contained in

$$\frac{1}{2}\left\langle J^\dagger \chi^i \right\rangle = -\psi^{j\,\dagger}\chi_{c2}^{ij} - \frac{1}{\sqrt{2}}\epsilon^{ijk}\psi^{j\,\dagger}\chi_{c1}^k + \frac{1}{\sqrt{3}}\psi^{i\,\dagger}\chi_{c0} + \eta_c^\dagger h_c^i\,, \tag{7.26}$$

where the fields $J = \vec{\psi}\cdot\vec{\sigma} + \eta_c$ and $\vec{\chi} = \sigma^j\left(-\chi_{c2}^{ij} - \frac{1}{\sqrt{2}}\epsilon^{ijk}\chi_{c1}^k + \frac{1}{\sqrt{3}}\delta^{ij}\chi_{c0}\right) + h_c^i$ [55, 170] annihilate the S-wave and P-wave charmonium states, respectively, and $\langle\cdots\rangle$ denotes the trace in spinor space. This means that the rescattering interaction strength for $\chi_{c2}\,p \to J/\psi\,p$ or $\chi_{c0}\,p \to J/\psi\,p$ is of similar size as that for the $\chi_{c1}\,p \to J/\psi\,p$. One might naively expect enhancements at both the $\chi_{c2}\,p$ and $\chi_{c0}\,p$ thresholds in the $J/\psi\,p$ invariant mass as well. However, this is not the case. As we have shown in Eq. (7.3), at leading order in α_s, the charmoium is produced by the $[\bar{c}\gamma^\mu(1-\gamma_5)c]$ current. This current has no projection onto the χ_{c0} or χ_{c2}. The production of the $\chi_{c0,c2}$ in the b decays can come only from higher-order QCD corrections which are suppressed. Indeed, there is no enhancement at the $\chi_{c2}\,p$ and $\chi_{c0}\,p$ thresholds in Λ_b decays, which is consistent with our expectation.

7.4 Discussions

In conclusion, what we have shown here is that the present information on the narrow structure around 4.45 GeV observed by the LHCb Collaboration is compatible with kinematical effects around the $\chi_{c1}\,p$ threshold: First, it is located exactly at the $\chi_{c1}\,p$ threshold. Second, the mass of the four-star well-established $\Lambda(1890)$ coincidentally makes the triangle singularity on the physical boundary located at the $\chi_{c1}\,p$ threshold, despite a small shift into the complex plane due to the finite width of the $\Lambda(1890)$, and

third, the χ_{c1}, instead of the χ_{c0} or χ_{c2}, can be easily produced in the weak decays of the Λ_b by the $V-A$ current so that there can be an evident effect at the $\chi_{c1}\,p$, but not the $\chi_{c0}\,p$ or $\chi_{c2}\,p$, threshold.

Therefore, the most important question regarding the structure around 4.45 GeV is whether it is just a kinematical effect or a real resonance. As discussed in Ref. [264], kinematical singularities, including both the normal threshold and the triangle singularity, cannot produce a narrow near-threshold peak in the elastic channel, which is the $\chi_{c1}\,p$ in this case. The reason is the interaction strength in the elastic channel controls the threshold behavior, and there can be a narrow near-threshold peak only when the interaction in the elastic channel is strong enough to produce a pole in the S-matrix which corresponds to a real resonance. On the contrary, one cannot simply determine the interaction strength for the inelastic channel ($\chi_{c1}\,p \to J/\psi\,p$ in our case) because it can always interfere with a direct production of the final state. Thus, the question can be answered by analyzing the process $\Lambda_b^0 \to K^-\chi_{c1}\,p$: if there is a narrow structure just above threshold in the $\chi_{c1}\,p$ invariant mass distribution, then the structure cannot be just a kinematical effect and calls for the existence of a real pentaquark-like exotic resonance, otherwise, one cannot conclude the $P_c(4450)$ to be another exotic hadron.

CHAPTER 8

Summary

The underlying structure of the newly observed exotic states which can not be accommodated within the traditional quark model is extremely interesting. To distinguish theoretical models of the underlying structures of the exotica is the current urgent task. In this thesis, we mainly focused on two parts. One is the investigation of inclusive prompt production of the S-wave loosely bound state at hadron colliders, the other one is the study of the rescattering of final states in heavy hadron decays.

The prompt production of the hadronic molecules is a subject still under development. The study on the production can serve as a reference for further experimental investigation for the properties of these states.

Inclusive prompt production of S-wave loosely bound states

In Chapter 3, we derived the formula to estimate the cross sections of the inclusive productions of charm-strange states at the LHC by using the amplitudes from unitarized heavy hadron chiral perturbation theory for the heavy-light mesons. We assume that the charm-strange states $D^*_{s0}(2317)$, $D_{s1}(2460)$, $D_{sJ}(2860)$ and $D_{s2}(2910)$ are S-wave loosely bound states of a kaon and a nonstrange charmed meson. Based on this assumption, the charmed meson–kaon pairs will be produced first by using two Monte Carlo event generators, Herwig and Pythia. After the production of the constituents, these D_{sJ} states will be formed through the final state interactions between them which can be described by effective field theory. Our results show that these charm-strange bound state can be copiously produced at the LHC. The measurements can not only be able to test the molecular description and production mechanism, but will also allow to gain deeper insights into the interaction between heavy and light mesons.

In addition, we also studied the production of the exotic hadrons with hidden heavy flavor, namely the XYZ quarkonium-like states at hadron colliders in Chapter 4 under the same molecular assumption. We primarily focus on the production of the X_b which is bottom analogue of the $X(3872)$ with $B\bar{B}^*$ components and its spin partner X_{b2} at the LHC and the Tevatron. Since the $X(3872)$ has been studied experimentally and theoretically, we also revisited the production of the $X(3872)$, and compared the obtained results with the experimental data and other theoretical results. Our results for the $X(3872)$ agree with the experiments. And according to our results, the future prospect for the production of its spin partner and bottom analogs is promising at LHC based on the accumulated data. This calls for an urgent experimental analysis.

In order to take the effect of the rescattering of the constituent mesons into account, we make use

of the Migdal-Waton theorem to derive the factorized formula for the production rate. However, one may doubt the use of the Migdal-Watson approach, because of a huge numbers of hadrons comoving with the molecular components. The hadrons near the constituent mesons with a small relative momentum can be investigated by using the event generators. Nevertheless the interaction strength between a hadron with a constituent of the would-be loosely bound S-wave molecule is much smaller than the one between the two constituents. Ultimately, we are able to derive an estimate of the production rates for these particles at the order-of-magnitude accuracy.

In order to clarify the intriguing properties and finally decipher the underlying structure of the exotic states, more accurate data and new processes involving their production will be helpful.

The rescattering effect of the final states can enhance the transitions when the Landau singularities appear in a specific kinematical region. This region is associated with the solution of the Landau equation. In particular, the threshold and anomalous threshold singularities arise in the triangle diagram. From the triangle diagrams, we can not only find the kinematics region where the transitions get enhanced, but also find the available intermediate mesons contribute to a peak or enhancement in the transitions.

Rescattering of final states in heavy hadron decays

In Chapter 5, we discussed the triangle diagrams for the production of the spin partner of $X(3872)$ through charmonium decay with the associated emission of a photon in electron–positron collisions by using an effective Lagrangian approach. The spin partner $X_2(4012)$ was predicted by the heavy quark spin symmetry is a $D^*\bar{D}^*$ bound state with quantum numbers $J^{PC} = 2^{++}$. The results show that the ideal energy region to observe the $X_2(4012)$ in e^+e^- annihilations is from 4.4 GeV to 4.5 GeV, due to the presence of the S-wave $\bar{D}^*D_1(2420)$ and $\bar{D}^*D_2(2460)$ thresholds, respectively. We also point out that it will be difficult to observe the $\gamma X_2(4012)$ at the e^+e^- center-of-mass energy around 4.26 GeV.

We studied the hindered magnetic dipole transitions between two P-wave bottomonia, $\chi_b(nP)$ and $h_b(n'P)$ with $n \neq n'$, by exploring the effect of the intermediate meson in Chapter 6. In the transitions, the coupled-channel effects originating from the coupling of quarkonia to a pair of heavy and anti-heavy mesons can play a dominant role and are expected to lead to partial widths much larger than the quark model predictions. We estimated these partial widths which, however, are very sensitive to unknown coupling constants related to the vertices $\chi_{b0}(nP)B\bar{B}$. But the ratios of the decay widths for the $2P$ to $1P$ bottomonia lead to very different values from the quenched quark model. These differences can be tested in future experiments. A measurement of the hindered $M1$ transitions can shed light on the coupled-channel dynamics in these transitions and hence on the size of the coupling constants. We also suggest to check the coupled-channel effects by comparing results from quenched and fully dynamical lattice QCD calculations.

Some of the exotic hadron candidates may be just originated from kinematical effects, as not every peak should be attributed to the existence of a resonance. In Chapter 7, we investigated the newly observed narrow pentaquark-like structure at 4.45 GeV by the LHCb Collaboration in the $J/\psi\, p$ invariant mass distribution in the $\Lambda_b^0 \to J/\psi\, K^-\, p$ decay. We found that it is compatible with kinematical effects of the rescattering from $\chi_{c1}\, p$ to $J/\psi\, p$. On the one hand, the peak is located exactly at the $\chi_{c1}\, p$ threshold and the mass of the four-star well-established $\Lambda(1890)$ can make the anomalous threshold singularity from a triangle diagram coincidentally at the $\chi_{c1}\, p$ threshold. On the other hand, there is a narrow structure at the $\chi_{c1}\, p$ threshold but not at the $\chi_{c0}\, p$ and $\chi_{c2}\, p$ thresholds. Therefore, we need more evidences to conclude whether that structure corresponds to a

real exotic resonance. We proposed to measure the process $\Lambda_b^0 \to K^- \chi_{c1}\, p$. If the same structure at 4.45 GeV exists in the $\chi_{c1}\, p$ invariant mass distribution as well, then it cannot be just a kinematical effect but is a real resonance, otherwise, one cannot conclude that the $P_c(4450)$ is another exotic hadron.

There must exists triangle singularity in the $\Lambda_b^0 \to J/\psi\, K^-\, p$ decay. Therefore, the full amplitude analysis should also include the triangle singularity in addition to possible Breit-Wigner amplitudes. How much the triangle singularity could contribute to the peak is not clear so far. This analysis should be done in the future. If the final state rescattering is enough to describe the experimental data, there is no need for the new states. Nevertheless, the inclusion of the triangle singularity would change the fit results.

APPENDIX A

Kinematics

A.1 Kinematics of two-body scattering

For the two-body scattering

$$A(p_1, m_1) + B(p_2, m_2) \to C(p_3, m_3) + D(p_4, m_4), \tag{A.1}$$

the Mandelstam variables are defined as

$$\begin{aligned} s &= (p_1 + p_2)^2 = (p_3 + p_4)^2, \\ t &= (p_1 - p_3)^2 = (p_2 - p_4)^2, \\ &= m_1^2 + m_3^2 - 2E_1E_3 + 2|\vec{p}_1||\vec{p}_3|\cos\theta, \\ u &= (p_1 - p_4)^2 = (p_2 - p_3)^2. \end{aligned} \tag{A.2}$$

They are not independent and satisfy the constraint for the on-shell particles

$$s + t + u = m_1^2 + m_2^2 + m_3^2 + m_4^2. \tag{A.3}$$

The Mandelstam variables are invariant in all frames, we can deal with them in the simple center-of-mass frame, in which the quantities will be denoted by an asterisk. In this frame, we have

$$\begin{aligned} \sqrt{s} &= E_1^* + E_2^*, \\ |\vec{p}_1^*| &= |\vec{p}_2^*|, \end{aligned}$$

It is easy to get the energies and momenta in terms of the invariants

$$\begin{aligned} E_1^* &= \frac{s + m_1^2 - m_2^2}{2\sqrt{s}}, \\ E_2^* &= \frac{s + m_2^2 - m_1^2}{2\sqrt{s}}, \\ E_3^* &= \frac{s + m_3^2 - m_4^2}{2\sqrt{s}}, \end{aligned}$$

$$
\begin{aligned}
E_4^* &= \frac{s+m_4^2-m_3^2}{2\sqrt{s}}, \\
|\vec{p}_1^*| &= |\vec{p}_2^*| = \frac{\sqrt{\lambda(s,m_1^2,m_2^2)}}{2\sqrt{s}}, \\
|\vec{p}_3^*| &= |\vec{p}_4^*| = \frac{\sqrt{\lambda(s,m_3^2,m_4^2)}}{2\sqrt{s}},
\end{aligned}
$$

where $\lambda(s,m_i^2,m_j^2) = [s-(m_i+m_j)^2][s-(m_i-m_j)^2]$. Inserting the above equations to Eq. (A.3), we have

$$
\begin{aligned}
t(s,\cos\theta) &= m_1^2+m_3^2-\frac{1}{2s}(s+m_1^2-m_2^2)(s+m_3^2-m_4^2) \\
&\quad +\frac{1}{2s}\sqrt{\lambda(s,m_1^2,m_2^2)\lambda(s,m_3^2,m_4^2)}\cos\theta,
\end{aligned} \tag{A.4}
$$

and

$$
\begin{aligned}
u(s,\cos\theta) &= m_1^2+m_2^2+m_3^2+m_4^2-s-t \\
&= -(s-m_2^2-m_4^2)+\frac{1}{2s}(s+m_1^2-m_2^2)(s+m_3^2-m_4^2) \\
&\quad -\frac{1}{2s}\sqrt{\lambda(s,m_1^2,m_2^2)\lambda(s,m_3^2,m_4^2)}\cos\theta.
\end{aligned} \tag{A.5}
$$

A.2 Kinematics of two-body decays

In Chapter 5 and Chapter 6, we deal with two-body decays. Here we will show some general properties of these processes. For the decay of a particle with mass M into two particles with mass m_1 and m_2

$$
A(P,M) \to B(p_1,m_1)+C(p_2,m_2), \tag{A.6}
$$

where $P^2=M^2$, $p_1^2=m_2^2$ and $p_2^2=m_2^2$. In the rest frame of the decaying particle, $P=(M,\vec{0})$. The energy conservation gives $M=E_1+E_2$, where E_1 and E_2 are the energy of particle B and C, respectively. The momentum conservation gives $\vec{p}_1+\vec{p}_2=0$. Thus, we have

$$
E_1 = \frac{M^2+m_1^2-m_2^2}{2M}, \quad E_2 = \frac{M^2+m_2^2-m_1^2}{2M}, \tag{A.7}
$$

and

$$
|\vec{p}_1| = |\vec{p}_2| = \frac{\left[\left(M^2-(m_1+m_2)^2\right)\left(M^2-(m_1-m_2)^2\right)\right]^{1/2}}{2M}. \tag{A.8}
$$

The decay width reads

$$
d\Gamma = \frac{1}{32\pi^2}\frac{|\vec{p}_1|}{M^2}\,|\mathcal{M}|^2\,d\Omega, \tag{A.9}
$$

where $d\Omega = d\phi_1 d(\cos\theta_1)$ is the solid angle of particle B.

The processes in Chapter 5 and Chapter 6 include (axial-)vector and tensor particles. Since we are not interested in their polarizations, we can average over the spin states of initial particle and sum over the

spin states of final particles, then integrate over the solid angle. The sum over polarization for vector is written as

$$\Pi^{\mu\nu}(q,m) = -g^{\mu\nu} + \frac{q^\mu q^\nu}{m^2}. \tag{A.10}$$

For a vector meson, if we extract the polarization vector $\epsilon^*_\mu(q,\lambda)$ from the amplitude $\mathcal{M}$ and define $\mathcal{M}^\mu(q)$ to be the rest of the amplitude, the decay width will be proportional to

$$\begin{aligned}\sum_\lambda \left|\epsilon^*_\mu(q,\lambda)\mathcal{M}^\mu(q)\right|^2 &= \sum_\lambda \epsilon^*_\mu(q,\lambda)\mathcal{M}^\mu(q)\epsilon_\nu(q,\lambda)\mathcal{M}^{\nu*}(q) \\ &= \Pi^{\mu\nu}(q,m)\mathcal{M}^\mu(q)\mathcal{M}^{\nu*}(q).\end{aligned} \tag{A.11}$$

For a tensor meson, if we again extract the polarization tensor $\epsilon^*_{\mu\alpha}(q,\lambda)$ from the amplitude $\mathcal{M}$ and define $\mathcal{M}^{\mu\alpha}(q)$ to be the rest of the amplitude, we have

$$\begin{aligned}\sum_\lambda \left|\epsilon^*_{\mu\alpha}(q,\lambda)\mathcal{M}^{\mu\alpha}(q)\right|^2 &= \sum_\lambda \epsilon^*_{\mu\alpha}(q,\lambda)\mathcal{M}^{\mu\alpha}(q)\epsilon_{\nu\beta}(q,\lambda)\mathcal{M}^{\nu\beta*}(q) \\ &= \left[\frac{1}{2}\left(\Pi_{\mu\alpha}\Pi_{\nu\beta} + \Pi_{\mu\beta}\Pi_{\alpha\nu}\right) - \frac{1}{3}\Pi_{\mu\nu}\Pi_{\alpha\beta}\right]\mathcal{M}^{\mu\alpha}(q)\mathcal{M}^{\nu\beta*}(q).\end{aligned} \tag{A.12}$$

For a photon, if we extract the polarization vector $\epsilon^*_\mu(q,\lambda)$ from the amplitude $\mathcal{M}$ and define $\mathcal{M}^\mu(q)$ to be the rest of the amplitude, we have

$$\begin{aligned}\sum_\lambda \left|\epsilon^*_\mu(q,\lambda)\mathcal{M}^\mu(q)\right|^2 &= \sum_\lambda \epsilon^*_\mu(q,\lambda)\mathcal{M}^\mu(q)\epsilon_\nu(q,\lambda)\mathcal{M}^{\nu*}(q) \\ &= \left(-g_{\mu\nu}\right)\mathcal{M}^\mu(q)\mathcal{M}^{\nu*}(q).\end{aligned} \tag{A.13}$$

The squared amplitude averaged over the polarizations is independent of the solid angle, we can obtain decay width

$$\Gamma = \frac{1}{(2J+1)8\pi}\sum_\lambda \left|\epsilon^*(q,\lambda)\cdot\mathcal{M}(q)\right|^2 \frac{|\vec{p}_1|}{M^2}, \tag{A.14}$$

where J denotes the spin of the decaying particle.

A.3 Kinematics of three-body decays

For the three-body scattering

$$A(P,M) \to B(p_1,m_1) + C(p_2,m_2) + D(p_3,m_3), \tag{A.15}$$

if we average over the spin states of decaying particle, the standard form for the Dalitz plot is

$$d\Gamma = \frac{1}{(2\pi)^3}\frac{1}{32M^3}\overline{|\mathcal{M}|^2}dm^2_{12}dm^2_{23}, \tag{A.16}$$

where $m_{ij}^2 = p_{ij}^2 = (p_i + p_j)^2$, then $m_{12}^2 + m_{23}^2 + m_{13}^2 = M^2 + m_1^2 + m_2^2 + m_3^2$. For a given value of m_{12}^2, m_{23}^2 reaches maximum and minimum values when $\vec{p}_2$ is antiparallel and parallel to $\vec{p}_3$, respectively. That is

$$\left(m_{23}^2\right)_{\text{max}} = \left(E_2^* + E_3^*\right)^2 - \left(\sqrt{E_2^{*2} - m_2^2} - \sqrt{E_3^{*2} - m_3^2}\right)^2, \tag{A.17}$$

$$\left(m_{23}^2\right)_{\text{mim}} = \left(E_2^* + E_3^*\right)^2 - \left(\sqrt{E_2^{*2} - m_2^2} + \sqrt{E_3^{*2} - m_3^2}\right)^2, \tag{A.18}$$

where $E_2^* = (m_{12}^2 - m_1^2 + m_2^2)/(2m_{12})$ and $E_3^* = (M^2 - m_{12}^2 - m_3^2)/(2m_{12})$ are the energies of particles C and D in the m_{12} rest frame. Dalitz plot is the scatter plot in m_{12}^2 and m_{23}^2. In Chapter 7, we plot the Dalitz plot of the process $\Lambda_b^0 \to K^- J/\psi\, p$ without taking into account the amplitude squared $\overline{|\mathcal{M}|^2}$. When the amplitude squared is taken into account, the allowed region of the plot will be populated with events.

APPENDIX B

Polarization vectors/tensors in the charmed meson–kaon scattering amplitudes

In fact, the scattering amplitude in Eq. (3.9) has a factor of the product of polarization vectors (if the scattered heavy meson is the D^* or D_1) or tensors (for the D_2), and the tree-level amplitude should be of the form

$$V(s,t,u)\,\vec{\epsilon}^{*(\lambda_1)}\cdot\vec{\epsilon}^{(\lambda_2)}, \tag{B.1}$$

where $\vec{\epsilon}^{*}\cdot\vec{\epsilon}$ means $\epsilon^*_\mu\epsilon_\mu$ if the scattered heavy meson is the D^* or D_1 and $\epsilon^*_{\mu\nu}\epsilon_{\nu\mu}$ for the D_2, and $\lambda_{1,2}$ denote the polarizations of the initial and final heavy mesons.

If we define

$$\Pi^{\mu\nu} = -g^{\mu\nu} + \frac{p^\mu p^\nu}{m^2}, \tag{B.2}$$

the sum over polarization for vector and tensor states are given by

$$\begin{aligned}
\sum_\lambda \epsilon^{(\lambda)}_\mu \epsilon^{*(\lambda)}_\nu &= \Pi^{\mu\nu}, \\
\sum_\lambda \epsilon^{(\lambda)}_{\mu\nu} \epsilon^{*(\lambda)}_{\alpha\beta} &= \frac{1}{2}\left(\Pi_{\mu\alpha}\Pi_{\nu\beta} + \Pi_{\mu\beta}\Pi_{\alpha\nu}\right) - \frac{1}{3}\Pi_{\mu\nu}\Pi_{\alpha\beta}.
\end{aligned} \tag{B.3}$$

Because the heavy mesons are highly nonrelativistic when we are interested in the near threshold region, we have

$$\begin{aligned}
\Pi^{00} &= -g^{00} + \frac{p^0 p^0}{m^2} = -1 + 1 = 0, \\
\Pi^{ij} &= -g^{ij} + \frac{p^i p^j}{m^2} = \delta^{ij}.
\end{aligned} \tag{B.4}$$

Thus the temporal component of the polarization vector can be neglected, and the nonrelativistic polarization summation formulae are given by

$$\begin{aligned}
\sum_\lambda \epsilon^{(\lambda)}_i \epsilon^{*(\lambda)}_j &= \delta_{ij}, \\
\sum_\lambda \epsilon^{(\lambda)}_{ij} \epsilon^{*(\lambda)}_{kl} &= \frac{1}{2}\left(\delta_{ik}\delta_{jl} + \delta_{il}\delta_{jk}\right) - \frac{1}{3}\delta_{ij}\delta_{kl},
\end{aligned} \tag{B.5}$$

where ϵ_{ij} is symmetric and traceless. At the one-loop level of the resummed S-wave amplitude, one has

$$\sum_{\lambda} V(s)\vec{\epsilon}^{*(\lambda_1)} \cdot \vec{\epsilon}^{(\lambda)} G(s) V(s) \vec{\epsilon}^{*(\lambda)} \cdot \vec{\epsilon}^{(\lambda_2)} = \vec{\epsilon}^{(\lambda_1)} \cdot \vec{\epsilon}^{(\lambda_2)} V(s) G(s) V(s), \tag{B.6}$$

As a result of Eq. (B.6), the inner product of the polarization vectors/tensors can be factorized out and becomes an overall factor of the resummed amplitude

$$\vec{\epsilon}^{*(\lambda_1)} \cdot \vec{\epsilon}^{(\lambda_2)} \frac{V(s)}{1 - G(s)V(s)}. \tag{B.7}$$

It looks different from the analogous equation in Refs. [70, 268], where the denominator of the resummed amplitude reads $1 - G(s)V(s)\left[1 + q_{\rm cm}^2/(3M_V)\right]$ for the pseudoscalar meson–vector meson scattering, where $q_{\rm cm}$ is the size of the momentum of the vector meson in the center-of-mass frame, and M_V is the vector meson mass. In the nonrelativistic limit, the additional factor $1 + q_{\rm cm}^2/(3M_V)$ is reduced to 1, and one gets the same equation as Eq. (B.7).

APPENDIX C

Unitarization

The S-matrix

$$S_{fi} = \langle f\,|S|\,i\rangle \tag{C.1}$$

represents the amplitude for the scattering from initial state $|i\rangle$ to final state $|f\rangle$. A momentum eigenstate can not contain any information about the positions of the particle in space. Hence they are likely to be widely separated in space and no interact at all. Therefore the S-matrix can be separated into two parts by writing

$$S = 1 + i\,T. \tag{C.2}$$

Unitarity of the S-matrix, $S\,S^\dagger = S^\dagger\,S = 1$ is derived from probability conservation, i.e. the total probability for any system to end up in some final state must be one. Thus,

$$T - T^\dagger = i\,T\,T^\dagger. \tag{C.3}$$

Then

$$\begin{aligned}\langle f\,|T|\,i\rangle - \left\langle f\left|T^\dagger\right|i\right\rangle &= i\sum_a \int \left[\prod_{i=1}^{n_a} \frac{d^3p_i}{2p_i^0(2\pi)^3}\right] \left\langle f\left|T^\dagger\right|a\right\rangle \langle a\,|T|\,i\rangle \times (2\pi)^4\delta^4(P_f - P_i) \\ &= i\sum_a \int d\Phi_a \left\langle f\left|T^\dagger\right|a\right\rangle \langle a\,|T|\,i\rangle\,,\end{aligned} \tag{C.4}$$

where the phase space of the intermediate state is

$$d\Phi_a = (2\pi)^4\delta^4(P_f - P_i) \prod_{i=1}^{n_a} \frac{d^3p_i}{2p_i^0(2\pi)^3}. \tag{C.5}$$

We also have

$$2i\,\mathrm{Im}\,T_{fi} = i\sum_a \int d\Phi_a T^*_{af} T_{ai}. \tag{C.6}$$

The phase space integral with two-body final states is given by

$$\begin{aligned}\int d\Phi_2 &= (2\pi)^4 \int \frac{d^3p}{(2\pi)^3 2p^0}\frac{d^3k}{(2\pi)^3 2k^0}\delta^4(P-p-k) \\ &= \int d\Omega \frac{q_{cm}}{16\pi^2\sqrt{s}}\theta(s-s_{th}) \\ &= 2\rho(s)\theta(s-s_{th}),\end{aligned} \tag{C.7}$$

where $s_{th} = (m_1+m_2)^2$ is the threshold and the phase space factor is defined as $\rho(s) = \frac{q_{cm}}{8\pi\sqrt{s}}$, with q_{cm} the three-momentum in the center-of-mass frame of two-body system $q_{cm} = \sqrt{(s-s_{th})(s-(m_1-m_2)^2)}/(2\sqrt{s})$. Therefore we have the relation

$$\mathrm{Im}\, T^{-1}(s) = \rho(s). \tag{C.8}$$

The infinite sum $T(s)$ of all scattering amplitude given by Lippman-Schwinger equation reads

$$\begin{aligned}T(s) &= \frac{1}{V^{-1}(s) - G(s)} \\ &= \frac{1}{V^{-1}(s) - \mathrm{Re}\, G(s) - i\,\mathrm{Im}\, G(s)},\end{aligned} \tag{C.9}$$

where $V(s)$ is the tree-level S-wave amplitude and $G(s)$ is the two-particle loop. Applying the Cutkosky's rule to the loop function, its imaginary part is related to the phase space factor

$$\mathrm{Im}\, G(s) = -\rho(s). \tag{C.10}$$

If we combine Eq. (C.8) and Eq. (C.9), it is obvious that $V(s)$ must be real as unitarity requires.

APPENDIX D

Loop integrals

D.1 Two-point loop integral

The relativistic scalar two-point loop integral is written as

$$i\int\frac{d^4q}{(2\pi)^4}\frac{1}{(q^2-m_1^2+i\epsilon)[(P-q)^2-m_2^2+i\epsilon]}. \tag{D.1}$$

In the center-of-mass frame ($P^\mu=\{E,\vec{0}\}$) and using the nonrelativistic approximation, we have

$$\begin{aligned} G(E) &= \frac{i}{4m_1m_2}\int\frac{d^4q}{(2\pi)^4}\frac{1}{(q^0-\frac{\vec{q}^2}{2m_1}-m_1+i\epsilon)(E-q^0-\frac{\vec{q}^2}{2m_2}-m_2+i\epsilon)} \\ &= \frac{1}{4m_1m_2}\int\frac{d^3q}{(2\pi)^3}\frac{1}{E-\frac{\vec{q}^2}{2\mu}-m_1-m_2}, \end{aligned} \tag{D.2}$$

where $\mu=m_1m_2/(m_1+m_2)$ is the reduced mass. The nonrelativistic form of the integral is related to the relativistic one as $G_{NR}(E)=4m_1m_2\,G(E)$.

D.1.1 Regulation of the loop integral

Obviously, the loop integral is divergent. But we can regularize the loop integral by taking a sharp cutoff $q_{\max}$ as the upper limit of the integral, then we get

$$\begin{aligned} G_{NR}(E,q_{\max}) &= \int_0^{q_{\max}}\frac{d^3q}{(2\pi)^3}\frac{1}{E-\frac{\vec{q}^2}{2\mu}-m_1-m_2} \\ &= -\frac{\mu}{\pi^2}\left(q_{\max}-k\tan^{-1}\left(\frac{q_{\max}}{k}\right)\right), \end{aligned} \tag{D.3}$$

where $k = \sqrt{2\mu(m_1 + m_2 - E - i\epsilon)}$ is the binding momentum. Besides, we can also use a regulator function $f_\Lambda(\vec{q})$ with the cutoff Λ in the integral. Then the nonrelativistic integral is written as

$$G_{NR}(E,\Lambda) = \int \frac{d^3q}{(2\pi)^3} \frac{f_\Lambda(\vec{q})}{E - \frac{\vec{q}^2}{2\mu} - m_1 - m_2}, \tag{D.4}$$

There are various choices for the regulator function, for example the dipole and the Gaussian form factors. Here we take the Gaussian form factor, $f_\Lambda(\vec{q}^{\,2}) = \exp\left(-2\vec{q}^{\,2}/\Lambda^2\right)$, to regularize the loop integral, the analytic expression for the integral is given by

$$G_{NR}(E,\Lambda) = -\frac{\mu}{\pi^2}\left[\sqrt{2\pi}\,\frac{\Lambda}{4} + \frac{\pi}{2}\,k\,e^{2k^2/\Lambda^2}\left(\mathrm{erfi}\left(\frac{\sqrt{2}\,k}{\Lambda}\right) - 1\right)\right], \tag{D.5}$$

the imaginary error function $\mathrm{erfi}(z) = (2/\sqrt{\pi})\int_0^z e^{t^2}dt$.

D.1.2 Riemann sheets in the loop integral

One might have noticed that the momentum k is a multivalued function of E and its branch point is at the threshold, which makes the loop function a multivalued function, too. Therefore, the loop function has two Riemann sheets corresponding to the two possible signs of the binding momentum.

The first sheet is in the range where $0 \le \mathrm{Arg}(E - m_1 - m_2) < 2\pi$, while the second one is in the rang where $-2\pi \le \mathrm{Arg}(E - m_1 - m_2) < 0$. If we move from the first Riemann sheet to the second one, we can simply change k by $-k$ in the loop function.

D.2 Three-point loop integrals in NREFT

In this section, we will show the calculation of three-point loop integrals in the NREFT. The calculation is based on the appendix of Ref. [170]. The relativistic scalar one-loop integral is written as

$$i\int \frac{d^dl}{(2\pi)^d} \frac{1}{(l^2 - m_1^2 + im_1\Gamma_1)[(P-l)^2 - m_2^2 + i\epsilon][(l-q)^2 - m_3^2 + i\epsilon]}, \tag{D.6}$$

in which we assign the meson with a mass m_1 a constant width Γ_1. Here at most one meson in the triangle diagram is allowed to have finite width, otherwise there would be not apparent threshold effect. In the rest frame of the initial particle ($P^\mu = \{M, \vec{0}\}$) and using the nonrelativistic approximation, we have

$$\begin{aligned}
I(m_1,m_2,m_3) &= \int \frac{d^dl}{(2\pi)^d} \frac{i/(8m_1m_2m_3)}{(l^0 - \frac{\vec{l}^2}{2m_1} - m_1 + i\frac{\Gamma_1}{2})(M - l^0 - \frac{\vec{l}^2}{2m_2} - m_2 + i\epsilon)[l^0 - q^0 - \frac{(\vec{l}-\vec{q})^2}{2m_3} - m_3 + i\epsilon]} \\
&= \frac{-i}{8m_1m_2m_3}\int \frac{d^dl}{(2\pi)^d} \frac{1}{(l^0 - \frac{\vec{l}^2}{2m_1} + i\frac{\Gamma_1}{2})(l^0 + b_{12} + \frac{\vec{l}^2}{2m_2} - i\epsilon)[l^0 - b_{23} + b_{12} - \frac{(\vec{l}-\vec{q})^2}{2m_3} + i\epsilon]} \\
&= \frac{\mu_{12}\mu_{23}}{2m_1m_2m_3}\int \frac{d^{d-1}l}{(2\pi)^{d-1}} \frac{1}{(\vec{l}^2 + c_{12} - i\mu_{12}\Gamma_1)(\vec{l}^2 - 2\frac{\mu_{23}}{m_3}\vec{l}\cdot\vec{q} + c_{23} - i\epsilon)},
\end{aligned}$$

where $b_{12} = m_1 + m_2 - M$, $b_{23} = b_{12} + m_3 - M + q^0$, $c_{12} = 2\mu_{12}b_{12}$, $c_{23} = 2\mu_{23}(b_{23} + \frac{\vec{q}^2}{2m_3})$ and $\mu_{ij} = m_i m_j/(m_i + m_j)$ are the reduced mass. In the above equation, we have shifted the integral variable and performed the contour integration over l^0. Next we can use Feynman parameters to combine the two denominators and then dimensional regularization to integrate the loop momentum,

$$\begin{aligned} I(m_1, m_2, m_3) &= \frac{\mu_{12}\mu_{23}}{2m_1m_2m_3}\int_0^1 dx \int \frac{d^{d-1}l}{(2\pi)^{d-1}} \frac{1}{[\vec{l}^2 - ax^2 + (c_{23} - c_{12} + i\mu_{12}\Gamma_1)x + c_{12} - i\mu_{12}\Gamma_1]^2} \\ &= \frac{\mu_{12}\mu_{23}}{16\pi m_1m_2m_3}\frac{1}{\sqrt{a}}\left[\tan^{-1}\left(\frac{c_{23} - c_{12} + i\mu_{12}\Gamma_1}{2\sqrt{a(c_{12} - i\mu_{12}\Gamma_1)}}\right) + \tan^{-1}\left(\frac{2a + c_{12} - i\mu_{12}\Gamma_1 - c_{23}}{2\sqrt{a(c_{23} - a)}}\right)\right], \end{aligned} \tag{D.7}$$

where $a = \left(\frac{\mu_{23}}{m_3}\right)^2 \vec{q}^{\,2}$.

Bibliography

[1] R. P. Feynman, M. Gell-Mann and G. Zweig,
Group U(6) × U(6) generated by current components, Phys. Rev. Lett. **13** (1964) 678.

[2] M. Gell-Mann, *A Schematic Model of Baryons and Mesons*, Phys. Lett. **8** (1964) 214.

[3] B. Aubert et al., *Observation of a narrow meson decaying to $D_s^+\pi^0$ at a mass of 2.32-GeV/c^2*, Phys. Rev. Lett. **90** (2003) 242001, arXiv: hep-ex/0304021 [hep-ex].

[4] D. Besson et al., *Observation of a narrow resonance of mass 2.46-GeV/c^2 decaying to $D_s^{*+}\pi^0$ and confirmation of the $D_{sJ}^*(2317)$ state*,
Phys. Rev. **D68** (2003) 032002, [Erratum: Phys. Rev.D75,119908(2007)],
arXiv: hep-ex/0305100 [hep-ex].

[5] A. Bondar et al., *Observation of two charged bottomonium-like resonances in Υ(5S) decays*, Phys. Rev. Lett. **108** (2012) 122001, arXiv: 1110.2251 [hep-ex].

[6] H.-X. Chen et al., *The hidden-charm pentaquark and tetraquark states* (2016),
arXiv: 1601.02092 [hep-ph].

[7] M. Ablikim et al., *Observation of $e^+e^- \to \gamma X(3872)$ at BESIII*,
Phys. Rev. Lett. **112**.9 (2014) 092001, arXiv: 1310.4101 [hep-ex].

[8] F.-K. Guo et al., *Production of the X(3872) in charmonia radiative decays*,
Phys. Lett. **B725** (2013) 127, arXiv: 1306.3096 [hep-ph].

[9] E. S. Swanson, *The New heavy mesons: A Status report*, Phys. Rept. **429** (2006) 243,
arXiv: hep-ph/0601110 [hep-ph].

[10] S.-L. Zhu, *New hadron states*, Int. J. Mod. Phys. **E17** (2008) 283,
arXiv: hep-ph/0703225 [hep-ph].

[11] S. Weinberg, *Pion scattering lengths*, Phys. Rev. Lett. **17** (1966) 616.

[12] Y. Tomozawa, *Axial vector coupling renormalization and the meson baryon scattering lengths*, Nuovo Cim. **A46** (1966) 707.

[13] F.-K. Guo et al., *Consequences of Heavy Quark Symmetries for Hadronic Molecules*,
Phys. Rev. **D88** (2013) 054007, arXiv: 1303.6608 [hep-ph].

[14] C. Bignamini et al., *Is the X(3872) Production Cross Section at Tevatron Compatible with a Hadron Molecule Interpretation?*, Phys. Rev. Lett. **103** (2009) 162001,
arXiv: 0906.0882 [hep-ph].

[15] T. Nakano et al.,
Evidence for a narrow $S = +1$ baryon resonance in photoproduction from the neutron,
Phys. Rev. Lett. **91** (2003) 012002, arXiv: hep-ex/0301020 [hep-ex].

[16] B. McKinnon et al., *Search for the Theta+ pentaquark in the reaction $\gamma d \to pK^-K^+n$*,
Phys. Rev. Lett. **96** (2006) 212001, arXiv: hep-ex/0603028 [hep-ex].

[17] K. Shirotori et al., *Search for the Θ^+ pentaquark via the $\pi^- p \to K^- X$ reaction at 1.92 GeV/c*,
Phys. Rev. Lett. **109** (2012) 132002, arXiv: 1203.3604 [nucl-ex].

[18] R. Aaij et al.,
Observation of $J/\psi p$ Resonances Consistent with Pentaquark States in $\Lambda_b^0 \to J/\psi K^- p$ Decays,
Phys. Rev. Lett. **115** (2015) 072001, arXiv: 1507.03414 [hep-ex].

[19] J. Z. Bai et al., *Observation of a near threshold enhancement in the $p\bar{p}$ mass spectrum from radiative $J/\psi \to \gamma p\bar{p}$ decays*, Phys. Rev. Lett. **91** (2003) 022001,
arXiv: hep-ex/0303006 [hep-ex].

[20] M. Ablikim et al.,
Spin-Parity Analysis of $p\bar{p}$ Mass Threshold Structure in J/ψ and ψ' Radiative Decays,
Phys. Rev. Lett. **108** (2012) 112003, arXiv: 1112.0942 [hep-ex].

[21] M. Z. Wang et al., *Observation of $B^+ \to p\bar{p}\pi^+$, $B^0 \to p\bar{p}K^0$, and $B^+ \to p\bar{p}K^{*+}$*,
Phys. Rev. Lett. **92** (2004) 131801, arXiv: hep-ex/0310018 [hep-ex].

[22] M.-Z. Wang et al., *Study of the baryon-antibaryon low-mass enhancements in charmless three-body baryonic B decays*, Phys. Lett. **B617** (2005) 141,
arXiv: hep-ex/0503047 [hep-ex].

[23] A. Datta and P. J. O'Donnell, *A New state of baryonium*, Phys. Lett. **B567** (2003) 273,
arXiv: hep-ph/0306097 [hep-ph].

[24] C.-K. Chua, W.-S. Hou and S.-Y. Tsai,
Possible hints and search for glueball production in charmless rare B decays,
Phys. Lett. **B544** (2002) 139, arXiv: hep-ph/0204186 [hep-ph].

[25] J. L. Rosner, *Low mass baryon anti-baryon enhancements in B decays*,
Phys. Rev. **D68** (2003) 014004, arXiv: hep-ph/0303079 [hep-ph].

[26] B. S. Zou and H. C. Chiang, *One pion exchange final state interaction and the p anti-p near threshold enhancement in $J/\psi \to \gamma p\bar{p}$ decays*, Phys. Rev. **D69** (2004) 034004,
arXiv: hep-ph/0309273 [hep-ph].

[27] A. Sibirtsev et al., *Near threshold enhancement of the $p\bar{p}$ mass spectrum in J/ψ decay*,
Phys. Rev. **D71** (2005) 054010, arXiv: hep-ph/0411386 [hep-ph].

[28] J. Haidenbauer, U.-G. Meißner and A. Sibirtsev,
Near threshold $p\bar{p}$ enhancement in B and J/ψ decay, Phys. Rev. **D74** (2006) 017501,
arXiv: hep-ph/0605127 [hep-ph].

[29] J. Haidenbauer, X.-W. Kang and U.-G. Meißner,
The electromagnetic form factors of the proton in the timelike region,
Nucl. Phys. **A929** (2014) 102, arXiv: 1405.1628 [nucl-th].

[30] X.-W. Kang, J. Haidenbauer and U.-G. Meißner,
Near-threshold $p\bar{p}$ invariant mass spectrum measured in J/ψ and ψ' decays,
Phys. Rev. **D91**.7 (2015) 074003, arXiv: 1502.00880 [nucl-th].

[31] J. L. Basdevant and S. Boukraa,
Successes and Difficulties of Unified Quark - Anti-quark Potential Models,
Z. Phys. **C28** (1985) 413.

[32] S. Godfrey and N. Isgur, *Mesons in a Relativized Quark Model with Chromodynamics*,
Phys. Rev. **D32** (1985) 189.

[33] M. Koll et al., *A Relativistic quark model for mesons with an instanton induced interaction*,
Eur. Phys. J. **A9** (2000) 73, arXiv: hep-ph/0008220 [hep-ph].

[34] R. Ricken et al., *The Meson spectrum in a covariant quark model*, Eur. Phys. J. **A9** (2000) 221,
arXiv: hep-ph/0008221 [hep-ph].

[35] B. Metsch et al., *The spectrum and strong decays of baryons in a relativistic quark model*,
Eur. Phys. J. **A18** (2003) 189.

[36] G. Zweig, *An SU(3) model for strong interaction symmetry and its breaking. Version 1* (1964).

[37] S. Weinberg, *Phenomenological Lagrangians*, Physica **A96** (1979) 327.

[38] J. Gasser and H. Leutwyler, *Chiral Perturbation Theory to One Loop*,
Annals Phys. **158** (1984) 142.

[39] J. Gasser and H. Leutwyler,
Chiral Perturbation Theory: Expansions in the Mass of the Strange Quark,
Nucl. Phys. **B250** (1985) 465.

[40] V. Bernard, N. Kaiser and U.-G. Meißner, *Chiral dynamics in nucleons and nuclei*,
Int. J. Mod. Phys. **E4** (1995) 193, arXiv: hep-ph/9501384 [hep-ph].

[41] V. Bernard and U.-G. Meißner, *Chiral perturbation theory*,
Ann. Rev. Nucl. Part. Sci. **57** (2007) 33, arXiv: hep-ph/0611231 [hep-ph].

[42] S. Scherer and M. R. Schindler, *A Primer for Chiral Perturbation Theory*,
Lect. Notes Phys. **830** (2012) pp.1.

[43] G. Burdman and J. F. Donoghue, *Union of chiral and heavy quark symmetries*,
Phys. Lett. **B280** (1992) 287.

[44] M. B. Wise, *Chiral perturbation theory for hadrons containing a heavy quark*,
Phys. Rev. **D45** (1992) 2188.

[45] M. Neubert, *Heavy quark symmetry*, Phys. Rept. **245** (1994) 259,
arXiv: hep-ph/9306320 [hep-ph].

[46] A. V. Manohar and M. B. Wise, *Heavy quark physics*,
Camb. Monogr. Part. Phys. Nucl. Phys. Cosmol. **10** (2000) 1.

[47] T.-M. Yan et al., *Heavy quark symmetry and chiral dynamics*,
Phys. Rev. **D46** (1992) 1148, [Erratum: Phys. Rev.D55,5851(1997)].

[48] R. Casalbuoni et al., *Phenomenology of heavy meson chiral Lagrangians*, Phys. Rept. **281** (1997) 145, arXiv: hep-ph/9605342 [hep-ph].

[49] S. R. Coleman, J. Wess and B. Zumino, *Structure of phenomenological Lagrangians. 1.*, Phys. Rev. **177** (1969) 2239.

[50] C. G. Callan Jr. et al., *Structure of phenomenological Lagrangians. 2.*, Phys. Rev. **177** (1969) 2247.

[51] F.-K. Guo, C. Hanhart and U.-G. Meißner, *On the extraction of the light quark mass ratio from the decays $\psi' \to J/\psi\pi^0(\eta)$*, Phys. Rev. Lett. **103** (2009) 082003, [Erratum: Phys. Rev. Lett.104,109901(2010)], arXiv: 0907.0521 [hep-ph].

[52] J. Hu and T. Mehen, *Chiral Lagrangian with heavy quark-diquark symmetry*, Phys. Rev. **D73** (2006) 054003, arXiv: hep-ph/0511321 [hep-ph].

[53] A. F. Falk, *Hadrons of arbitrary spin in the heavy quark effective theory*, Nucl. Phys. **B378** (1992) 79.

[54] A. F. Falk and M. E. Luke, *Strong decays of excited heavy mesons in chiral perturbation theory*, Phys. Lett. **B292** (1992) 119, arXiv: hep-ph/9206241 [hep-ph].

[55] S. Fleming and T. Mehen, *Hadronic Decays of the X(3872) to χ_{cJ} in Effective Field Theory*, Phys. Rev. **D78** (2008) 094019, arXiv: 0807.2674 [hep-ph].

[56] F. De Fazio, *Radiative transitions of heavy quarkonium states*, Phys. Rev. **D79** (2009) 054015, [Erratum: Phys. Rev.D83,099901(2011)], arXiv: 0812.0716 [hep-ph].

[57] A. M. Badalian et al., *Resonances in Coupled Channels in Nuclear and Particle Physics*, Phys. Rept. **82** (1982) 31.

[58] F.-K. Guo et al., *Production of charm-strange hadronic molecules at the LHC*, JHEP **05** (2014) 138, arXiv: 1403.4032 [hep-ph].

[59] P. Artoisenet and E. Braaten, *Production of the X(3872) at the Tevatron and the LHC*, Phys. Rev. **D81** (2010) 114018, arXiv: 0911.2016 [hep-ph].

[60] P. Artoisenet and E. Braaten, *Estimating the Production Rate of Loosely-bound Hadronic Molecules using Event Generators*, Phys. Rev. **D83** (2011) 014019, arXiv: 1007.2868 [hep-ph].

[61] A. Esposito et al., *A Mechanism for Hadron Molecule Production in p pbar(p) Collisions*, J. Mod. Phys. **4** (2013) 1569, arXiv: 1305.0527 [hep-ph].

[62] F.-K. Guo, U.-G. Meißner and W. Wang, *Production of charged heavy quarkonium-like states at the LHC and the Tevatron*, Commun. Theor. Phys. **61** (2014) 354, arXiv: 1308.0193 [hep-ph].

[63] B. Aubert et al., *Observation of a New D_s Meson Decaying to DK at a Mass of 2.86-GeV/c^2*, Phys. Rev. Lett. **97** (2006) 222001, arXiv: hep-ex/0607082 [hep-ex].

[64] M. Di Pierro and E. Eichten, *Excited heavy - light systems and hadronic transitions*, Phys. Rev. **D64** (2001) 114004, arXiv: hep-ph/0104208 [hep-ph].

[65] F.-K. Guo and U.-G. Meißner, *More kaonic bound states and a comprehensive interpretation of the D_{sJ} states*, Phys. Rev. **D84** (2011) 014013, arXiv: 1102.3536 [hep-ph].

[66] Q.-T. Song et al., *Charmed-strange mesons revisited: mass spectra and strong decays*, Phys. Rev. **D91** (2015) 054031, arXiv: 1501.03575 [hep-ph].

[67] S. Godfrey and I. T. Jardine, *Nature of the $D^*_{s1}(2710)$ and $D^*_{sJ}(2860)$ mesons*, Phys. Rev. **D89**.7 (2014) 074023, arXiv: 1312.6181 [hep-ph].

[68] T. Barnes, F. E. Close and H. J. Lipkin, *Implications of a DK molecule at 2.32 GeV*, Phys. Rev. **D68** (2003) 054006, arXiv: hep-ph/0305025 [hep-ph].

[69] E. van Beveren and G. Rupp, *Observed $D_s(2317)$ and tentative D(2030) as the charmed cousins of the light scalar nonet*, Phys. Rev. Lett. **91** (2003) 012003, arXiv: hep-ph/0305035 [hep-ph].

[70] E. E. Kolomeitsev and M. F. M. Lutz, *On Heavy light meson resonances and chiral symmetry*, Phys. Lett. **B582** (2004) 39, arXiv: hep-ph/0307133 [hep-ph].

[71] F.-K. Guo et al., *Dynamically generated 0+ heavy mesons in a heavy chiral unitary approach*, Phys. Lett. **B641** (2006) 278, arXiv: hep-ph/0603072 [hep-ph].

[72] F.-K. Guo, P.-N. Shen and H.-C. Chiang, *Dynamically generated 1+ heavy mesons*, Phys. Lett. **B647** (2007) 133, arXiv: hep-ph/0610008 [hep-ph].

[73] F.-K. Guo, C. Hanhart and U.-G. Meißner, *Implications of heavy quark spin symmetry on heavy meson hadronic molecules*, Phys. Rev. Lett. **102** (2009) 242004, arXiv: 0904.3338 [hep-ph].

[74] W. A. Bardeen, E. J. Eichten and C. T. Hill, *Chiral multiplets of heavy - light mesons*, Phys. Rev. **D68** (2003) 054024, arXiv: hep-ph/0305049 [hep-ph].

[75] M. A. Nowak, M. Rho and I. Zahed, *Chiral doubling of heavy light hadrons: BABAR 2317-MeV/c^2 and CLEO 2463 MeV/c^2 discoveries*, Acta Phys. Polon. **B35** (2004) 2377, arXiv: hep-ph/0307102 [hep-ph].

[76] T. Mehen and R. P. Springer, *Even- and odd-parity charmed meson masses in heavy hadron chiral perturbation theory*, Phys. Rev. **D72** (2005) 034006, arXiv: hep-ph/0503134 [hep-ph].

[77] K. A. Olive et al., *Review of Particle Physics*, Chin. Phys. **C38** (2014) 090001.

[78] P. L. Cho and M. B. Wise, *Comment on $D_s^* \to D_s\pi^0$ decay*, Phys. Rev. **D49** (1994) 6228, arXiv: hep-ph/9401301 [hep-ph].

[79] A. Faessler et al., *Strong and radiative decays of the $D^*_{s0}(2317)$ meson in the DK molecule picture*, Phys. Rev. **D76** (2007) 014005, arXiv: 0705.0254 [hep-ph].

[80] A. Faessler et al., *D^*K molecular structure of the $D_{s1}(2460)$ meson*, Phys. Rev. **D76** (2007) 114008, arXiv: 0709.3946 [hep-ph].

[81] M. F. M. Lutz and M. Soyeur, *Radiative and isospin-violating decays of D_s mesons in the hadrogenesis conjecture*, Nucl. Phys. **A813** (2008) 14, arXiv: 0710.1545 [hep-ph].

[82] F.-K. Guo et al., *Subleading contributions to the width of the $D^*_{s0}(2317)$*, Phys. Lett. **B666** (2008) 251, arXiv: 0806.3374 [hep-ph].

[83] M. F. M. Lutz et al., *Physics Performance Report for PANDA: Strong Interaction Studies with Antiprotons* (2009), arXiv: 0903.3905 [hep-ex].

[84] L. Liu et al., *Interactions of charmed mesons with light pseudoscalar mesons from lattice QCD and implications on the nature of the $D^*_{s0}(2317)$*, Phys. Rev. **D87**.1 (2013) 014508, arXiv: 1208.4535 [hep-lat].

[85] D. Mohler et al., *$D^*_{s0}(2317)$ Meson and D-Meson-Kaon Scattering from Lattice QCD*, Phys. Rev. Lett. **111**.22 (2013) 222001, arXiv: 1308.3175 [hep-lat].

[86] M. Cleven et al., *Light meson mass dependence of the positive parity heavy-strange mesons*, Eur. Phys. J. **A47** (2011) 19, arXiv: 1009.3804 [hep-ph].

[87] S. Cho et al., *Multi-quark hadrons from Heavy Ion Collisions*, Phys. Rev. Lett. **106** (2011) 212001, arXiv: 1011.0852 [nucl-th].

[88] S. Cho et al., *Studying Exotic Hadrons in Heavy Ion Collisions*, Phys. Rev. **C84** (2011) 064910, arXiv: 1107.1302 [nucl-th].

[89] J. S. Lange, *The PANDA experiment: Hadron physics with antiprotons at FAIR*, Int. J. Mod. Phys. **A24** (2009) 369.

[90] R. Aaij et al., *Study of D_{sJ} decays to $D^+K^0_S$ and D^0K^+ final states in pp collisions*, JHEP **10** (2012) 151, arXiv: 1207.6016 [hep-ex].

[91] J. A. Oller and E. Oset, *Chiral symmetry amplitudes in the S wave isoscalar and isovector channels and the sigma, f0(980), a0(980) scalar mesons*, Nucl. Phys. **A620** (1997) 438, [Erratum: Nucl. Phys.A652,407(1999)], arXiv: hep-ph/9702314 [hep-ph].

[92] J. A. Oller and E. Oset, *N/D description of two meson amplitudes and chiral symmetry*, Phys. Rev. **D60** (1999) 074023, arXiv: hep-ph/9809337 [hep-ph].

[93] J. A. Oller and U.-G. Meißner, *Chiral dynamics in the presence of bound states: Kaon nucleon interactions revisited*, Phys. Lett. **B500** (2001) 263, arXiv: hep-ph/0011146 [hep-ph].

[94] J. Nieves and E. Ruiz Arriola, *Bethe-Salpeter approach for unitarized chiral perturbation theory*, Nucl. Phys. **A679** (2000) 57, arXiv: hep-ph/9907469 [hep-ph].

[95] B. Borasoy et al., *A Gauge invariant chiral unitary framework for kaon photo- and electroproduction on the proton*, Eur. Phys. J. **A34** (2007) 161, arXiv: 0709.3181 [nucl-th].

[96] F.-K. Guo et al., *S wave K pi scattering and effects of kappa in $J/\psi \to \bar{K}^{*0}(892)K^+\pi^-$*, Nucl. Phys. **A773** (2006) 78, arXiv: hep-ph/0509050 [hep-ph].

[97] K. M. Watson, *The Effect of final state interactions on reaction cross-sections*, Phys. Rev. **88** (1952) 1163.

[98] A. B. Migdal, *The theory of nuclear reactions with production of slow particles*, Sov. Phys. JETP **1** (1955) 2.

[99] C. Bignamini et al., *More loosely bound hadron molecules at CDF?*, Phys. Lett. **B684** (2010) 228, arXiv: 0912.5064 [hep-ph].

[100] U.-G. Meißner and J. A. Oller, *$J/\psi \to \phi\pi\pi(K\bar{K})$ decays, chiral dynamics and OZI violation*, Nucl. Phys. **A679** (2001) 671, arXiv: hep-ph/0005253 [hep-ph].

[101] T. Sjostrand, S. Mrenna and P. Z. Skands, *A Brief Introduction to PYTHIA 8.1*, Comput. Phys. Commun. **178** (2008) 852, arXiv: 0710.3820 [hep-ph].

[102] M. Bahr et al., *Herwig++ Physics and Manual*, Eur. Phys. J. **C58** (2008) 639, arXiv: 0803.0883 [hep-ph].

[103] A. Buckley et al., *Rivet user manual*, Comput. Phys. Commun. **184** (2013) 2803, arXiv: 1003.0694 [hep-ph].

[104] URL: https://twiki.cern.ch/twiki/bin/view/AtlasPublic/LuminosityPublicResults.

[105] URL: https://twiki.cern.ch/twiki/bin/view/CMSPublic/LumiPublicResults.

[106] B. Aubert et al., *Study of D_{sJ} decays to D^*K in inclusive e^+e^- interactions*, Phys. Rev. **D80** (2009) 092003, arXiv: 0908.0806 [hep-ex].

[107] *Measurement of D^* meson production cross sections in pp collisions at $\sqrt{s} = 7$ TeV with the ATLAS detector* (2011).

[108] F.-K. Guo et al., *Production of the bottom analogs and the spin partner of the $X(3872)$ at hadron colliders*, Eur. Phys. J. **C74**.9 (2014) 3063, arXiv: 1402.6236 [hep-ph].

[109] S. Godfrey, "Topics in Hadron Spectroscopy in 2009", *Particles and fields. Proceedings, Meeting of the Division of the American Physical Society, DPF 2009, Detroit, USA, July 26-31, 2009*, 2009, arXiv: 0910.3409 [hep-ph], URL: https://inspirehep.net/record/834347/files/arXiv:0910.3409.pdf.

[110] C. Amsler et al., *Review of Particle Physics*, Phys. Lett. **B667** (2008) 1.

[111] S. K. Choi et al., *Observation of a narrow charmonium - like state in exclusive $B^{+-} \to K^{+-}\pi^+\pi^- J/\psi$ decays*, Phys. Rev. Lett. **91** (2003) 262001, arXiv: hep-ex/0309032 [hep-ex].

[112] B. Aubert et al., *Study of the $B \to J/\psi K^-\pi^+\pi^-$ decay and measurement of the $B \to X(3872)K^-$ branching fraction*, Phys. Rev. **D71** (2005) 071103, arXiv: hep-ex/0406022 [hep-ex].

[113] A. Abulencia et al., *Analysis of the quantum numbers J^{PC} of the $X(3872)$*, Phys. Rev. Lett. **98** (2007) 132002, arXiv: hep-ex/0612053 [hep-ex].

[114] G. Gokhroo et al.,
Observation of a Near-threshold $D^0\bar{D}^0\pi^0$ Enhancement in $B \to D^0\bar{D}^0\pi^0 K$ Decay,
Phys. Rev. Lett. **97** (2006) 162002, arXiv: hep-ex/0606055 [hep-ex].

[115] B. Aubert et al., *Search for $B^+ \to X(3872)K^+$, $X(3872) \to J/\psi\gamma$*,
Phys. Rev. **D74** (2006) 071101, arXiv: hep-ex/0607050 [hep-ex].

[116] R. Aaij et al., *Determination of the X(3872) meson quantum numbers*,
Phys. Rev. Lett. **110** (2013) 222001, arXiv: 1302.6269 [hep-ex].

[117] B. Aubert et al.,
Search for a charged partner of the X(3872) in the B meson decay $B \to X^- K$, $X^- \to J/\psi\pi^-\pi^0$,
Phys. Rev. **D71** (2005) 031501, arXiv: hep-ex/0412051 [hep-ex].

[118] N. A. Tornqvist,
Isospin breaking of the narrow charmonium state of Belle at 3872-MeV as a deuson,
Phys. Lett. **B590** (2004) 209, arXiv: hep-ph/0402237 [hep-ph].

[119] C. Hanhart et al.,
Reconciling the X(3872) with the near-threshold enhancement in the $D^0\bar{D}^{*0}$ final state,
Phys. Rev. **D76** (2007) 034007, arXiv: 0704.0605 [hep-ph].

[120] K. Abe et al., "Evidence for $X(3872) \to \gamma J/\psi$ and the sub-threshold decay $X(3872) \to \omega J/\psi$",
Lepton and photon interactions at high energies. Proceedings, 22nd International Symposium, LP 2005, Uppsala, Sweden, June 30-July 5, 2005, 2005, arXiv: hep-ex/0505037 [hep-ex].

[121] D. Gamermann and E. Oset, *Isospin breaking effects in the X(3872) resonance*,
Phys. Rev. **D80** (2009) 014003, arXiv: 0905.0402 [hep-ph].

[122] B. Aubert et al., *A Study of $B \to X(3872)K$, with $X(3872) \to J/\psi\pi^+\pi^-$*,
Phys. Rev. **D77** (2008) 111101, arXiv: 0803.2838 [hep-ex].

[123] M. Butenschoen, Z.-G. He and B. A. Kniehl,
NLO NRQCD disfavors the interpretation of X(3872) as $\chi_{c1}(2P)$, Phys. Rev. **D88** (2013) 011501,
arXiv: 1303.6524 [hep-ph].

[124] M. Suzuki, *The X(3872) boson: Molecule or charmonium*, Phys. Rev. **D72** (2005) 114013,
arXiv: hep-ph/0508258 [hep-ph].

[125] W.-S. Hou, *Searching for the bottom counterparts of $X(3872)$ and Y(4260) via $\pi^+\pi^-\Upsilon$*,
Phys. Rev. **D74** (2006) 017504, arXiv: hep-ph/0606016 [hep-ph].

[126] A. Ali et al., *A case for hidden $b\bar{b}$ tetraquarks based on $e^+e^- \to b\bar{b}$ cross section between $\sqrt{s} = 10.54$ and 11.20 GeV*, Phys. Lett. **B684** (2010) 28, arXiv: 0911.2787 [hep-ph].

[127] N. A. Tornqvist,
From the deuteron to deusons, an analysis of deuteron - like meson meson bound states,
Z. Phys. **C61** (1994) 525, arXiv: hep-ph/9310247 [hep-ph].

[128] M. Karliner and S. Nussinov,
The doubly heavies: $\bar{Q}Q\bar{q}q$ and $QQ\bar{q}\bar{q}$ tetraquarks and QQq baryons, JHEP **07** (2013) 153,
arXiv: 1304.0345 [hep-ph].

[129] T. Aushev et al., *Physics at Super B Factory* (2010), arXiv: 1002.5012 [hep-ex].

[130] A. E. Bondar et al., *Heavy quark spin structure in Z_b resonances*, Phys. Rev. **D84** (2011) 054010, arXiv: 1105.4473 [hep-ph].

[131] M. B. Voloshin, *Radiative transitions from Upsilon(5S) to molecular bottomonium*, Phys. Rev. **D84** (2011) 031502, arXiv: 1105.5829 [hep-ph].

[132] T. Mehen and J. W. Powell, *Heavy Quark Symmetry Predictions for Weakly Bound B-Meson Molecules*, Phys. Rev. **D84** (2011) 114013, arXiv: 1109.3479 [hep-ph].

[133] J. Nieves and M. P. Valderrama, *The Heavy Quark Spin Symmetry Partners of the X(3872)*, Phys. Rev. **D86** (2012) 056004, arXiv: 1204.2790 [hep-ph].

[134] C. Hidalgo-Duque, J. Nieves and M. P. Valderrama, *Light flavor and heavy quark spin symmetry in heavy meson molecules*, Phys. Rev. **D87**.7 (2013) 076006, arXiv: 1210.5431 [hep-ph].

[135] J. Nieves and M. P. Valderrama, *Deriving the existence of $B\bar{B}^*$ bound states from the X(3872) and Heavy Quark Symmetry*, Phys. Rev. **D84** (2011) 056015, arXiv: 1106.0600 [hep-ph].

[136] M. T. AlFiky, F. Gabbiani and A. A. Petrov, *X(3872): Hadronic molecules in effective field theory*, Phys. Lett. **B640** (2006) 238, arXiv: hep-ph/0506141 [hep-ph].

[137] B. Grinstein et al., *Chiral perturbation theory for f_{D_s}/f_D and B_{B_s}/B_B*, Nucl. Phys. **B380** (1992) 369, arXiv: hep-ph/9204207 [hep-ph].

[138] M. P. Valderrama, *Power Counting and Perturbative One Pion Exchange in Heavy Meson Molecules*, Phys. Rev. **D85** (2012) 114037, arXiv: 1204.2400 [hep-ph].

[139] B. Reisert et al., *Charm production studies at CDF*, Nucl. Phys. Proc. Suppl. **170** (2007) 243.

[140] J. Alwall et al., *MadGraph 5 : Going Beyond*, JHEP **06** (2011) 128, arXiv: 1106.0522 [hep-ph].

[141] B. Aubert et al., *Measurements of the absolute branching fractions of $B^\pm \to K^\pm X(c\bar{c})$*, Phys. Rev. Lett. **96** (2006) 052002, arXiv: hep-ex/0510070 [hep-ex].

[142] S.-K. Choi et al., *Bounds on the width, mass difference and other properties of $X(3872) \to \pi^+\pi^- J/\psi$ decays*, Phys. Rev. **D84** (2011) 052004, arXiv: 1107.0163 [hep-ex].

[143] T. Aushev et al., *Study of the $B \to X(3872)(D^{*0}\bar{D}^0)K$ decay*, Phys. Rev. **D81** (2010) 031103, arXiv: 0810.0358 [hep-ex].

[144] P. del Amo Sanchez et al., *Evidence for the decay $X(3872) \to J/\psi\omega$*, Phys. Rev. **D82** (2010) 011101, arXiv: 1005.5190 [hep-ex].

[145] B. Aubert et al., *Evidence for $X(3872) \to \psi(2S)\gamma$ in $B^\pm \to X(3872)K^\pm$ decays, and a study of $B \to c\bar{c}\gamma K$*, Phys. Rev. Lett. **102** (2009) 132001, arXiv: 0809.0042 [hep-ex].

[146] V. Bhardwaj et al., *Observation of $X(3872) \to J/\psi\gamma$ and search for $X(3872) \to \psi'\gamma$ in B decays*, Phys. Rev. Lett. **107** (2011) 091803, arXiv: 1105.0177 [hep-ex].

[147] G. Bauer, *The X(3872) at CDF II*, Int. J. Mod. Phys. **A20** (2005) 3765, arXiv: hep-ex/0409052 [hep-ex].

[148] S. Chatrchyan et al., *Measurement of the X(3872) production cross section via decays to $J/\psi\pi\pi$ in pp collisions at $\sqrt{(s)} = 7$ TeV*, JHEP **04** (2013) 154, arXiv: 1302.3968 [hep-ex].

[149] S. Chatrchyan et al., *Search for a new bottomonium state decaying to $\Upsilon(1S)\pi^+\pi^-$ in pp collisions at $\sqrt{s} = 8$ TeV*, Phys. Lett. **B727** (2013) 57, arXiv: 1309.0250 [hep-ex].

[150] S. Chatrchyan et al., *Measurement of the $\Upsilon(1S)$, $\Upsilon(2S)$, and $\Upsilon(3S)$ cross sections in pp collisions at $\sqrt{s} = 7$ TeV*, Phys. Lett. **B727** (2013) 101, arXiv: 1303.5900 [hep-ex].

[151] S. Chatrchyan et al., *Search for a new bottomonium state decaying to $\Upsilon(1S)\pi^+\pi^-$ in pp collisions at $\sqrt{s} = 8$ TeV*, Phys. Lett. **B727** (2013) 57, arXiv: 1309.0250 [hep-ex].

[152] G. Li and W. Wang, *Hunting for the X_b via radiative decays*, Phys. Lett. **B733** (2014) 100, arXiv: 1402.6463 [hep-ph].

[153] URL: https://twiki.cern.ch/twiki/bin/view/Main/LHCb-Facts#Integrated_luminosity.

[154] "Physics at a High-Luminosity LHC with ATLAS", *Community Summer Study 2013: Snowmass on the Mississippi (CSS2013) Minneapolis, MN, USA, July 29-August 6, 2013*, 2013, arXiv: 1307.7292 [hep-ex], URL: https://inspirehep.net/record/1245017/files/arXiv:1307.7292.pdf.

[155] G. Aad et al., *Measurement of Upsilon production in 7 TeV pp collisions at ATLAS*, Phys. Rev. **D87**.5 (2013) 052004, arXiv: 1211.7255 [hep-ex].

[156] D. Acosta et al., *Observation of the narrow state $X(3872) \to J/\psi\pi^+\pi^-$ in $\bar{p}p$ collisions at $\sqrt{s} = 1.96$ TeV*, Phys. Rev. Lett. **93** (2004) 072001, arXiv: hep-ex/0312021 [hep-ex].

[157] V. M. Abazov et al., *Observation and properties of the $X(3872)$ decaying to $J/\psi\pi^+\pi^-$ in $p\bar{p}$ collisions at $\sqrt{s} = 1.96$ TeV*, Phys. Rev. Lett. **93** (2004) 162002, arXiv: hep-ex/0405004 [hep-ex].

[158] R. Aaij et al., *Observation of $X(3872)$ production in pp collisions at $\sqrt{s} = 7$ TeV*, Eur. Phys. J. **C72** (2012) 1972, arXiv: 1112.5310 [hep-ex].

[159] D. M. Asner et al., *Physics at BES-III*, Int. J. Mod. Phys. **A24** (2009) S1, arXiv: 0809.1869 [hep-ex].

[160] F.-K. Guo, U.-G. Meißner and Z. Yang, *Production of the spin partner of the X(3872) in e^+e^- collisions*, Phys. Lett. **B740** (2015) 42, arXiv: 1410.4674 [hep-ph].

[161] C.-Y. Wong, *Molecular states of heavy quark mesons*, Phys. Rev. **C69** (2004) 055202, arXiv: hep-ph/0311088 [hep-ph].

[162] E. S. Swanson, *$D\bar{D}^*$ and $D^*\bar{D}^*$ molecules*, J. Phys. Conf. Ser. **9** (2005) 79.

[163] R. Molina and E. Oset, *The Y(3940), Z(3930) and the X(4160) as dynamically generated resonances from the vector-vector interaction*, Phys. Rev. **D80** (2009) 114013, arXiv: 0907.3043 [hep-ph].

[164] Z.-F. Sun et al., *A note on the $B^*\bar{B}$, $B^*\bar{B}^*$, $D^*\bar{D}$, $\bar{D}^*\bar{D}^*$, molecular states*, Chin. Phys. **C36** (2012) 194.

[165] M. Albaladejo et al., *Decay widths of the spin-2 partners of the X(3872)*, Eur. Phys. J. **C75**.11 (2015) 547, arXiv: 1504.00861 [hep-ph].

[166] L. Maiani et al., *Diquark-antidiquarks with hidden or open charm and the nature of X(3872)*, Phys. Rev. **D71** (2005) 014028, arXiv: hep-ph/0412098 [hep-ph].

[167] A. Margaryan and R. P. Springer, *Using the decay $\psi(4160) \to X(3872)\gamma$ to probe the molecular content of the X(3872)*, Phys. Rev. **D88**.1 (2013) 014017, arXiv: 1304.8101 [hep-ph].

[168] S. Fleming et al., *Pion interactions in the $X(3872)$*, Phys. Rev. **D76** (2007) 034006, arXiv: hep-ph/0703168 [hep-ph].

[169] Fayyazuddin and Riazuddin, *Heavy quark spin symmetry and D mesons*, Phys. Rev. **D48** (1993) 2224.

[170] F.-K. Guo et al., *Effect of charmed meson loops on charmonium transitions*, Phys. Rev. **D83** (2011) 034013, arXiv: 1008.3632 [hep-ph].

[171] F.-K. Guo, U.-G. Meißner and C.-P. Shen, *Enhanced breaking of heavy quark spin symmetry*, Phys. Lett. **B738** (2014) 172, arXiv: 1406.6543 [hep-ph].

[172] X. Li and M. B. Voloshin, *Suppression of the S-wave production of $(3/2)^+ + (1/2)^-$ heavy meson pairs in e^+e^- annihilation*, Phys. Rev. **D88**.3 (2013) 034012, arXiv: 1307.1072 [hep-ph].

[173] G.-J. Ding, *Are Y(4260) and Z_2^+ are D_1D or D_0D^* Hadronic Molecules?*, Phys. Rev. **D79** (2009) 014001, arXiv: 0809.4818 [hep-ph].

[174] Q. Wang, C. Hanhart and Q. Zhao, *Decoding the riddle of $Y(4260)$ and $Z_c(3900)$*, Phys. Rev. Lett. **111**.13 (2013) 132003, arXiv: 1303.6355 [hep-ph].

[175] M. Cleven et al., *$Y(4260)$ as the first S-wave open charm vector molecular state?*, Phys. Rev. **D90**.7 (2014) 074039, arXiv: 1310.2190 [hep-ph].

[176] S. Weinberg, *Evidence That the Deuteron Is Not an Elementary Particle*, Phys. Rev. **137** (1965) B672.

[177] M. Cleven et al., *Bound state nature of the exotic Z_b states*, Eur. Phys. J. **A47** (2011) 120, arXiv: 1107.0254 [hep-ph].

[178] Fayyazuddin and O. H. Mobarek, *Radiative decay of $D_2(2460)$ and $D_1(2420)$*, Phys. Rev. **D50** (1994) 2329.

[179] J. G. Körner, D. Pirjol and K. Schilcher, *Radiative decays of the P wave charmed mesons*, Phys. Rev. **D47** (1993) 3955, arXiv: hep-ph/9212220 [hep-ph].

[180] S. Godfrey, *Properties of the charmed P-wave mesons*, Phys. Rev. **D72** (2005) 054029, arXiv: hep-ph/0508078 [hep-ph].

[181] L. D. Landau, *On analytic properties of vertex parts in quantum field theory*, Nucl. Phys. **13** (1959) 181.

[182] F.-K. Guo, U.-G. Meißner and Z. Yang, *Hindered magnetic dipole transitions between P-wave bottomonia* (2016), arXiv: 1604.00770 [hep-ph].

[183] J. P. Lees et al., *Evidence for the $h_b(1P)$ meson in the decay $\Upsilon(3S) \to \pi^0 h_b(1P)$*, Phys. Rev. **D84** (2011) 091101, arXiv: 1102.4565 [hep-ex].

[184] M. B. Voloshin, *Hadronic transitions from $\Upsilon(3S)$ TO 1 p wave singlet bottomonium level*, Sov. J. Nucl. Phys. **43** (1986) 1011, [Yad. Fiz.43,1571(1986)].

[185] S. Godfrey and J. L. Rosner, *Production of singlet P wave $c\bar{c}$ and $b\bar{b}$ states*, Phys. Rev. **D66** (2002) 014012, arXiv: hep-ph/0205255 [hep-ph].

[186] U. Tamponi et al., *First observation of the hadronic transition $\Upsilon(4S) \to \eta h_b(1P)$ and new measurement of the $h_b(1P)$ and $\eta_b(1S)$ parameters*, Phys. Rev. Lett. **115**.14 (2015) 142001, arXiv: 1506.08914 [hep-ex].

[187] F.-K. Guo, C. Hanhart and U.-G. Meißner, *Extracting the light quark mass ratio m_u/m_d frombottomoniatransitions*, Phys. Rev. Lett. **105** (2010) 162001, arXiv: 1007.4682 [hep-ph].

[188] S. Godfrey and K. Moats, *Bottomonium Mesons and Strategies for their Observation*, Phys. Rev. **D92**.5 (2015) 054034, arXiv: 1507.00024 [hep-ph].

[189] J.-F. Liu and G.-J. Ding, *Bottomonium Spectrum with Coupled-Channel Effects*, Eur. Phys. J. **C72** (2012) 1981, arXiv: 1105.0855 [hep-ph].

[190] E. Eichten et al., *Charmonium: Comparison with Experiment*, Phys. Rev. **D21** (1980) 203.

[191] K. Heikkila, S. Ono and N. A. Tornqvist, *Heavy $c\bar{c}$ and $b\bar{b}$ quarkonium states and unitarity effects*, Phys. Rev. **D29** (1984) 110, [Erratum: Phys. Rev.D29,2136(1984)].

[192] E. J. Eichten, K. Lane and C. Quigg, *New states above charm threshold*, Phys. Rev. **D73** (2006) 014014, [Erratum: Phys. Rev.D73,079903(2006)], arXiv: hep-ph/0511179 [hep-ph].

[193] M. R. Pennington and D. J. Wilson, *Decay channels and charmonium mass-shifts*, Phys. Rev. **D76** (2007) 077502, arXiv: 0704.3384 [hep-ph].

[194] T. Barnes and E. S. Swanson, *Hadron loops: General theorems and application to charmonium*, Phys. Rev. **C77** (2008) 055206, arXiv: 0711.2080 [hep-ph].

[195] B.-Q. Li, C. Meng and K.-T. Chao, *Coupled-Channel and Screening Effects in Charmonium Spectrum*, Phys. Rev. **D80** (2009) 014012, arXiv: 0904.4068 [hep-ph].

[196] I. V. Danilkin and Yu. A. Simonov,
Channel coupling in heavy quarkonia: Energy levels, mixing, widths and new states,
Phys. Rev. **D81** (2010) 074027, arXiv: 0907.1088 [hep-ph].

[197] J. Ferretti et al., *Bottomonium self-energies due to the coupling to the meson-meson continuum*,
Phys. Rev. **C86** (2012) 015204.

[198] Z.-Y. Zhou and Z. Xiao,
Comprehending heavy charmonia and their decays by hadron loop effects,
Eur. Phys. J. **A50**.10 (2014) 165, arXiv: 1309.1949 [hep-ph].

[199] H. J. Lipkin and S. F. Tuan,
OZI Violating Dipion Decays of Heavy Quarkonia via an Intermediate Heavy Meson Pair State,
Phys. Lett. **B206** (1988) 349.

[200] P. Moxhay, *Coupled Channel Effects in the Decay Υ (3s) $\to$ Υ (1s) $\pi^+\pi^-$*,
Phys. Rev. **D39** (1989) 3497.

[201] H.-Y. Zhou and Y.-P. Kuang,
Coupled channel effects in hadronic transitions in heavy quarkonium systems,
Phys. Rev. **D44** (1991) 756.

[202] C. Meng and K.-T. Chao, *Scalar resonance contributions to the dipion transition rates of $\Upsilon(4S, 5S)$ in the re-scattering model*, Phys. Rev. **D77** (2008) 074003,
arXiv: 0712.3595 [hep-ph].

[203] C. Meng and K.-T. Chao,
$\Upsilon(4S, 5S) \to \Upsilon(1S)\eta$ transitions in the rescattering model and the new BaBar measurement,
Phys. Rev. **D78** (2008) 074001, arXiv: 0806.3259 [hep-ph].

[204] Yu. A. Simonov and A. I. Veselov, *Bottomonium dipion transitions*,
Phys. Rev. **D79** (2009) 034024, arXiv: 0804.4635 [hep-ph].

[205] G. Li and Q. Zhao, *Revisit the radiative decays of J/ψ and $\psi' \to \gamma\eta_c(\gamma\eta_c')$*,
Phys. Rev. **D84** (2011) 074005, arXiv: 1107.2037 [hep-ph].

[206] T. Mehen and D.-L. Yang, *On the Role of Charmed Meson Loops in Charmonium Decays*,
Phys. Rev. **D85** (2012) 014002, arXiv: 1111.3884 [hep-ph].

[207] D.-Y. Chen, X. Liu and X.-Q. Li, *Anomalous dipion invariant mass distribution of the $\Upsilon(4S)$ decays into $\Upsilon(1S)\pi^+\pi^-$ and $\Upsilon(2S)\pi^+\pi^-$*, Eur. Phys. J. **C71** (2011) 1808,
arXiv: 1109.1406 [hep-ph].

[208] F.-K. Guo and U.-G. Meißner,
Examining coupled-channel effects in radiative charmonium transitions,
Phys. Rev. Lett. **108** (2012) 112002, arXiv: 1111.1151 [hep-ph].

[209] R. Mussa, *a talk at B2TIP-II, Krakow*.

[210] F.-K. Guo et al., *Novel analysis of the decays $\psi' \to h_c\pi^0$ and $\eta_c' \to \chi_{c0}\pi^0$*,
Phys. Rev. **D82** (2010) 034025, arXiv: 1002.2712 [hep-ph].

[211] W. Detmold, C.-J. D. Lin and S. Meinel,
Axial couplings and strong decay widths of heavy hadrons, Phys. Rev. Lett. **108** (2012) 172003, arXiv: 1109.2480 [hep-lat].

[212] F. Bernardoni et al., *Precision lattice QCD computation of the $B^*B\pi$ coupling*,
Phys. Lett. **B740** (2015) 278, arXiv: 1404.6951 [hep-lat].

[213] J. M. Flynn et al., *The $B^*B\pi$ Coupling Using Relativistic Heavy Quarks*,
Phys. Rev. **D93**.1 (2016) 014510, arXiv: 1506.06413 [hep-lat].

[214] R. Aaij et al.,
Measurement of the $\chi_b(3P)$ mass and of the relative rate of $\chi_{b1}(1P)$ and $\chi_{b2}(1P)$ production,
JHEP **10** (2014) 88, arXiv: 1409.1408 [hep-ex].

[215] P. Colangelo, F. De Fazio and T. N. Pham,
Nonfactorizable contributions in B decays to charmonium: The Case of $B^- \to K^- h_c$,
Phys. Rev. **D69** (2004) 054023, arXiv: hep-ph/0310084 [hep-ph].

[216] J. F. Amundson et al., *Radiative D^* decay using heavy quark and chiral symmetry*,
Phys. Lett. **B296** (1992) 415, arXiv: hep-ph/9209241 [hep-ph].

[217] R. Lewis and R. M. Woloshyn, *Excited Upsilon Radiative Decays*,
Phys. Rev. **D84** (2011) 094501, arXiv: 1108.1137 [hep-lat].

[218] R. Lewis and R. M. Woloshyn, *More about excited bottomonium radiative decays*,
Phys. Rev. **D86** (2012) 057501, arXiv: 1207.3825 [hep-lat].

[219] C. Hughes et al., *Hindered M1 Radiative Decay of $\Upsilon(2S)$ from Lattice NRQCD*,
Phys. Rev. **D92** (2015) 094501, arXiv: 1508.01694 [hep-lat].

[220] K. Azizi, H. Sundu and J. Y. Sungu,
Semileptonic transition of P wave bottomonium $\chi_{b0}(1P)$ to B_c meson,
Eur. Phys. J. **A48** (2012) 108, arXiv: 1207.5922 [hep-ph].

[221] F.-K. Guo, C. Hanhart and U.-G. Meißner,
Mass splittings within heavy baryon isospin multiplets in chiral perturbation theory,
JHEP **09** (2008) 136, arXiv: 0809.2359 [hep-ph].

[222] F.-K. Guo et al., *How to reveal the exotic nature of the $P_c(4450)$*,
Phys. Rev. **D92**.7 (2015) 071502, arXiv: 1507.04950 [hep-ph].

[223] Q. Wang, X.-H. Liu and Q. Zhao,
Photoproduction of hidden charm pentaquark states $P_c^+(4380)$ and $P_c^+(4450)$,
Phys. Rev. **D92** (2015) 034022, arXiv: 1508.00339 [hep-ph].

[224] V. Kubarovsky and M. B. Voloshin,
Formation of hidden-charm pentaquarks in photon-nucleon collisions,
Phys. Rev. **D92**.3 (2015) 031502, arXiv: 1508.00888 [hep-ph].

[225] M. Karliner and J. L. Rosner, *Photoproduction of Exotic Baryon Resonances*,
Phys. Lett. **B752** (2016) 329, arXiv: 1508.01496 [hep-ph].

[226] Y. Huang et al.,
Photoproduction of hidden-charm states in $\gamma p \to \bar{D}^{*0}\Lambda_c^+$ reaction near threshold (2016), arXiv: 1604.05969 [nucl-th].

[227] Q.-F. Lü et al.,
Neutral hidden charm pentaquark states $P_c^0(4380)$ and $P_c^0(4450)$ in $\pi^- p \to J/\psi n$ reaction, Phys. Rev. **D93**.3 (2016) 034009, arXiv: 1510.06271 [hep-ph].

[228] X.-H. Liu and M. Oka, *Understanding the nature of the heavy pentaquarks and searching for them in pion-induced reactions* (2016), arXiv: 1602.07069 [hep-ph].

[229] S. K. Choi et al., *Observation of a resonance-like structure in the $\pi^{+-}\psi'$ mass distribution in exclusive $B \to K\pi^{+-}\psi'$ decays*, Phys. Rev. Lett. **100** (2008) 142001, arXiv: 0708.1790 [hep-ex].

[230] R. Aaij et al., *Observation of the resonant character of the $Z(4430)^-$ state*, Phys. Rev. Lett. **112**.22 (2014) 222002, arXiv: 1404.1903 [hep-ex].

[231] M. Ablikim et al.,
Observation of a Charged Charmoniumlike Structure in $e^+e^- \to \pi^+\pi^- J/\psi$ at $\sqrt{s}$ =4.26GeV, Phys. Rev. Lett. **110** (2013) 252001, arXiv: 1303.5949 [hep-ex].

[232] Z. Q. Liu et al.,
Study of $e^+e^- \to \pi^+\pi^- J/\psi$ and Observation of a Charged Charmoniumlike State at Belle, Phys. Rev. Lett. **110** (2013) 252002, arXiv: 1304.0121 [hep-ex].

[233] M. Ablikim et al.,
Observation of a charged charmoniumlike structure in $e^+e^- \to (D^*\bar{D}^*)^\pm\pi^\mp$ at $\sqrt{s}$ = 4.26GeV, Phys. Rev. Lett. **112**.13 (2014) 132001, arXiv: 1308.2760 [hep-ex].

[234] R. Chen et al., *Identifying exotic hidden-charm pentaquarks*, Phys. Rev. Lett. **115**.13 (2015) 132002, arXiv: 1507.03704 [hep-ph].

[235] H.-X. Chen et al., *Towards exotic hidden-charm pentaquarks in QCD*, Phys. Rev. Lett. **115**.17 (2015) 172001, arXiv: 1507.03717 [hep-ph].

[236] L. Roca, J. Nieves and E. Oset, *LHCb pentaquark as a $\bar{D}^*\Sigma_c - \bar{D}^*\Sigma_c^*$ molecular state*, Phys. Rev. **D92**.9 (2015) 094003, arXiv: 1507.04249 [hep-ph].

[237] J.-J. Wu et al., *Prediction of narrow N^* and Λ^* resonances with hidden charm above 4 GeV*, Phys. Rev. Lett. **105** (2010) 232001, arXiv: 1007.0573 [nucl-th].

[238] J.-J. Wu et al.,
Dynamically generated N^* and Λ^* resonances in the hidden charm sector around 4.3 GeV, Phys. Rev. **C84** (2011) 015202, arXiv: 1011.2399 [nucl-th].

[239] Z.-C. Yang et al., *The possible hidden-charm molecular baryons composed of anti-charmed meson and charmed baryon*, Chin. Phys. **C36** (2012) 6, arXiv: 1105.2901 [hep-ph].

[240] C. W. Xiao, J. Nieves and E. Oset, *Combining heavy quark spin and local hidden gauge symmetries in the dynamical generation of hidden charm baryons*, Phys. Rev. **D88** (2013) 056012, arXiv: 1304.5368 [hep-ph].

[241] A. Mironov and A. Morozov, *Is the pentaquark doublet a hadronic molecule?*, JETP Lett. **102**.5 (2015) 271, arXiv: 1507.04694 [hep-ph].

[242] L. Maiani, A. D. Polosa and V. Riquer, *The New Pentaquarks in the Diquark Model*, Phys. Lett. **B749** (2015) 289, arXiv: 1507.04980 [hep-ph].

[243] Z.-G. Wang, *Analysis of $P_c(4380)$ and $P_c(4450)$ as pentaquark states in the diquark model with QCD sum rules*, Eur. Phys. J. **C76**.2 (2016) 70, arXiv: 1508.01468 [hep-ph].

[244] S. M. Flatte, *Coupled - Channel Analysis of the pi eta and K anti-K Systems Near K anti-K Threshold*, Phys. Lett. **B63** (1976) 224.

[245] C. Hanhart et al., *Practical Parametrization for Line Shapes of Near-Threshold States*, Phys. Rev. Lett. **115**.20 (2015) 202001, arXiv: 1507.00382 [hep-ph].

[246] D. I. O. R. J. Eden P. V. Landshoff and J. C. Polkinghorne, *The Analytic S -Matrix*, 1966.

[247] T. S. Chang, *Introduction to Dispersion Relation (2 volumes, in Chinese, written in 1965)*, 1980.

[248] C. Schmid, *Final-State Interactions and the Simulation of Resonances*, Phys. Rev. **154** (5 1967) 1363, URL: http://link.aps.org/doi/10.1103/PhysRev.154.1363.

[249] I. J. R. Aitchison, *Unitarity, Analyticity and Crossing Symmetry in Two- and Three-hadron Final State Interactions* (2015), arXiv: 1507.02697 [hep-ph].

[250] X.-H. Liu, M. Oka and Q. Zhao, *Searching for observable effects induced by anomalous triangle singularities*, Phys. Lett. **B753** (2016) 297, arXiv: 1507.01674 [hep-ph].

[251] J.-J. Wu et al., *The Puzzle of anomalously large isospin violations in $\eta(1405/1475) \to 3\pi$*, Phys. Rev. Lett. **108** (2012) 081803, arXiv: 1108.3772 [hep-ph].

[252] X.-G. Wu et al., *Understanding the property of $\eta(1405/1475)$ in the J/ψ radiative decay*, Phys. Rev. **D87**.1 (2013) 014023, arXiv: 1211.2148 [hep-ph].

[253] Q. Wang, C. Hanhart and Q. Zhao, *Systematic study of the singularity mechanism in heavy quarkonium decays*, Phys. Lett. **B725**.1-3 (2013) 106, arXiv: 1305.1997 [hep-ph].

[254] M. Mikhasenko, B. Ketzer and A. Sarantsev, *Nature of the $a_1(1420)$*, Phys. Rev. **D91**.9 (2015) 094015, arXiv: 1501.07023 [hep-ph].

[255] N. N. Achasov, A. A. Kozhevnikov and G. N. Shestakov, *Isospin breaking decay $\eta(1405) \to f_0(980)\pi^0 \to 3\pi$*, Phys. Rev. **D92**.3 (2015) 036003, arXiv: 1504.02844 [hep-ph].

[256] I. T. Lorenz, H. W. Hammer and U.-G. Meißner, *New structures in the proton-antiproton system*, Phys. Rev. **D92**.3 (2015) 034018, arXiv: 1506.02282 [hep-ph].

[257] J. L. Rosner, *Threshold effect and $\pi^{+-}\psi(2S)$ peak*, Phys. Rev. **D76** (2007) 114002, arXiv: 0708.3496 [hep-ph].

[258] D. V. Bugg, *How Resonances can synchronise with Thresholds*, J. Phys. **G35** (2008) 075005, arXiv: 0802.0934 [hep-ph].

[259] D. V. Bugg, *An Explanation of Belle states $Z_b(10610)$ and $Z_b(10650)$*, Europhys. Lett. **96** (2011) 11002, arXiv: 1105.5492 [hep-ph].

[260] E. S. Swanson, *Z_b and Z_c Exotic States as Coupled Channel Cusps*, Phys. Rev. **D91**.3 (2015) 034009, arXiv: 1409.3291 [hep-ph].

[261] D.-Y. Chen, X. Liu and T. Matsuki, *Reproducing the $Z_c(3900)$ structure through the initial-single-pion-emission mechanism*, Phys. Rev. **D88**.3 (2013) 036008, arXiv: 1304.5845 [hep-ph].

[262] A. P. Szczepaniak, *Triangle Singularities and XYZ Quarkonium Peaks*, Phys. Lett. **B747** (2015) 410, arXiv: 1501.01691 [hep-ph].

[263] J. L. Rosner, *Effects of S-wave thresholds*, Phys. Rev. **D74** (2006) 076006, arXiv: hep-ph/0608102 [hep-ph].

[264] F.-K. Guo et al., *Could the near-threshold XYZ states be simply kinematic effects?*, Phys. Rev. **D91**.5 (2015) 051504, arXiv: 1411.5584 [hep-ph].

[265] M. Beneke and L. Vernazza, *$B \to \chi_{cJ} K$ decays revisited*, Nucl. Phys. **B811** (2009) 155, arXiv: 0810.3575 [hep-ph].

[266] A. V. Anisovich et al., *Three-particle physics and dispersion relation theory*, Hackensack, USA: World Scientific, 2013, ISBN: 9780814478809, URL: http://www.worldscientific.com/worldscibooks/10.1142/8779.

[267] S. Coleman and R. E. Norton, *Singularities in the physical region*, Nuovo Cim. **38** (1965) 438.

[268] L. Roca, E. Oset and J. Singh, *Low lying axial-vector mesons as dynamically generated resonances*, Phys. Rev. **D72** (2005) 014002, arXiv: hep-ph/0503273 [hep-ph].

Acknowledgements

First, I wish to express my deepest gratitude to my supervisors, Prof. Dr. Ulf-G.Meißner and Prof. Feng-Kun Guo. Their deep knowledge of physics and constant support have benefited me enormously. Without them, this thesis would not have been possible. Moreover, I am truly grateful for suggesting my participation in some conferences and workshops and supporting me to visit the Institute of Theoretical Physics in Beijing. In addition, thanks to Prof. Wei Wang for the nice collaboration and many helpful discussions.

Secondly, I would also like to thank Dr. Qian Wang and Prof. Dr. Christoph Hanhart for the helpful discussions. Thanks to Prof. Juan M. Nieves Pamplona for his kind hospitality when I was in Valencia. I am grateful to the secretary, Barbara Kraus, for her help. Christian Jost and Bernard Metsch are also acknowledged for the computer issues. Thanks to Prof. Dr. Bastian Kubis, Christopher Helmes, Dr. Maxim Mai and Menglin Du for their kind help.

At last, I can never express how grateful I am to my parents and sister, they always help and support me.

Publications of important parts of the dissertation

Published journal articles

- "How to reveal the exotic nature of the $P_c(4450)$,"
  F. K. Guo, U.-G. Meißner, W. Wang and Z. Yang,
  Phys. Rev. D **92**, 071502.

- "Production of the spin partner of the X(3872) in e^+e^- collisions,"
  F. K. Guo, U.-G. Meißner and Z. Yang,
  Phys. Lett. B **740**, 42 (2015).

- "Production of charm-strange hadronic molecules at the LHC,"
  F. K. Guo, U.-G. Meißner, W. Wang and Z. Yang,
  JHEP **1405**, 138.

- "Production of the bottom analogs and the spin partner of the $X(3872)$ at hadron colliders,"
  F. K. Guo, U.-G. Meißner, W. Wang and Z. Yang,
  Eur. Phys. J. C **74**, no. 9, 3063 (2014).

Articles under review

- "Hindered magnetic dipole transitions between P-wave bottomonia,"
  F. K. Guo, U.-G. Meißner and Z. Yang,
  arXiv:1604.00770 [hep-ph].